

N71-17446

NASA CR-103025

THE JOHNS HOPKINS UNIVERSITY  
APPLIED PHYSICS LABORATORY  
SILVER SPRING, MARYLAND

S2P-2-396

November 1970

FINAL REPORT  
MAGNETIC ATTITUDE CONTROL SYSTEM FOR  
HEAO

prepared for  
Marshall Space Flight Center  
under NASA Defense Purchase Request No. H-65027A

SPACE DEVELOPMENT DEPARTMENT  
JOHNS HOPKINS UNIVERSITY  
APPLIED PHYSICS LABORATORY  
8621 GEORGIA AVENUE  
SILVER SPRING, MARYLAND

CASE FILE  
COPY

### ACKNOWLEDGEMENT

This report has been prepared and edited by F. F. Mobley and B. E. Tossman. The authors wish to recognize the contributions of D. Yost and J. Wildes in the application of optimal control techniques to this study, and to C. E. Williams for assistance in computer simulation. This work at APL has been under the direction of H. B. Riblet, Project Engineer.

The authors also wish to recognize the valuable contributions made by the Marshall Space Flight Center technical representatives B. G. Davis and D. N. Schultz in the course of discussions of our results.

TABLE OF CONTENTS

	Page
ABSTRACT .....	1
I SUMMARY .....	2
II INTRODUCTION.....	5
A. HEAO Concept, Mission and Control Requirements .....	5
1. Scanning Mode .....	7
2. Pointing Mode .....	7
B. Possibilities of Magnetic Control and Advantages .....	8
III INVESTIGATION OF PROBLEM .....	10
A. Purpose and Scope .....	10
B. Design Approach for a Magnetic Control System .....	11
C. Derivation of Optimal Control Law Coefficients .....	13
D. Magnetic Control System Synthesis and Performance .....	18
1. Fixed Parameters for HEAO-A Simulations .....	18
2. Effects due to Wheel Momentum, Weighting Ratio and Dipole Moments.....	18
a. Performance with 2000 ft-lb-sec Wheel..	20
b. Performance with 1000 ft-lb-sec Wheel..	24
c. Performance with 500 ft-lb-sec Wheel..	24
d. Performance with Zero Momentum Flywheel .....	28
3. Effects due to Magnetic Control Algorithms.	30
a. Available Component Algorithm .....	30
b. Single Component Algorithm .....	31
c. Two Component Algorithm .....	35
d. Combinations of Algorithms .....	37
4. Effects due to Sensor Deadband.....	39

TABLE OF CONTENTS - Continued

	Page
E. Baseline Magnetic Attitude Control System-Design and Performance.....	41
1. System Components.....	41
2. Algorithm Switching Logic.....	41
3. Baseline System Performance.....	42
a. Solar Pointing Scan Mode- Winter Solstice.....	42
b. Solar Pointing Scan Mode- Vernal Equinos.....	42
c. Galactic Pole Pointing.....	45
d. Worst Case Declination.....	45
e. Large Angle Maneuvers and Scan Rate Capture.....	45
F. Pointing Mode.....	54
1. Introduction to Problem of Pointing Mode Performance.....	54
2. Fixed Speed Wheel.....	54
3. Variable Speed Wheel- Y-Pointing Mode.....	56
4. Variable Speed Wheel- Z-Pointing Mode.....	62
IV CONCLUSIONS.....	65
REFERENCES.....	68
APPENDIX A. MAGNETIC TORQUER DESIGN.....	A-1
APPENDIX B. MATHEMATICAL MODEL OF THE EARTH'S MAGNETIC FIELD.....	B-1
APPENDIX C. COMPUTER PROGRAM FOR HEAO-A SIMULATION.....	C-1
APPENDIX D. DERIVATION OF OPTIMAL CONTROL LAW COEFFICIENTS.....	D-1
APPENDIX E. DERIVATION OF LINEARIZED EQUATIONS OF MOTION.....	E-1

LIST OF ILLUSTRATIONS

Figure	Title	Page
1	Baseline Performance—Solar Pointing Scan Mode at Winter Solstice.....	3
2	Y-Pointing Mode with Wheel Modulation.....	4
3	HEAO Component Arrangement.....	6
4	HEAO-A Attitude Control System Concept.....	12
5	HEAO-A with 2000 ft-lb-sec Wheel (Case #14)....	21
6	Magnetic Control Dipole Moments for HEAO-A with 2000 ft-lb-sec wheel (Case #14).....	22
7	HEAO-A with 2000 ft-lb-sec Wheel Magnetic Control and $10^3$ a-t-m <sup>2</sup> Dipole Limits (Case #16).....	23
8	HEAO with 1000 ft-lb-sec Wheel and Magnetic Control, $10^3$ a-t-m <sup>2</sup> Dipole Limits (Case #18)...	25
9	Scan Mode Control with 500 ft-lb-sec Wheel (Case #73).....	26
10	HEAO with 500 ft-lb-sec Wheel and Magnetic Control (Case #19).....	27
11	HEAO with No Wheel, All Magnetic Control (Case #17).....	29
12	Available Component Algorithm Performance (Case #118).....	32
13	Production of Spin Rate Magnetic Control Torque.....	34
14	Production of Pointing Control Torque.....	38
15	Baseline Magnetic Torquer Algorithm.....	42
16	Baseline Performance—Solar Pointing Scan Mode at Winter Solstice (Case #80).....	44
17	Scan Mode, Sun at Vernal Equinox (Case #90)....	45
18	Galactic Scan (RAN = 180°)(Case #82).....	47
19	Galactic Scan, Worst Case (RAN = 0°.....	48
20	Worst Case Declination of Scan Axis (Case #21).....	49
21	Capture from 45° Elevation Error (Case #30)....	51
22	Capture from Large Initial Scan Rate (Case #69).....	52
23	Capture from Extreme Initial Conditions (Case #95).....	53
24	Y-Pointing Mode with Wheel Modulation.....	55

LIST OF ILLUSTRATIONS (continued)

Figure	Title	Page
25	Y-Pointing Mode with Wheel Modulation (Case #79).....	57
26	Assumed Motor Torque Characteristics.....	58
27	Y-Pointing Mode with Wheel Modulation and Gravity-Gradient Compensation (Case #112).....	61
28	Z-Pointing Mode Performance with Wheel Speed Modulation.....	63
A-1	Electromagnet Design-Comparison of Materials.....	A-11
D-1	Block Diagram of the Linearized System (Scan Mode).....	D-7
D-2	Block Diagram of the Linearized System (Pointing Mode).....	D-8

LIST OF TABLES

Table	Title	Page
I	Optimal Control Cases Investigated.....	14
II	Optimal Gains for Scan Mode.....	16
III	Optimal Gains for the Pointing Mode.....	17
IV	HEAO-A Study Parameters.....	19
V	Effect of Deadband on Scan Mode Performance....	40

## ABSTRACT

Marshall Space Flight Center has undertaken a scientific satellite project named the High Energy Astronomy Observatory (HEAO). It is conceived as a very large satellite (30 ft long by 10 ft diameter) weighing about 25,000 lbs, to be launched by a Titan III rocket into a 2000 n.mile altitude orbit. It is intended to carry large radiation detector experiments for measuring X-rays, gamma rays, and cosmic rays, and lead to mapping of sources of radiation in the celestial sphere. Control of the satellite attitude in space would be achieved in part by magnetic devices interacting with the earth's magnetic field to provide control torques. Closed loop control would be used to achieve pointing accuracies of 1 degree. This report describes the synthesis and design trade-offs inherent to a closed loop magnetic control system, the selection of a baseline control system for HEAO-A and the performance of this system in both experiment scan and pointing modes.



## I SUMMARY

Computer simulations of closed loop attitude control of HEAO with only magnetic control torques indicate that the desired pointing control cannot be obtained due to large gravity-gradient disturbance torques. However, addition to the system of a modest momentum wheel of 1000 ft-lb-sec momentum provides enough gyro-stabilization to HEAO to give short-term attitude stabilization, and the magnetic torquing system can work effectively against long-term disturbances to meet the desired pointing requirements. A typical result of computer simulation of this case is shown in Figure 1. This case shows that the total error angle is maintained at less than 1 degree over a 24 hour period and probably could be maintained indefinitely.

Another satellite operating mode requires another axis to be pointed to 1 degree, and the wheel axis be maintained within  $\pm 37$  degrees of the sun-line to obtain the necessary solar array power. We have found the constant speed momentum wheel with magnetic control inadequate for this case. However, by providing variable wheel speed capability, and operating the wheel to produce control torques by wheel speed variation we have been successful in obtaining the desired control accuracy. Figure 2, shows a typical result of computer simulation of this case.

We have found that magnetic torquers can be limited to maximum dipole values of  $\pm 10^3$  ampere-turn-meter<sup>2</sup> without compromising the system performance. This has important implications on the weight and electrical power demands of the magnetic control system.

(CASE #80)

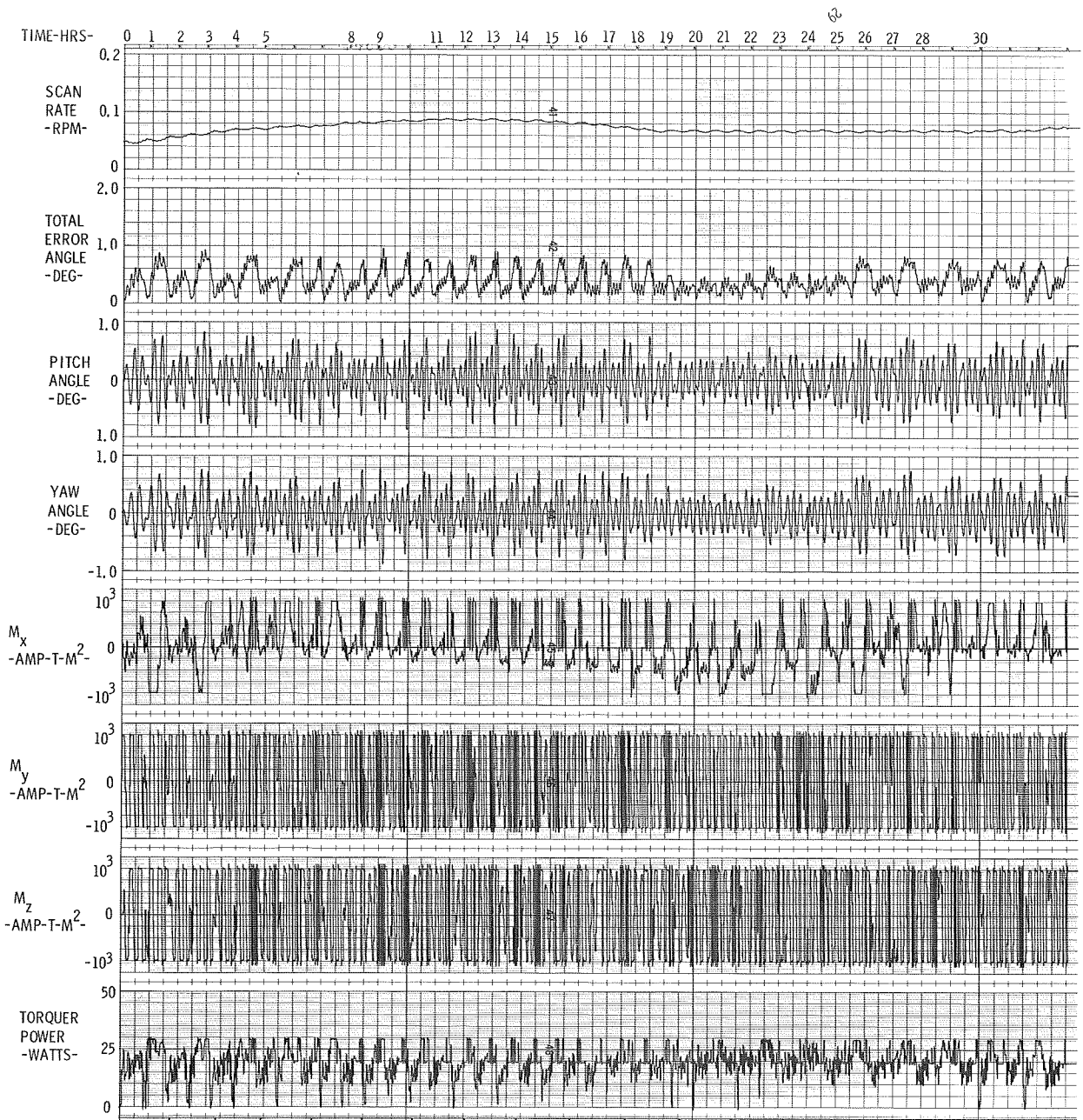


Fig. 1 SCAN MODE, SOLAR POINTING OF WINTER SOLSTICE

POINT AT RA=0°, DE=0°  
CONTROL LAW #24, ALGORITHM #2, WITH DEADBANDS  
HEAO-A RUN #79

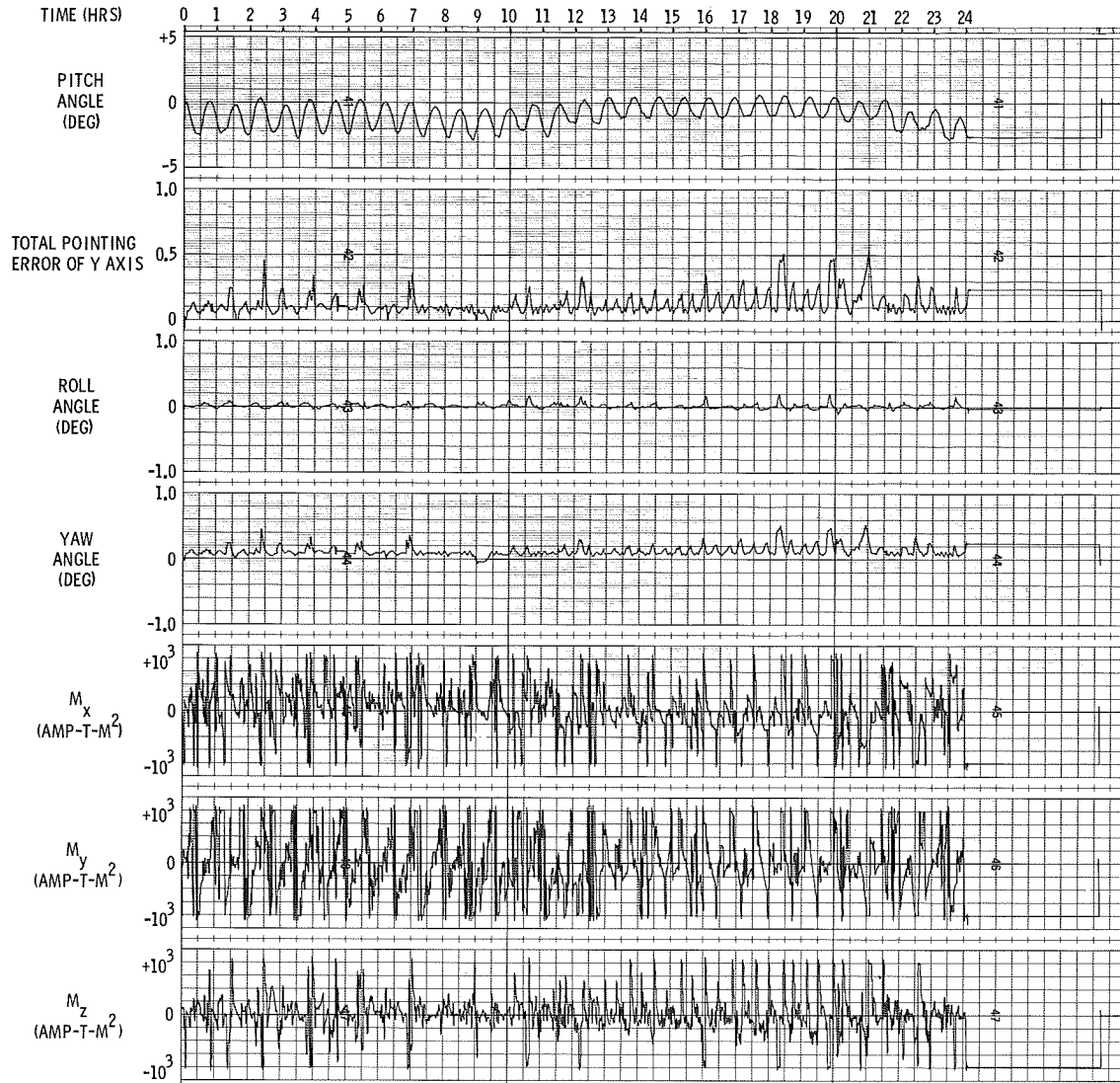


Fig. 2 Y POINTING MODE WITH WHEEL MODULATION

## II. INTRODUCTION

### A. HEAO-A Concept, Mission and Control Requirements

The High Energy Astronomy Observatory satellite is conceived as a large satellite capable of carrying large detectors or experiments into low altitude orbit for astronomical research in broad ranges of the electromagnetic and particle spectra.

The primary objective of HEAO-A will be a complete survey of the celestial sphere to locate all sources of X-rays, gamma-rays, and cosmic-rays whose radiation falls within the range of instrument sensitivities and spectral range. The secondary objective will be to study some of these sources in more detail by pointing the spacecraft for limited periods of time.

The baseline concept developed by NASA Marshall Space Flight Center for the HEAO-A satellite calls for a total payload weight of 25,000 lbs of which 14,000 lbs would be experiment equipment. It would be assembled in an octagonal cylinder 30 ft long by 9 ft across flats, and launched by a Titan III-D rocket into a circular orbit of 200 n.miles altitude and 28.5 degree inclination. A minimum orbital lifetime of one year is required. The estimated average power consumption of the satellite is 660 watts.

1  
6  
1

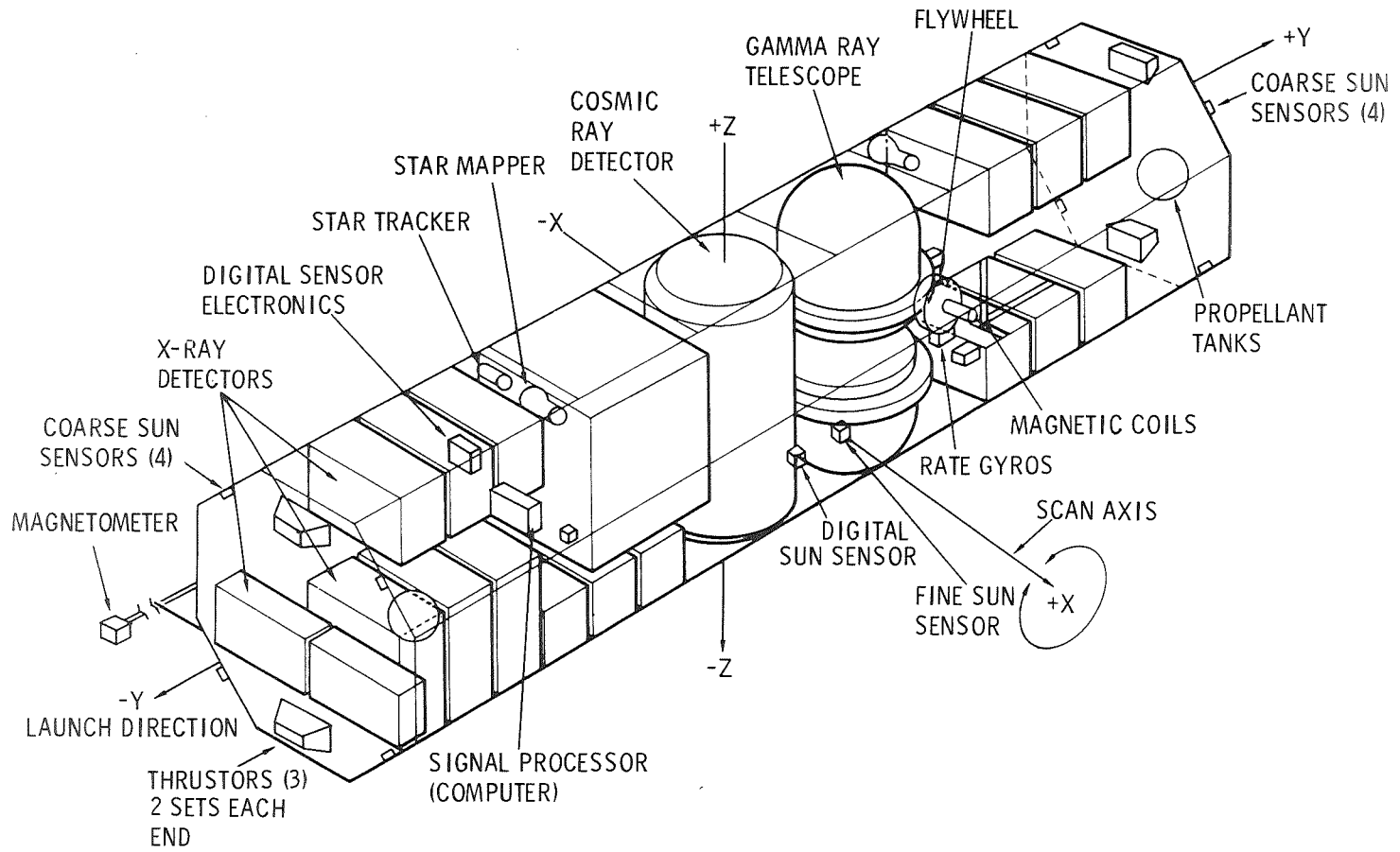


Fig. 3 HEAO COMPONENT ARRANGEMENT

Figure 3 shows the spacecraft concept with some indication of possible internal arrangement of subsystems. This figure also defines the axis system for subsequent discussion.

Solar cell arrays would be mounted on the +X rectangular face and the two adjacent faces. The cells will generate power to support the spacecraft functions. Therefore, except for limited periods of time, the spacecraft must be oriented so that the +X axis is pointed in the vicinity of the sun. There are two operating modes for the experiment which have been defined, consistent with this characteristic, the scanning mode, and the pointing mode.

### Scanning Mode

In this mode the satellite will rotate at 0.05 rpm ( $\pm 0.05$  rpm) about the X axis, with the +X axis pointed at the sun to an accuracy of 1 degree. Various experiments will detect radiation along the Y and Z axes. These axes will scan the celestial sphere as the satellite rotates and survey a region of the sky. As the sun appears to move in the celestial sphere about 1 deg/day, in about 180 days the entire celestial sphere will have been surveyed by the experiment detectors.

A variation of the scanning mode is the galactic scan mode. In this case the satellite spin axis is oriented near the galactic poles so that the experiments scan for sources in the galactic plane. The spin axis must also be within  $37^\circ$  of the sun-line to provide adequate power. Obviously this can only be done at certain times of the year when the sun approaches the galactic pole.

### Pointing Mode

In this mode one of the experiment axes (either Y or Z) will be oriented to remain fixed on some celestial sources for continuous sensing. The required alignment accuracy is  $\pm 1$  degree. At the same time the +X axis must be oriented to within some angle of the sun line ( $\sim 37$  degrees) to assure adequate power generation by the solar arrays.

A closed-loop attitude control system would be used in both modes. Sun sensors (for the scanning mode) and star sensors (for the pointing mode) would be used to provide error angles for the control system. An inertial platform or strap-down gyro system might also be used for error angle information. A gyro system would be used to sense satellite rotation rates. The angle and rate information would be used in some sort of angle or digital controller which would activate the appropriate torque generators to correct the satellite attitude and maintain it within the desired limits.

#### B. Possibility of Magnetic Control and Advantages

Various torque generators are being considered for HEAO-A, including gas jet thrusters, reaction wheels, and magnetic torquers reacting with the earth's magnetic field.

Gas jet thrusters have the advantage that the torque can be directly applied to the desired axis. Hardware and control systems using these devices have proven performance in spacecraft applications. However the gas supply is not unlimited, and eventual consumption of the supply limits the lifetime of the satellite.

Reaction wheels have proven performance but power consumption and system complexity are disadvantages.

Magnetic torquing has been used extensively in attitude control of small satellites, viz. the TIROS satellite,<sup>(1)</sup> the Direct Measurement Explorer-A,<sup>(2)</sup> the DODGE satellite,<sup>(3)</sup> and others.<sup>(4,5)</sup> It is simple in concept, and unlimited in lifetime. Power consumption can be minimized by careful design. The major limitation however is one of basic physics, namely that at any instant of time, with a given magnetic field of the earth at the satellite,  $\vec{H}$ , no control torque can be generated with a component parallel to the vector  $\vec{H}$ . This is because the torque  $\vec{T}$  produced by the interaction of a satellite magnetic dipole  $\vec{M}$  with the earth's field is given by the vector cross product.

$$\vec{T} = \vec{M} \times \vec{H}$$

Clearly the torque is perpendicular to both  $\vec{M}$  and  $\vec{H}$  and has no component parallel with  $\vec{H}$ . The dipole  $\vec{M}$  can be arbitrarily oriented in the satellite by energizing three orthogonal electromagnets or air coils, even so the resultant torque is perpendicular to  $\vec{H}$ .

Therefore when the "controller" recognizes the need for torque parallel to  $\vec{H}$  to correct some attitude error, it finds that it cannot produce the desired torque with magnetic torquers.

It is for this reason primarily, that applications of magnetic torquing has been limited to special applications where the fundamental limitation could be tolerated. One aspect of the earth's magnetic field which makes the problem tolerable is that the orientation of the field changes with time as the satellite proceeds in orbit around the earth. Therefore it may be possible to produce the desired torque if the controller can wait for the field direction to change sufficiently. This is true for all orbits, even equatorial, because of the tilt in the earth's dipole field, and also for satellites in synchronous orbit because the field direction (in inertial space) changes with a period of 24 hours.

This requirement for delay in taking corrective action forces compromise on the control performance. As a general rule precise three-axis stabilization of a spacecraft against large and arbitrary disturbances cannot be achieved with all magnetic control. However modest stabilization against small, predictable disturbances is in some cases, feasible.

It is the purpose of our study here to explore this possibility for HEAO-A. The desired orientation accuracy of the scan axis of  $\pm 1$  degree (in the scanning mode) appears challenging for magnetic control. However the satellite is large and heavy, and subjected to relatively small disturbances. This helps to ease the problem. So there is a reasonable basis for considering the feasibility of all magnetic control, at least for some phases of the mission if not all, with significant advantage to the spacecraft lifetime and complexity if it can be achieved.



### III INVESTIGATION OF PROBLEM

#### A. Purpose and Scope

The purpose of study is to provide guidelines for subsequent design of the satellite. As such our approach has been to seek and identify problem areas, explore the effects of various schemes and parameters, and in general establish a baseline approach for use in the latter stages of satellite design.

Many real and practical problems of control system design evolve from the peculiarities of the attitude sensors - their errors, noise characteristics, sampling characteristics, etc. Our focus here however is on magnetic control and its capabilities. We have therefore chosen to assume ideal characteristics for the sensor systems for the most part.

The "controller" takes sensor outputs and "computes" control action via built-in algorithms and logic, some of which may be subject to change by ground command. We have assumed idealized controller characteristics, i.e. we assume that it does exactly what we require of it.

The assumptions focus our study on the problem of magnetic torquing.

This section considers HEAO-A attitude requirements and investigates control system trade-offs and performance. The investigation includes the effects on pointing performance due to:

- (a) wheel momentum
- (b) magnetic torquer limits
- (c) control law coefficients
- (d) magnetic control algorithm
- (e) noise and deadband on attitude sensors, and
- (f) large angle and rate errors.

From this investigation a control system is synthesized which meets mission requirements using minimum sized control system elements. The performance of this baseline system is examined in detail.

## B. Design Approach for a Magnetic Control System

Synthesis of a magnetic control system is far from straightforward due to grossly non-analytic aspects of the problem. First it must be noted that inherent limitations exist in the use of magnetic torquers for three-axis attitude control. To restate the problem simply, no component of the desired torque vector can be generated which is parallel to the local magnetic field. Second, the magnetic field of the earth is quite complex and accurate performance predictions cannot be made with linear dynamical models or simplified representations of the earth's magnetic field. APL simulations employed full nonlinear equations of motion and 48 terms of a spherical harmonic expansion of the magnetic field.

The non-analytic aspects and limitations imposed by a magnetic torquing system require a trial and error design synthesis rather than a straightforward solution. There is one aspect of the problem which does lend itself, however, to exact solution and that is evaluation of the instantaneous desired torque vector needed for optimal control. Producing that torque vector magnetically is subsequently solved by trial and error techniques. The overall system design was therefore divided into two parts:

- (a) given spacecraft attitude errors and rates, determine the desired torque vector which in an optimal sense will control the pointing error with some minimum of control effort, and
- (b) given the desired torque vector and attitude of the magnetic field relative to the spacecraft generate magnetic dipole moments which will effect the desired control.

The two-step control system synthesis requires then (a) determination of optimal control law coefficients and an investigation of the effect of the assumed optimization criteria and (b) synthesis of a magnetic control algorithm and investigation of the effect of variations in its design. Coupled into the problem are effects due to wheel momentum, dipole moment limits, sensor deadband and large angular motion.

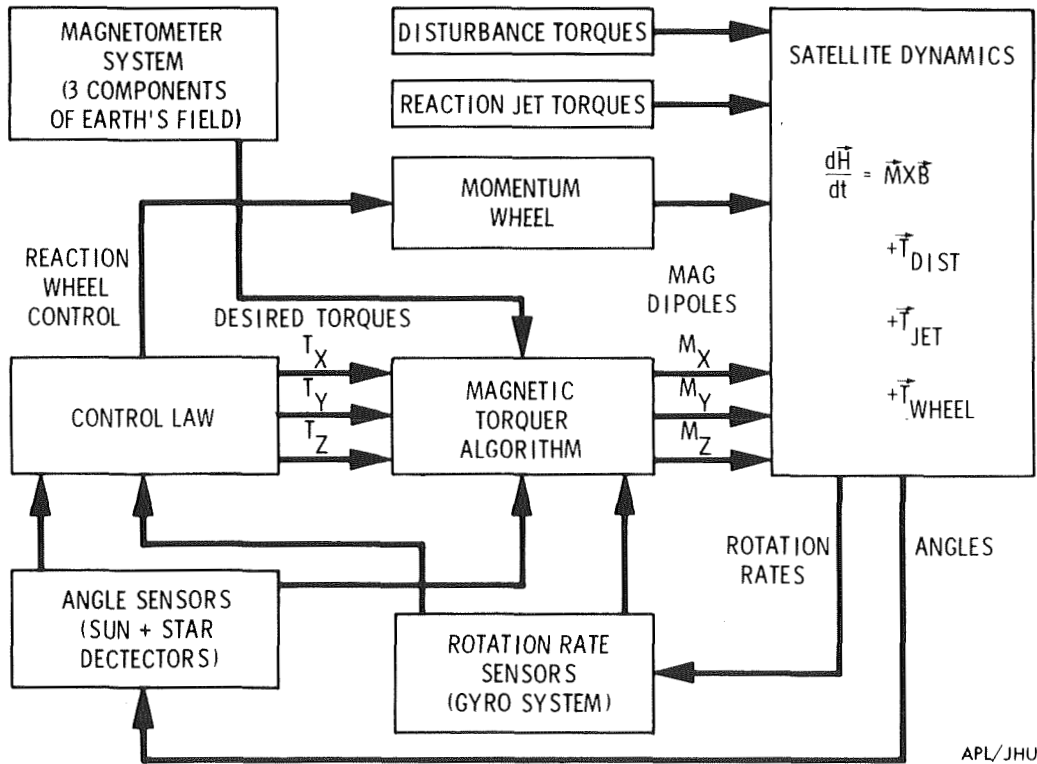


Fig. 4 HEAO-A ATTITUDE CONTROL SYSTEM CONCEPT

The complex coupling inherent to the magnetic control of HEAO-A is illustrated in the block diagram of Figure 4. A breakdown of the total magnetic control system into a control law section and torquer algorithm section enables the optimization of each on a more tractable basis.

### C. Derivation of Optimal Control Law Coefficients

This section describes the HEAO-A attitude control law designed to minimize control effort while maintaining pointing and scan rate control. The analysis is detailed in Appendix D and is based on linearized dynamical equations of motion. Output from the optimal control law is the desired control torque vector. There is no limitation of magnetic interaction imposed at this phase. It is assumed that a control torque can be obtained in any direction. Three modes of operation are studied: a scan mode, and two pointing modes.

The control system must meet certain requirements:

- (1) Given any initial error (roll spin rate, roll angle, pitch angle, or yaw angle), the system must reduce this error to a tolerable value.
- (2) Given an external disturbance on the satellite the control system must reduce the effects of this disturbance to an acceptable error.

The object of the control law is to take the measured attitude and rate errors of the satellite and, from this information, compute torques which must be applied to the satellite to minimize these errors and at the same time minimize the control effort required.

Mathematically, this objective of optimal control is to choose the control torque vector  $\bar{T}$  in such a way as to minimize the quadratic performance index

$$J = \frac{1}{2} \int_0^{\infty} \left[ (q/r)_1 y^2 + (q/r)_2 p^2 + (q/r)_3 \dot{r}_e^2 + T_x^2 + T_y^2 + T_z^2 \right] dt$$

Where:

- y = yaw angle (positive rotation about z axis)
- p = pitch angle (positive rotation about y axis)
- r = roll angle (positive rotation about x axis)
- $\dot{r}_e$  = roll rate error
- $T_x$  = control torque about the x axis.
- $T_y$  = control torque about the y axis
- $T_z$  = control torque about the z axis
- q/r = error to torque weighting ratio

For the <sup>POINTING</sup> scan modes,  $\dot{r}$  is replaced by the r, the roll angle.

The optimal solution for the control torque is derived by computer solution. Table I lists the set of cases investigated for HEAO-A. In Table I

- $H_x$  = momentum of the x axis momentum wheel
- $\dot{r}_o$  = nominal roll rate = constant

Table I OPTIMAL CONTROL CASES INVESTIGATED

Mode	Control Law No.	q/r weighting ratio	$H_x$	$\dot{r}_o$
			-ft-lb-sec-	-rpm-
Scan Mode	14	100(p,y),10( $\dot{r}$ )	1000	.05
	15	100(p,y),10( $\dot{r}$ )	500	.05
	16	100(p,y),10( $\dot{r}$ )	0	.05
	17	100(p,y),10( $\dot{r}$ )	0	0
	18	100(p,y),10( $\dot{r}$ )	0	.10
	19	100(p,y),10( $\dot{r}$ )	2000	.05
	20	600(p,y),10( $\dot{r}$ )	0	.05
	21	600(p,y),10( $\dot{r}$ )	0	.10
	22	600(p,y),10( $\dot{r}$ )	0	0
Pointing				
Mode I	23	100(r,y),1(p)	0	0
(Y pointing)	24	100(r,y),1(p)	1000	0
	25	100(r,y),1(p)	500	0
Pointing				
Mode II	26	100(r,p),1(y)	0	0
(Z pointing)	27	100(r,p),1(y)	1000	0
	28	100(r,p),1(y)	500	0

The general form of the optimal control torque is given by a linear combination of errors and rates, viz.,

$$T_x = -k_{11}y - k_{12}\dot{y} - k_{13}p - k_{14}\dot{p} - k_{15}r - k_{16}(\dot{r} - \dot{r}_{\text{desired}})$$

$$T_y = -k_{21}y - k_{22}\dot{y} - k_{23}p - k_{24}\dot{p} - k_{25}r - k_{26}\dot{r}$$

$$T_z = -k_{31}y - k_{32}\dot{y} - k_{33}p - k_{34}\dot{p} - k_{35}r - k_{36}\dot{r}$$

Tables II and III list the coefficients  $k_{ij}$  for each of the cases listed in Table I. All coefficients are based on the moments of inertia

$$\begin{aligned} I_x &= 5.0 \times 10^4 \text{ kg-m}^2 \quad (36,870 \text{ slug-ft}^2) \\ I_y &= 5.4 \times 10^3 \text{ kg-m}^2 \quad (3982. \text{ slug-ft}^2) \\ I_z &= 4.8 \times 10^4 \text{ kg-m}^2 \quad (35400 \text{ slug-ft}^2) \end{aligned}$$

Several of the control coefficients are identically zero, namely

$$\left. \begin{array}{cccc} k_{11} & k_{12} & k_{13} & k_{14} \\ k_{25} & k_{26} & k_{35} & k_{36} \end{array} \right\} = 0$$

For the scan mode  $k_{15}$  is zero since roll angle is not an attitude error parameter. Tables II and III list all non-zero coefficients. Units for the coefficients are in the MKS system where the torques computed are in newton-meters, angles expressed in radians and rates expressed in radians/second.

TABLE II

## OPTIMAL GAINS FOR SCAN MODE

Control Case #	$\dot{i}_0$ -rpm-	$H_x$ -ft-lb-sec	$q/r$	(N-M <sup>2</sup> /RAD N-M <sup>2</sup> /RAD/SEC) OPTIMAL GAINS							$k_{36}$	
				$k_{21}$	$k_{22}$	$k_{23}$	$k_{24}$	$k_{31}$	$k_{32}$	$k_{33}$		$k_{34}$
14	.05	1000	100	9.740	.03699	2.264	156.5	2.264	466.5	-9.740	.004163	3.14
15	.05	500	100	7.904	.1291	6.126	257.4	6.125	767.4	-7.904	.01452	3.14
16	.05	0	100	-.2722	-.008142	9.996	328.7	9.996	980.4	.2722	-.0009150	3.14
17	0	0	100	0.0	0.0	10.0	328.8	9.999	980.6	0.0	0.0	3.14
18	.10	0	100	-.5441	-.01626	9.985	328.6	9.985	979.8	.5442	-.001828	3.14
19	.05	2000	100	9.982	.004753	.5868	79.66	.5868	237.5	-9.982	.0005308	3.14
20	.05	0	6000	-.7578	-.009609	77.46	915.1	77.46	2729.0	.7578	-.001079	3.14
21	.10	0	6000	-1.516	-.01899	77.45	915.0	77.45	2728.8	1.516	-.002135	3.14
22	0	0	6000	0.0	0.0	77.46	915.1	77.46	2729.1	0.0	0.0	3.14

\* It is noted that coefficient  $k_{36}$  is completely independent of all other elements and is a function only of the weighting ratio for control about the X (roll) axis. In actual control simulations  $k_{36}$  was varied to determine optimal control with a magnetic system. The value suggested on this basis was 500.



TABLE III  
OPTIMAL GAINS FOR THE POINTING MODE

MODE	CASE #	$\dot{i}_o$ (rpm)	$H_x$ ft-lb- sec	$q/x$	OPTIMAL GAINS										
					$k_{21}$	$k_{22}$	$k_{23}$	$k_{24}$	$k_{31}$	$k_{32}$	$k_{33}$	$k_{34}$	$k_{35}$	$k_{36}$	
II (Y)	1	0	0	100	0.0	0.0	.99995	103.97	9.9993	980.55	0.0	0.0	9.9993	<del>k<sub>35</sub></del>	<del>k<sub>36</sub></del>
	2	0	1000	100	9.9834	18.166	.057402	78.514	.57511	75.173	- .99665	2.0425	10.0	10.0	1000.0
	3	0	500	100	9.7846	117.23	.20634	141.28	2.0644	160.05	- .97805	13.181	10.0	10.0	1000.0
III (Z)	1	0	0	100	0.0	0.0	10.0	328.8	.99994	310.07	0.0	0.0	10.0	10.0	1000.0
	2	0	1000	100	.94391	-62.807	3.0234	115.99	.29888	441.91	-9.5319	-7.0616	10.0	10.0	1000.0
	3	0	500	100	.65427	-231.14	7.5607	213.93	.75574	577.05	-6.5448	-25.988	10.0	10.0	1000.0



## D. Magnetic Control System Synthesis and Performance

### 1. Fixed parameters for HEAO-A simulations

Section C develops the optimal control law for HEAO-A which minimizes some measure of the squares of the error angles and squares of the control torques. A flight system would include a control law section (as shown in Figure 4) which continuously (or on a sampled data bases) generates the three components of the desired torque vector.

It remains then to synthesize a magnetic control system which best generates this desired torque vector. Evaluation of this control system is strongly dependent on specific orbit parameters, modelling of earth's magnetic field, and orientation of the scan axis. A large number of exact computer simulations are thus required to establish attitude performance.

Subsequent sections discuss the effects on attitude behavior due to control system parameters as based on digital computer simulations. Table IV lists those parameters held constant throughout all simulations.

### 2. Effects due to Wheel Momentum, Weighting Ratio and Dipole Limits

The most critical parameter in the HEAO-A system is the wheel momentum. It is desirable to determine the minimum wheel momentum necessary to achieve pointing control. Investigation of the effect on performance due to wheel momentum is closely coupled to the control law coefficients and limits on dipole moments. The effect of large wheel momentum is to reduce motion of the pointing axis so that magnetic control is more easily accomplished. This means that the control torques and thus dipole moment size can be reduced and also that magnetic control effort can be delayed until the local field vector is in a more favorable orientation.

For smaller values of wheel momentum greater magnetic control action is required to maintain pointing control and action must be taken almost continuously. This need for increased control action requires greater dipole limits, larger

Table IV  
HEAO-A Study Parameters

Satellite Moments of Inertia

$$I_x = 36,920 \text{ slug-ft}^2$$

$$I_y = 3,992 \text{ slug-ft}^2$$

$$I_z = 35,187 \text{ slug-ft}^2$$

Flywheel Momentum 0 to 2000 ft-lb-sec

Orbit

Altitude 200 n.miles

Inclination 28.5 deg

Eccentricity 0

Rt. Ascension of Node 0 deg or 180 deg.

Earth's Magnetic Field 48 term expansion

Control Modes

Celestial Scan (Solar Pointing to  $\pm 1$  deg)

Galactic Scan (Galactic pole pointing to  $\pm 1$  deg)

Pointing Mode (Y axis to  $\pm 1$  deg, X axis to  $\pm 37$  deg of sun)

control law coefficients, and places more demand on the magnetic control algorithms to produce the best control for arbitrary orientations of the local magnetic field.

Increasing dipole limits does not in itself immediately produce better magnetic control. What it does is to allow the magnetic torque vector to increase in magnitude and perhaps allow the magnetic torque vector to more closely align with an intended torque vector.

A second ingredient needed for increased magnetic interaction is increased weighting ratio. The weighting ratio (called  $q/r$  in Section II, C.) controls the degree of importance attached to angular error versus torque magnitude in the optimization integral. Increasing the weighting ratio places more emphasis on reducing the pointing error and calls for increased torques from the control law to do so. Generally it is necessary to increase the limits on dipole moment when the weighting ratio is increased. If not, the increased demand for control action is not generated by the torquers.

The specific values of wheel momentum investigated were 2000, 1000, 500, and 0 ft-lb-sec. The pointing and scan rate control performance as effected by weighting ratio and dipole limits on these wheel momenta is presented in the following sections.

a. 2000 ft-lb-sec wheel

For the 2000 ft-lb-sec flywheel HEAO-A run numbers 14 and 16, shown in Figures 5 through 7, are representative of scan mode performance. Run #14 has no limit on dipole moment; run #16 has  $10^3$  amp-turn- $m^2$  limits. For both runs the scan axis pointed at the sun at winter solstice and the weighting ratio was 100/1. In run #16, where the dipole moments were limited, pointing error peaks were about  $0.6^\circ$  and spin rate variations (from 0.05 rpm) were 0.025 rpm. Using smaller weighting ratio and further limiting the dipole moment size would increase the pointing and scan rate errors. The  $10^3$  amp-turn- $m^2$  design for a 2000 ft-lb-sec wheel appears to have considerable margin.

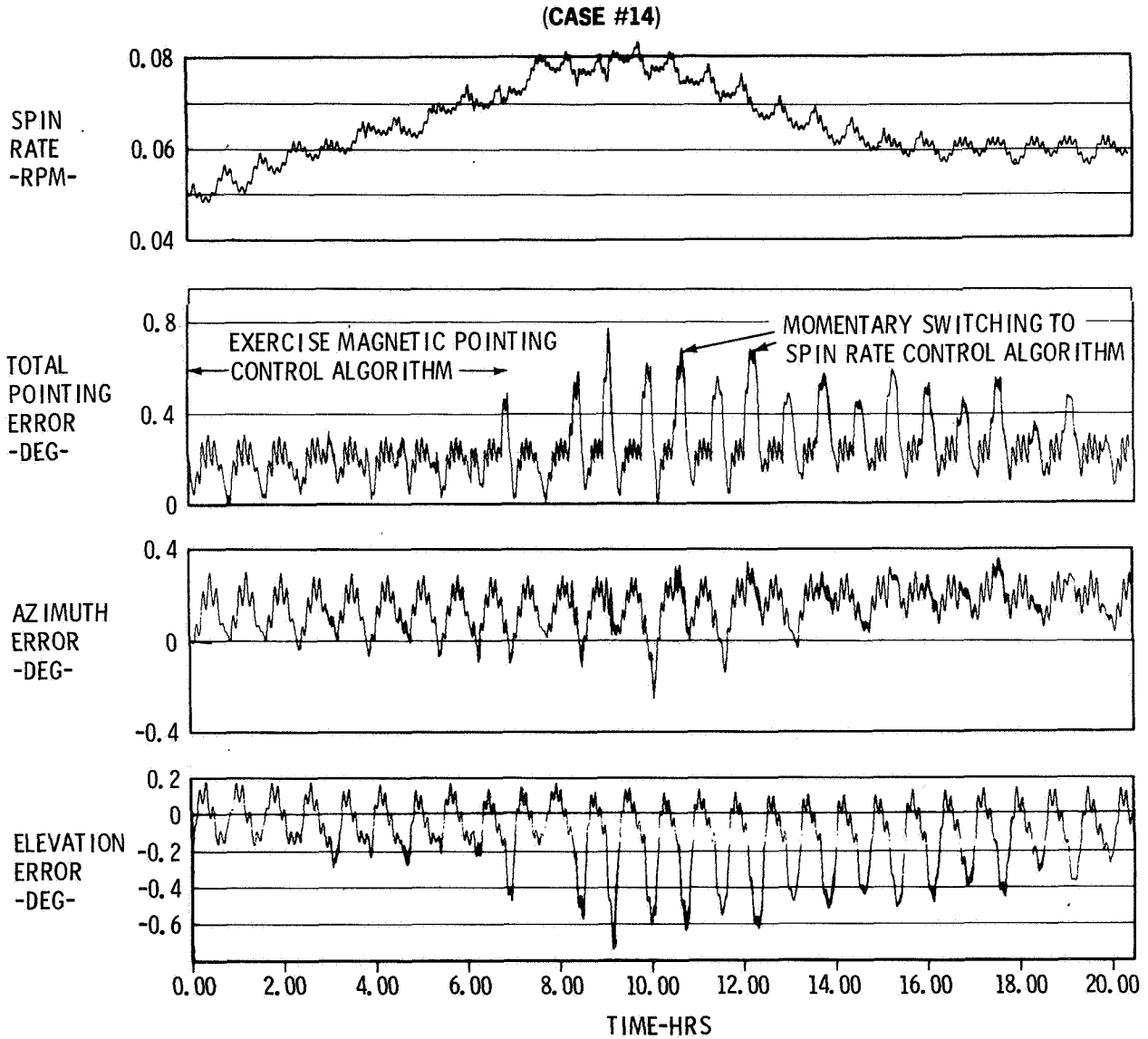


Fig. 5 HEAO WITH 2000 FT-LB-SEC WHEEL AND MAGNETIC CONTROL

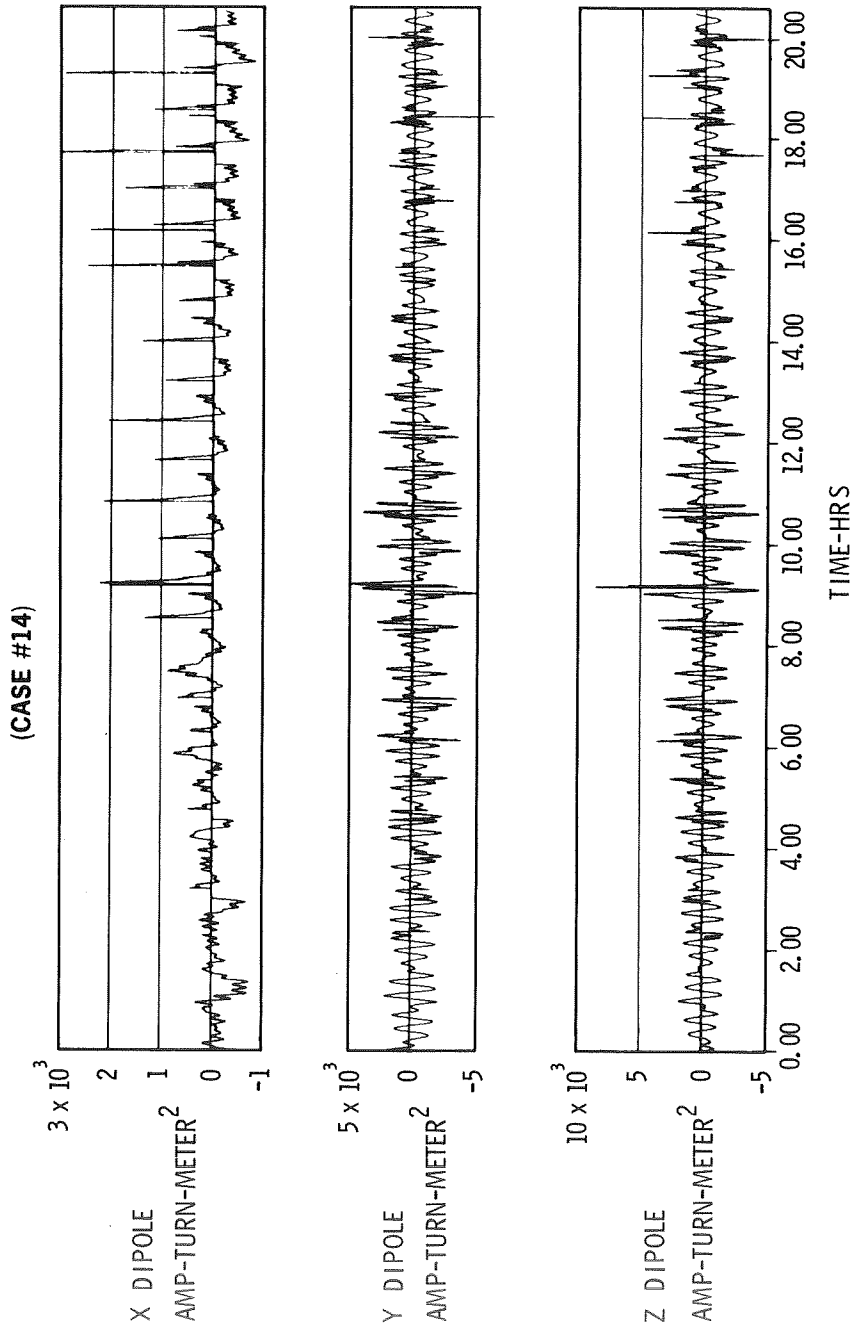
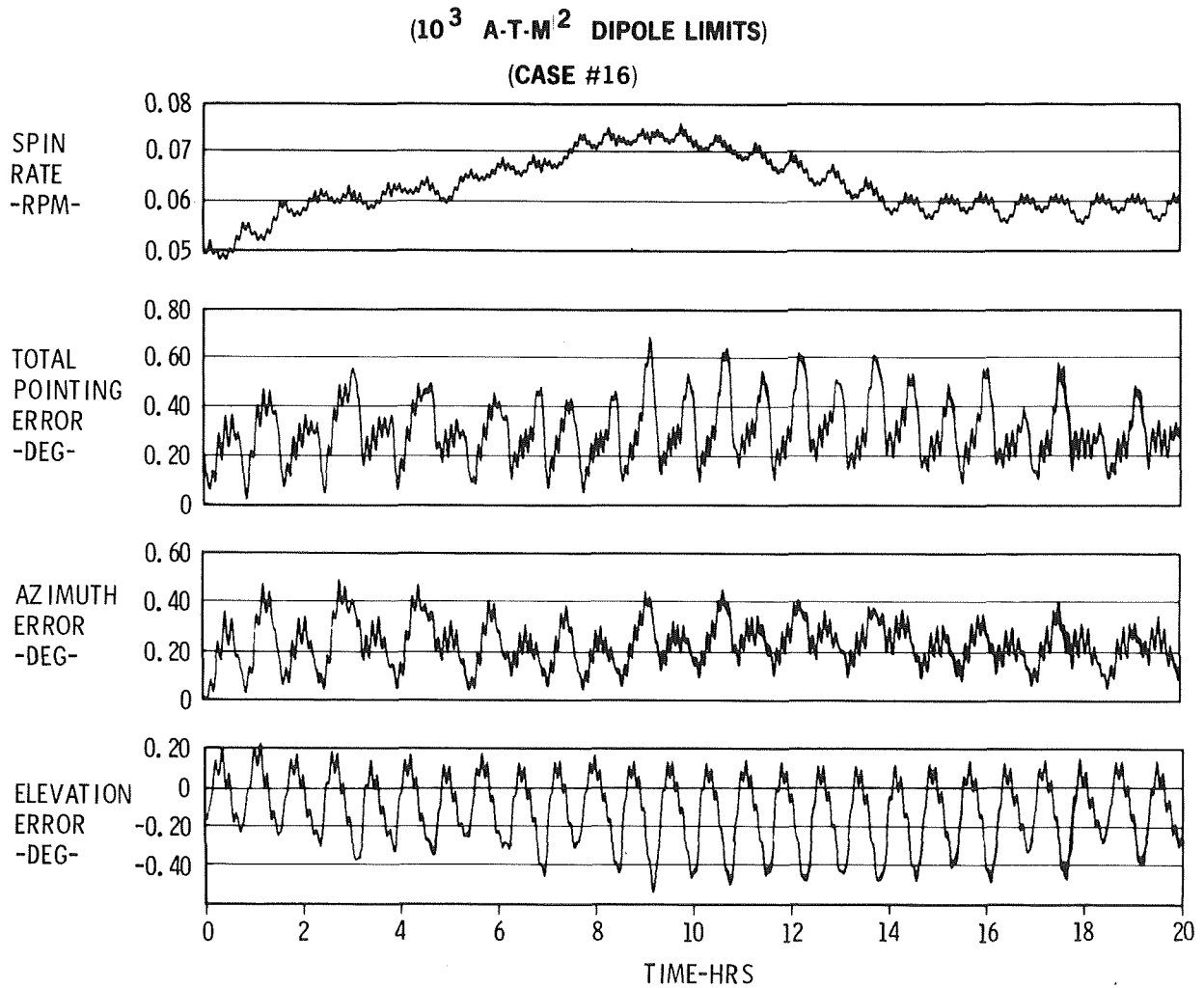


Fig. 6 MAGNETIC CONTROL DIPOLE MOMENTS FOR HEAD WITH 2000 FT.-LB-SEC WHEEL



**Fig. 7 HEAO WITH 2000 FT-LB-SEC WHEEL AND MAGNETIC CONTROL**

b. 1000 ft-lb-sec Wheel

HEAO-A run #18 (Figure 8) is representative of the pointing and scan rate control performance using a 1000 ft-lb-sec flywheel. The dipole limits were  $10^3$  amp-turn- $m^2$  and weighting ratio 100/1. During a 24 hour period the scan rate variation was below .05 rpm and peak pointing errors about  $0.9^\circ$ . Increasing the dipole moment limits alone would not improve pointing performance as most of the control actions call for dipoles of  $10^3$  or less. Pointing and scan rate performance could be improved by both increasing the weighting ratio (results in greater torque demand) and increasing the dipole moment limits. It was felt that the selection of 100/1 weighting ratio and  $10^3$  dipole limits represents a good compromise for a magnetic control design with a 1000 ft-lb-sec flywheel.

c. 500 ft-lb-sec Wheel

Current APL experience with HEAO-A simulations did not find satisfactory pointing and scan rate control using a 500 ft-lb-sec flywheel. HEAO-A run #73 (Figure 9) is representative performance. Pointing error peaks were generally close to  $1.0^\circ$  and occasionally greater. Scan rate exceeded 0.12 rpm. Dipole moment limits were  $10^3$  amp-turn- $m^2$  and weighting ratio was 100/1. Variation in the magnetic control algorithm succeeded in containing the scan rate to less than 0.09 rpm but pointing error peaks increased to  $1.5^\circ$  as shown in Figure 10.

Indicated in Figure 9 is the total torquer power in watts. This function is based on an assumed specific design for the torquers based on electromagnet and air coil design considerations discussed in Appendix A. The design assumed for HEAO-A consists of:

<u>Axis</u>	<u>Type</u>	<u>Weight lbs</u>	<u>Power* watts</u>
X	Coil	17.2	10
Y	Electromagnet	19.2	10
Z	Coil	17.2	10

\* The power level is that required to produce  $10^3$  amp-turn- $m^2$  of magnetic moment.

( $10^3$  A-T-M<sup>2</sup> DIPOLE LIMITS) CASE#18

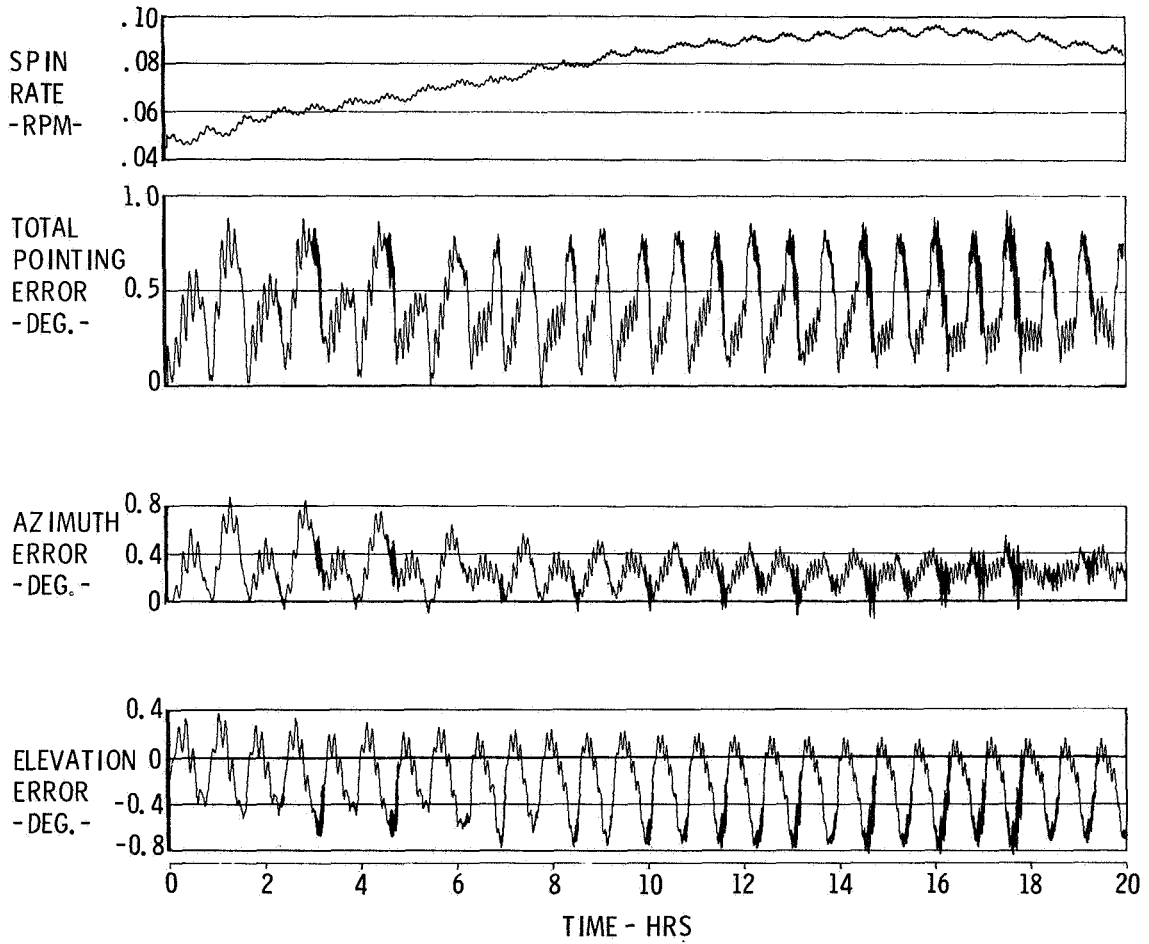


Fig. 8 HEAO WITH 1000 FT-LB-SEC WHEEL AND MAGNETIC CONTROL



CONTROL LAW #15, ALGORITHM #2, NO DEADBAND  
HEAO-A RUN #73

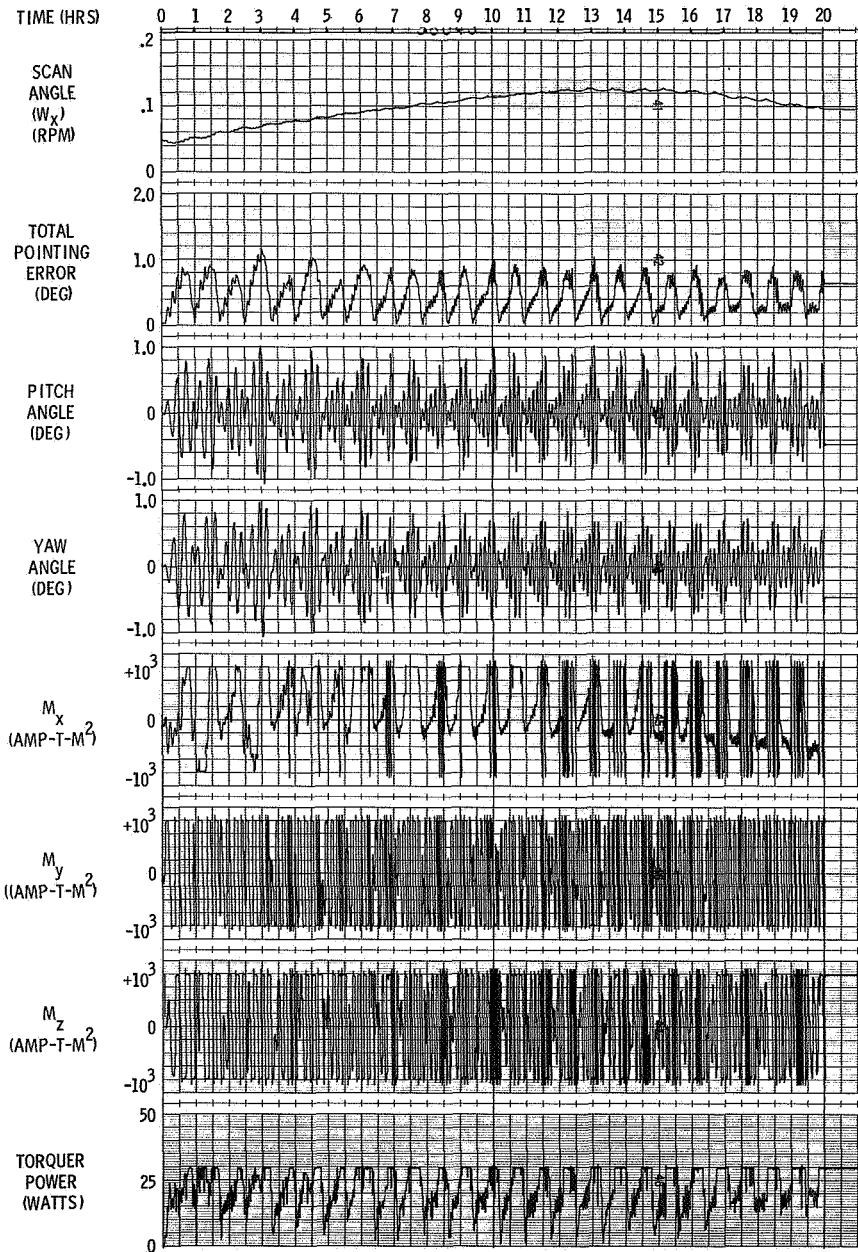


Fig. 9 SCAN MODE CONTROL WITH 500 FT-LB-SEC WHEEL

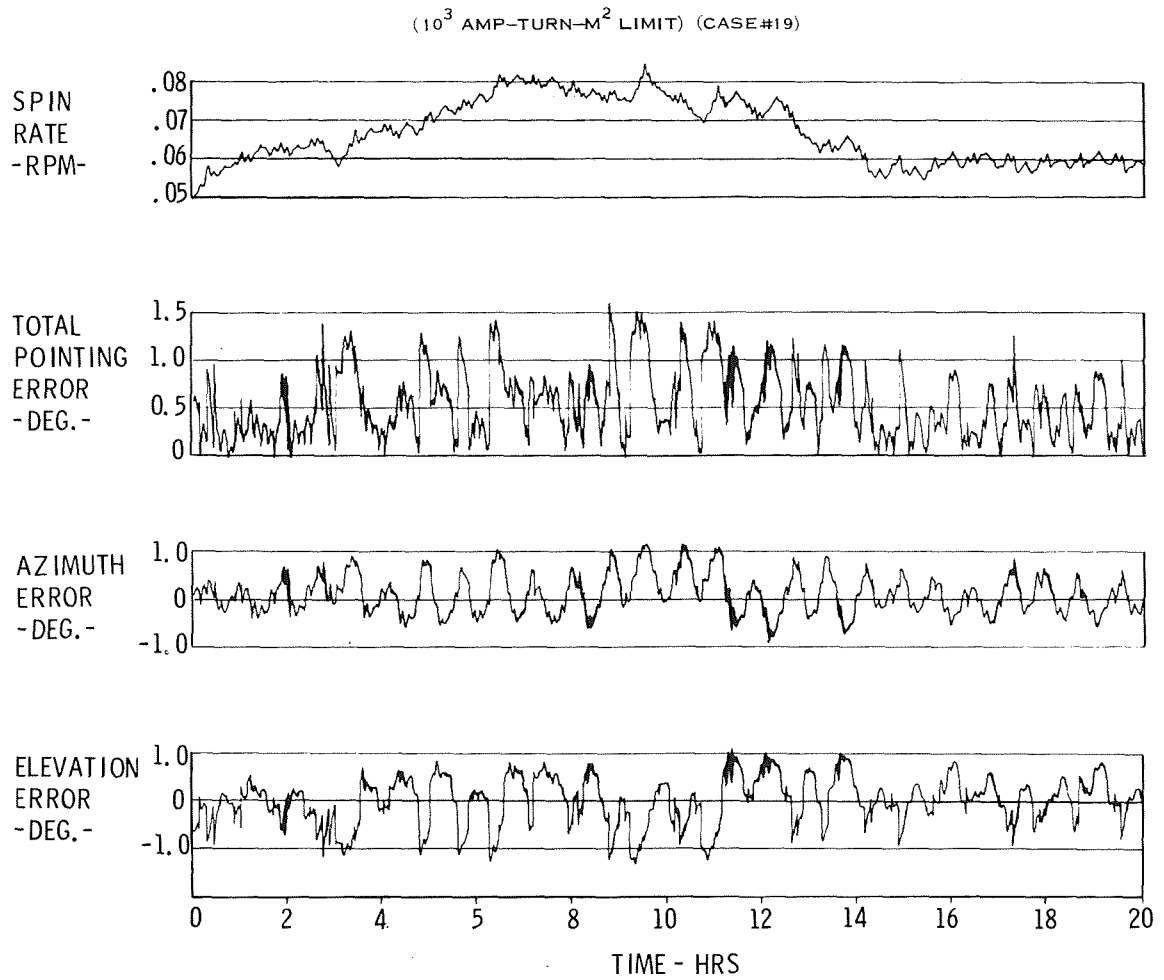


Fig. 10 HEAO WITH 500 FT-LB-SEC WHEEL AND MAGNETIC CONTROL

Although the dipole moment is proportional to the torquer current and the power dissipated is proportional to current squared, the total power drawn from a constant voltage source is linearly related to current. Thus the power function presented in the performance figures can be expressed by

$$\text{Power} = (M_x + M_y + M_z)/100. \text{ watts}$$

where

$M_{x,y,z}$  are dipole levels in amp-turn-m<sup>2</sup> units.

d. Zero Momentum Wheel

Numerous attempts were made to achieve some form of scan rate and pointing stability using no flywheel. HEAO-A run #17 (Figure 11) is perhaps characteristic of these attempts. The weighting ratio was 6000/1 and no limit imposed on dipole moments. The type of algorithm used is most critical for all magnetic control. The type found to achieve the best control for other flywheel values was employed here. In addition, the control law coefficients which were sensitive to scan rate were continuously evaluated. This provided a form of optimal control over a broad range of scan rates. It is noted that when a flywheel is used, the sensitivity of control law coefficients to scan rate is significantly reduced.

In the HEAO-A run #17, the magnetic control algorithm maintained pointing control to roughly 0.8° but lost scan rate control. The scan rate was 0.15 rpm after 20 hours simulation and increasing. A change in magnetic control algorithm might improve scan rate control but probably at the expense of losing pointing control. In summary, no successful combination of control law coefficients or control algorithms were found which provided for scan rate and pointing control with no flywheel assist.

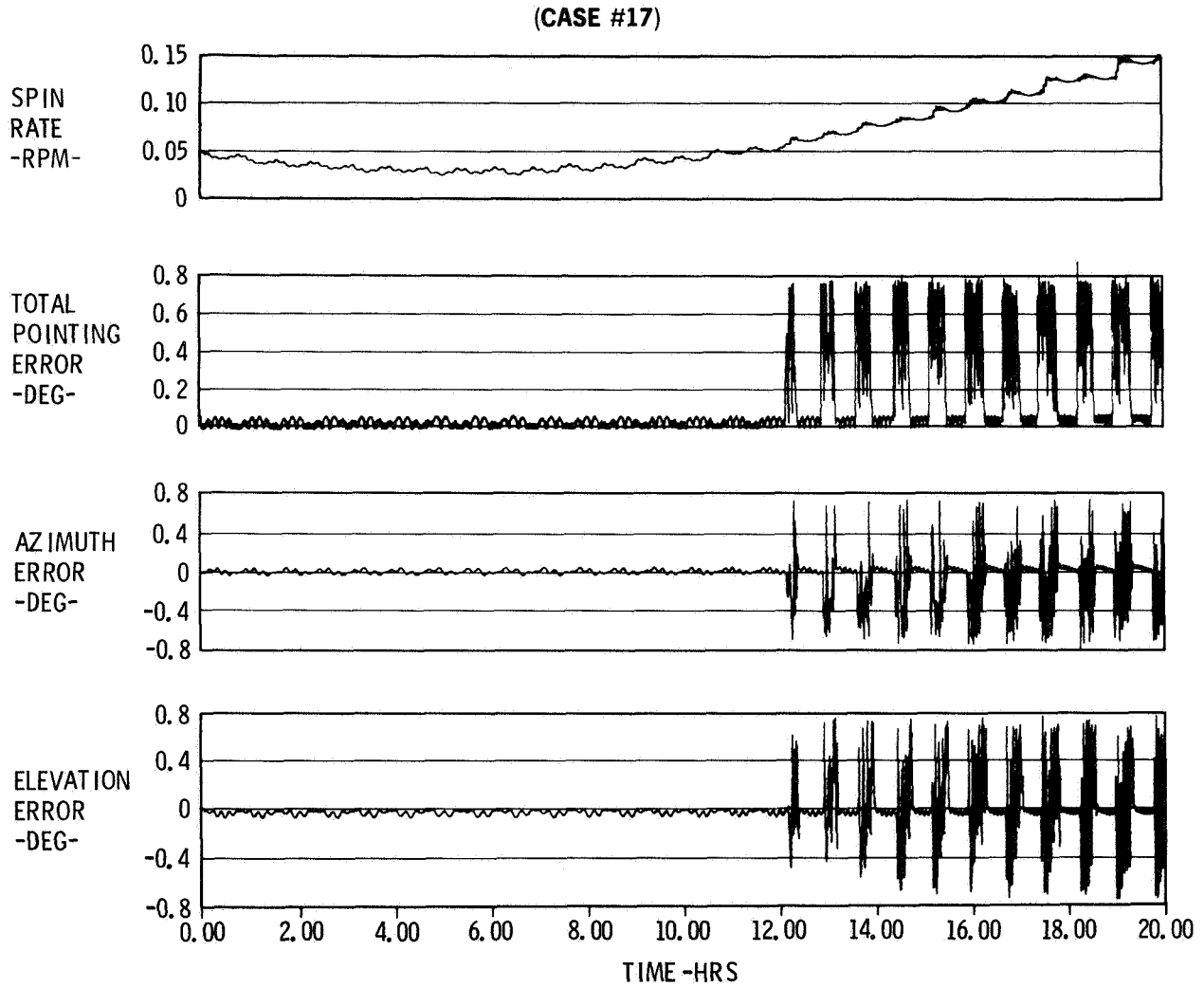


Fig. 11 HEAO WITH NO WHEEL, ALL MAGNETIC CONTROL

### 3. Magnetic Control Algorithms

The most intriguing aspect of the HEAO-A problem was the investigation of algorithms to achieve magnetic control. It is the algorithm which determines the dipole moment vector to be generated in an attempt to produce the desired torque vector. The algorithm makes its determination of dipole moment based on the orientation of the local magnetic field, the desired torque vector as computed from the optimal control law, and the attitude errors and rates. In this section various types of magnetic control algorithms are discussed and the type used to achieve HEAO-A stabilization explained.

#### a. Available Component Algorithm

This algorithm, although not found useful for HEAO-A stabilization, is presented since it is perhaps the most obvious. A dipole moment  $\vec{M}$  is computed according to the relation

$$\vec{M} = (\vec{H} \times \vec{T}_{des})/H^2 \quad (1)$$

where

$$\begin{aligned} \vec{T}_{des} &= \text{desired torque vector} \\ \vec{H} &= \text{earth's magnetic field vector} \end{aligned}$$

The dipole moment generated is normal to  $\vec{H}$  for conservation of effort. (It is noted that only that component of  $\vec{M}$  which is normal to  $\vec{H}$  has any effect in producing torque.) The torque produced by this dipole is

$$\vec{T} = \vec{M} \times \vec{H} = (\vec{H} \times \vec{T}_{des} \times \vec{H})/H^2$$

and is seen to be the component of  $\vec{T}_{des}$  which is normal to  $\vec{H}$  and in the plane containing  $\vec{T}_{des}$  and  $\vec{H}$ . The algorithm, then, produces that component of the desired torque vector which is able to be produced as governed by the orientation of the local magnetic field.

Specifically, the components of the torque vector produced are:

$$T_i = T_{i\text{-desired}} - (\vec{H} \cdot \vec{T}_{des})H_i/H^2 \quad (i = x, y, z)$$

In effect, the components of the desired torque vector are rarely produced, but are altered by a proportionate amount of the component of  $\vec{T}_{des}$  parallel to  $\vec{H}$ .

The disadvantage of this algorithm is that the torque generated is overly dependent on the orientation of  $\vec{H}$ . Suppose for example, it is essential to produce some measure of the pointing control components of  $\vec{T}_{des}$ , else pointing control be lost. This algorithm generally will not achieve that desired goal.

This lack of performance is indicated in run #118 (Figure 12) in which pointing, controlled easily by other algorithms, is lost by the "available component" algorithm. The pointing errors exceed  $1.4^\circ$ .

b. Single Component Algorithm

To clarify the major deficiency of the "available component" algorithm the "single component" algorithm is presented. Owing to one of its advantages, the "single component" algorithm was used in conjunction with other algorithms to achieve HEAO-A stabilization.

The essence of this algorithm is that one of the components of  $\vec{T}_{des}$  (say  $T_x$ ,  $T_y$ , or  $T_z$ ) is selected to be the most important component to be produced at any given time. Suppose, for example, that the scan rate is above the desired limit while pointing is under control. Then it would be desirable to generate as much of the scan rate component of  $\vec{T}_{des}$  as possible.

It must be noted that this aspect of producing, in full magnitude, a particular component of the desired torque vector can be achieved by the "available component" algorithm by amplifying the dipole moment vector given in Equation (1). To produce the  $i^{th}$  component of the desired torque vector identically the amplification factor is:

$$T_{i-des} \left[ T_{i-des} - H_i (\vec{H} \cdot \vec{T}) / H^2 \right]$$

(CASE #118)

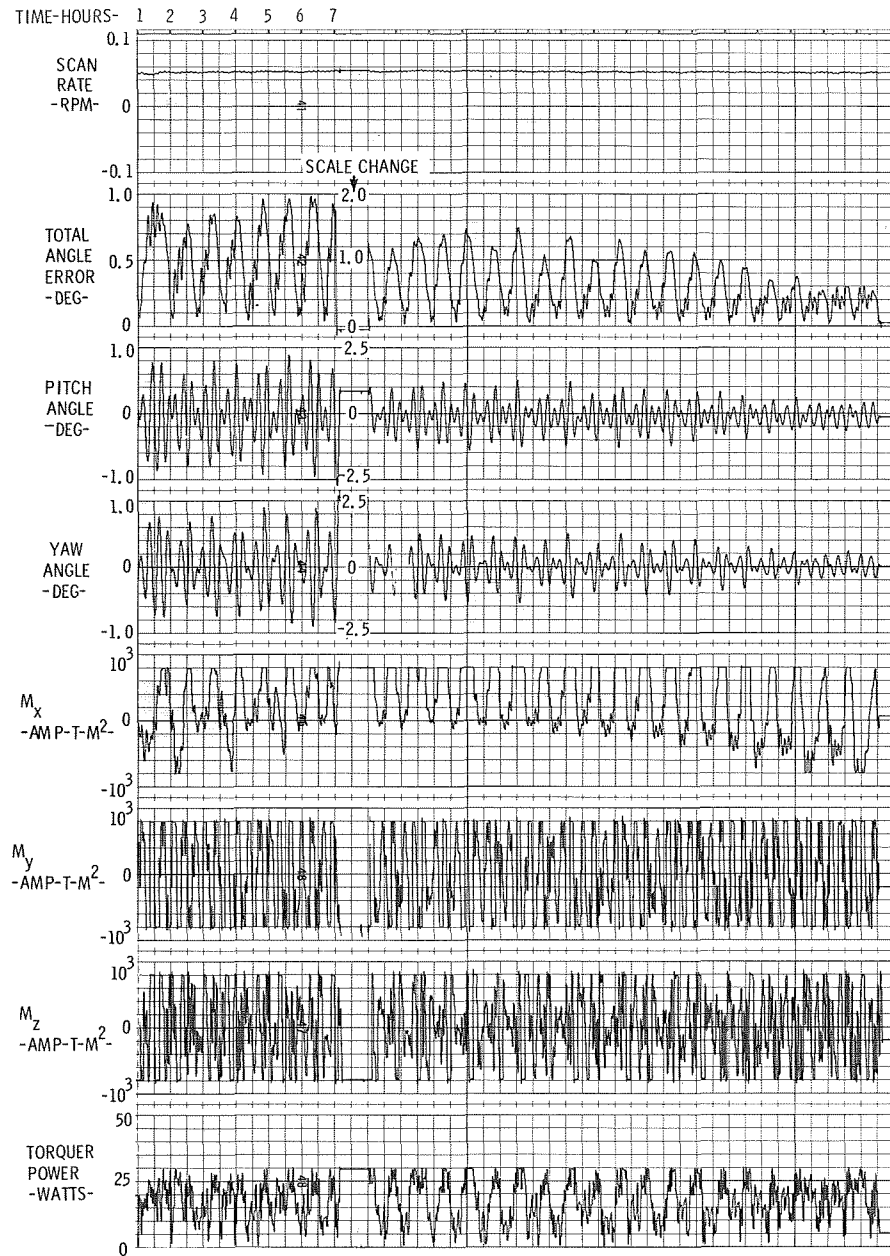


Fig. 12 AVAILABLE COMPONENT ALGORITHM PERFORMANCE

The disadvantage to this amplification is that the other two components of torque may be significantly larger than wanted.

A more straightforward technique of producing a single component of the desired torque vector is one that has been used in magnetic spin rate control of numerous APL attitude control system designs. If it is the X-axis component of desired torque that is to be produced, a dipole moment is generated in the satellite y-z plane which is normal to the y-z component of the local magnetic field. Figure 13 illustrates these vector properties. The dipole moment components for this x-axis component of  $T_{des}$  are:

$$\begin{aligned} M_x &= 0 \\ M_y &= kH_z \\ M_z &= -kH_y \\ \text{where } k &= T_{x-des} / (H_y^2 + H_z^2) \end{aligned}$$

Several disadvantages to this algorithm are that (1) owing to the division by  $\bar{H}_y^2 + \bar{H}_z^2$  ( $= \bar{H}_{yz}$ ) the dipole moment called for may be excessive if  $\bar{H}_{yz}$  is small, and (2) the torque components  $\bar{T}_y$  and  $\bar{T}_z$  produced are not functionally related to their respective desired torque components. This "single component" algorithm, however, has been used with success in achieving HEAO-A spin rate control. For total control, it must be used in conjunction with other algorithms (to be discussed) and used only under certain conditions. Suggested conditions include:

- (a) when spin rate error has exceeded some deadband, say  $\pm 0.2$  rpm.
- (b) when the magnetic field is oriented near the spacecraft y-z plane, say within  $35^\circ$ , and
- (c) only when the pointing axis is well controlled, say better than  $0.75^\circ$ .



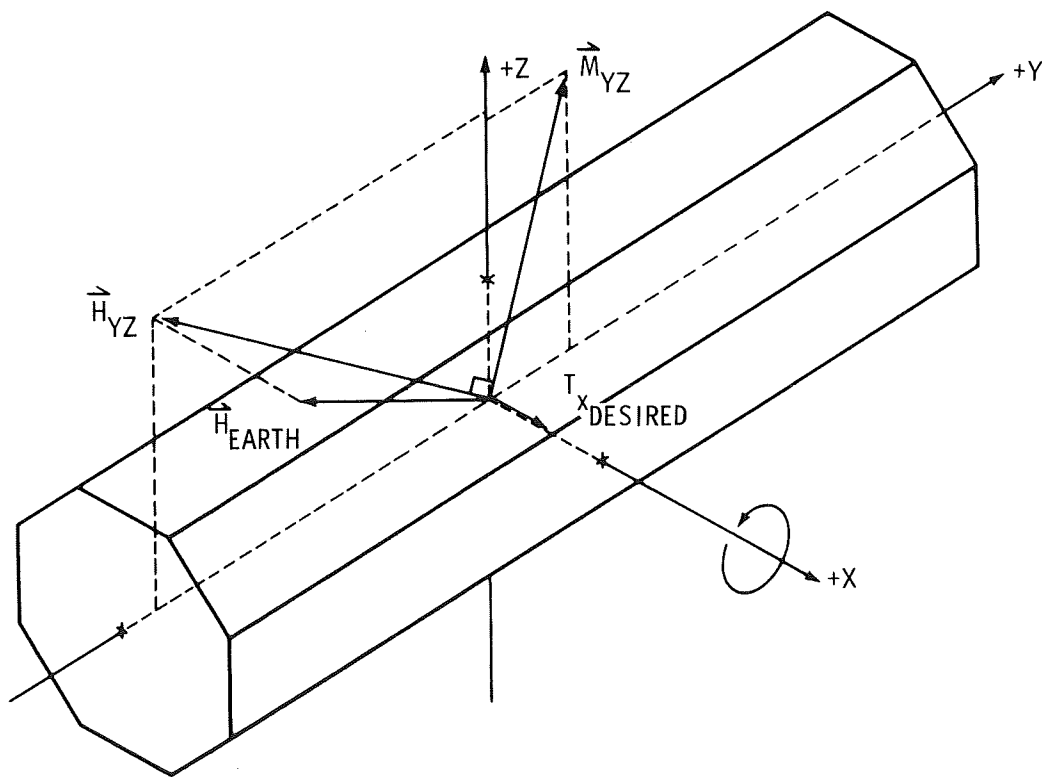


Fig. 13 PRODUCTION OF SPIN RATE MAGNETIC CONTROL TORQUE

c. Two Component Algorithm

The "two component" algorithm presented in this section has been employed extensively to achieve HEAO-A pointing control. It effects the production (subject to dipole moment limits) of two components of the desired torque vector. For the X-axis scan mode, these components have been the y and z components as they are the components, that govern pointing of the scan axis.

To produce the desired torque components, a dipole moment  $\bar{M}$  is generated whose components are determined by simultaneous solution of three of the following four equations

(a) the three component equations of

$$\bar{M} \times \bar{H} = \bar{T}_{des}$$

$$M_y H_z - M_z H_y = T_{x-des} \quad (2-a)$$

$$M_z H_x - M_x H_z = T_{y-des} \quad (2-b)$$

$$M_x H_y - M_y H_x = T_{z-des} \quad (2-c)$$

and (b) a relation insuring that  $\bar{M}$  is normal to  $\bar{H}$

$$(\bar{M} \cdot \bar{H} = 0) \quad (3)$$

$$M_x H_x + M_y H_y + M_z H_z = 0$$

To produce the desired y and z components of  $T_{des}$  Eqs 2-b, 2-c and 3 are solved simultaneously. To produce the x and z desired torque components Eqs(2-a),(2-c) and(3) are solved simultaneously. Similar procedure is used for generating the x and y desired torque components. For completeness, the solutions for the components of  $\bar{M}$  for each case follow:

1) X-Y Desired Components of Torque

$$M_x = \frac{-T_{x-des}(H_x H_y) - T_{y-des}(H_y^2 + H_z^2)}{H_z H^2}$$

$$M_y = \frac{T_{x-des}(H_x^2 + H_z^2) + T_{y-des}(H_x H_y)}{H_z H^2}$$

$$M_z = \frac{-T_{x-des} H_y + T_{y-des} H_x}{H^2}$$

2) X-Z Desired Components of Torque

$$M_x = \frac{T_{x-des}(H_x H_z) + T_{z-des}(H_y^2 + H_z^2)}{H_y H^2}$$

$$M_y = \frac{T_{x-des} H_z - T_{z-des} H_x}{H^2}$$

$$M_z = \frac{-T_{x-des}(H_x^2 + H_y^2) - T_{z-des}(H_x H_z)}{H_y H^2}$$

3) Y-Z Desired Components of Torque

$$M_x = \frac{-T_{y-des} H_z + T_{z-des} H_y}{H^2}$$

$$M_y = \frac{-T_{y-des}(H_y H_z) - T_{z-des}(H_x^2 + H_z^2)}{H_x H^2}$$

$$M_z = \frac{T_{y-des}(H_x^2 + H_y^2) + T_{z-des}(H_y H_z)}{H_x H^2}$$

Vector properties of the torque produced, as compared to the desired torque vector are shown in Figure 14. This example shows the production of the y and z components of  $\vec{T}_{des}$  for pointing control. A dipole moment  $\vec{M}$  is generated which is normal to  $\vec{H}$ . This dipole produces a torque  $\vec{T}_{produced}$  which has identically the same component in the y-z plane as the desired torque vector,  $\vec{T}_{des}$ .

The advantage of the use of these "two component" algorithms is that exact torque components necessary to maintain pointing control can be produced almost continuously. The disadvantages are that (a) the dipole moments called for may be inordinately large depending on the magnetic field orientation and (b) the component of torque on the third axis is completely arbitrary and could hinder spin rate control.

#### d. Combinations of Algorithms

HEAO-A stabilization was achieved by switching between a "two component" algorithm for pointing control and a "single component" algorithm for scan rate control. The detailed switching logic is discussed in the section on the baseline control system. This combination of algorithms plus switching logic is referred to as Algorithm #1 for the baseline system.

A second combination of algorithms has also been successfully used to achieve HEAO-A pointing and spin rate control. This combination switches from one "two component" algorithm to another depending on pointing and spin rate errors. The y-z component algorithm is used to maintain pointing control.

When spin rate control is needed (i.e. torquing about the x-axis) either the x-y or x-z torque component algorithms are used. If the Y-axis acceleration demand (i.e.  $T_{y-des}/I_y$ ) is greater than the Z-axis acceleration demand ( $T_{z-des}/I_z$ ), then the x-y torque component algorithm is used. Thus the desired torque about the spin axis (x) and the Y-axis is produced. If the Z-axis acceleration demand is greater than the

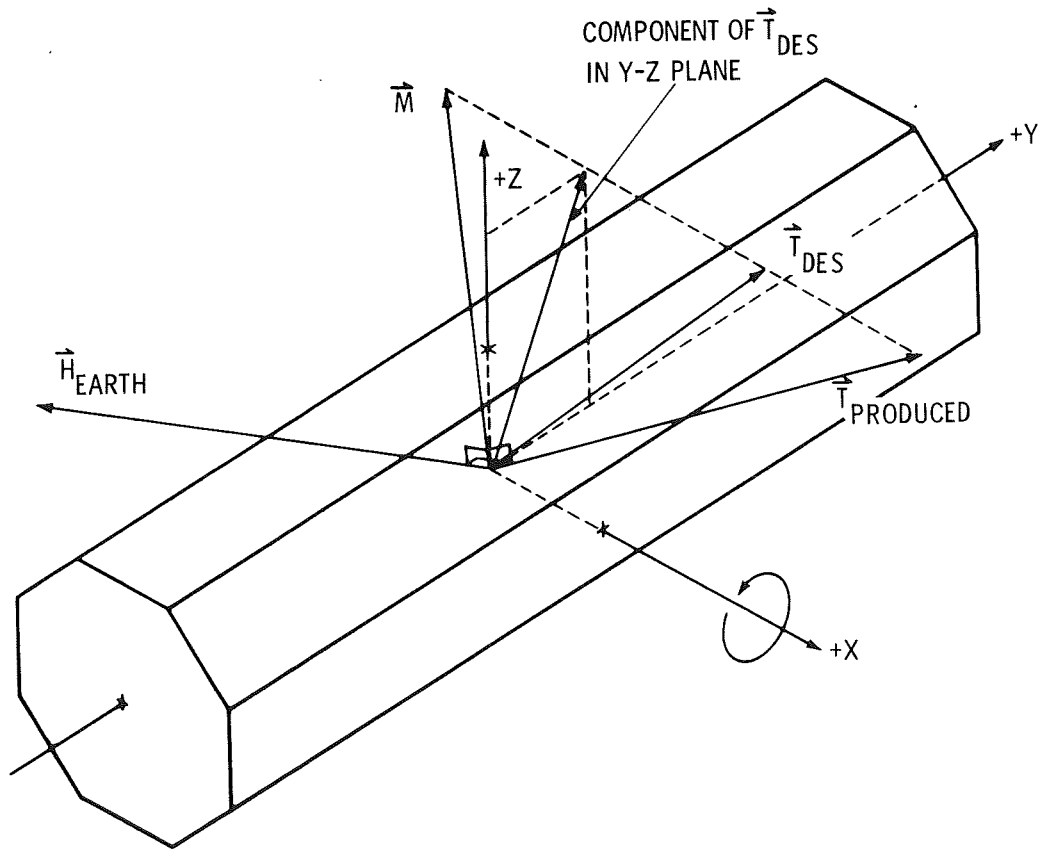


Fig. 14 PRODUCTION OF POINTING CONTROL TORQUE

Y demand, the x-z torque component algorithm is used. This system is also discussed in the baseline system description and is referred to as Algorithm #2. It is comparable in performance to Algorithm #1.

It is clear that additional optimization of algorithms and switching logic can be studied. The results of such study could result in increased pointing and spin rate performance while using a smaller flywheel.

#### 4. Effects due to Sensor Deadband

This section considers the effect of deadband in attitude and rate sensors on control performance. Deadband eliminates noise effects when attitude errors are small and allows the system to conserve control effort unless really needed. Deadband is used on the attitude sensor outputs and comes into effect when computing the desired torque vector. That contribution to desired torque due to a particular angle or rate (see Equation on page 15 ) is set to zero if that angle or rate is within the deadband; otherwise, the contribution to desired torque is computed normally.

Various levels of deadband were investigated as well as combinations of angle and rate deadband. The results of that investigation are presented here.

For a nominally stabilized condition, the error angles which measure the right ascension and declination of the sun in body coordinates vary from zero to about  $0.8^\circ$ . Roughly three-fourths of the time these angles are greater than  $0.1^\circ$  and half the time greater than  $0.2^\circ$ . This suggests that if angle deadbands much greater than  $0.1^\circ$  are used considerable information necessary for pointing control may be lost.

Angular rates about the y and z axes vary sinusoidally, the nominal amplitude being about  $3 \times 10^{-4}$  rpm with occasional peaks to about  $3 \times 10^{-3}$  rpm. Roughly one-half of the time, the angular rates exceed  $1 \times 10^{-4}$  rpm.

TABLE V  
 Effect of Deadband on Scan Mode Performance

<u>Deadband</u>	<u>Rate</u> <u>-rpm-</u>	<u>Peak Pointing Error</u> <u>-degrees-</u>	<u>Scan Rate Error</u> <u>-rpm-</u>
0	0	0.85°	0.040
0.1	0	0.90°	0.046
0.2	0	0.95°	0.054
0.1	10 <sup>-4</sup>	0.90°	0.046
0.2	2x10 <sup>-4</sup>	1.0°	0.058

A series of runs was made in which the angle deadband ranged from zero to  $0.2^\circ$  and the deadband on rates varied from zero to  $2 \times 10^{-4}$  rpm. All runs in this series were made for the winter solstice scan mode. Simulation results of that study are summarized in the Table V.

The conclusion of this study is that a combined deadband of  $0.1^\circ$  on angle and  $10^{-4}$  rpm on rate can be tolerated without severely compromising pointing and scan rate control. It remains to verify the acceptability of deadband for all orientations of the scan axis.

## E. Baseline Magnetic Attitude Control System-Design and Performance

### 1. System Components

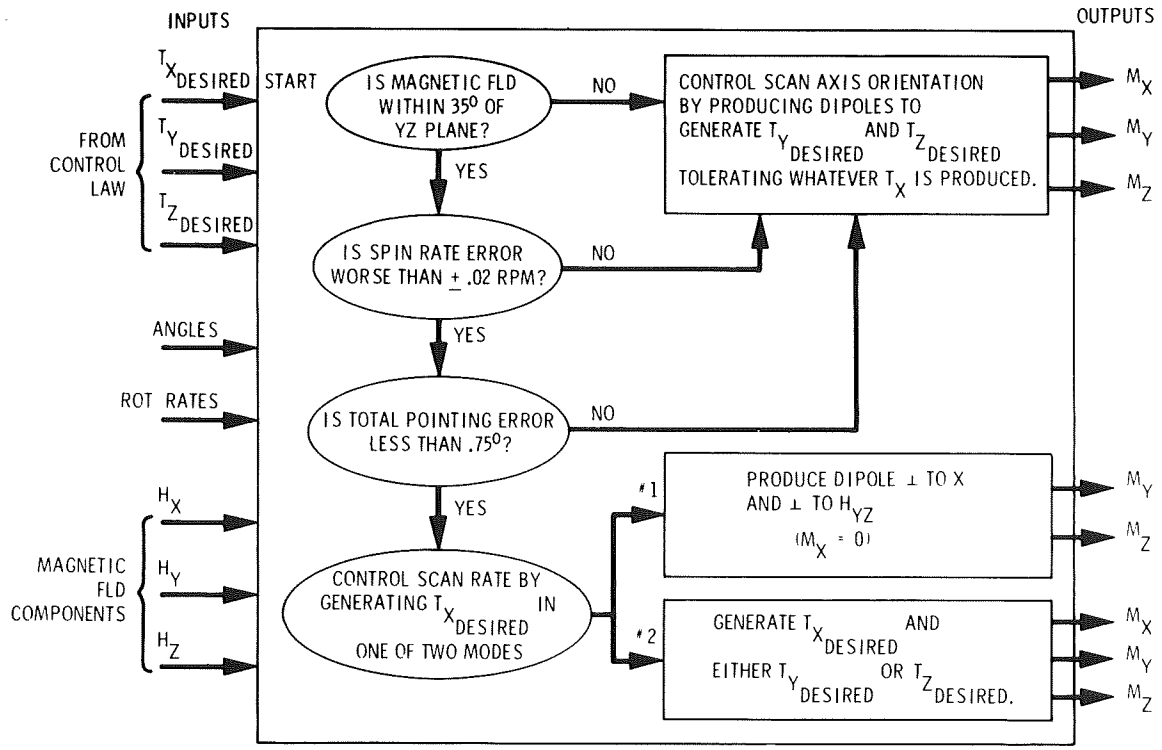
As a result of the investigations into the effect of wheel momentum, control law coefficients, dipole moment sizing, magnetic control algorithms and deadband, a baseline control system was established which appeared to have good global performance. This baseline system consists of:

- a) momentum wheel of 1000 ft-lb-sec
- b) magnetic torquers of 1000 amp-turn- $m^2$  maximum dipole
- c) a deadband of  $0.1^\circ$  on angle sensors and  $10^{-4}$  rpm on rate sensors.
- d) combination of one and two component control algorithms with switching logic called Algorithm #1.

### 2. Algorithm Switching Logic

The algorithm switching logic for the baseline system is shown in Figure 15. Inputs to this magnetic control section are components of the desired torque vector, attitude errors and rates and magnetic field components. Most of the time the y-z component control algorithm is used to maintain pointing control. Spin rate control is considered if the pointing error is less than  $0.75^\circ$ . Spin rate control action is taken if three conditions are satisfied:





APL JHU

Fig. 15 BASELINE MAGNETIC TORQUER ALGORITHM

- a) the magnetic field is within  $35^\circ$  of the y-z plane,
- b) the total pointing error is less than  $0.75^\circ$ , and
- c) the error in spin rate is worse than  $\pm 0.02$  rpm.

If scan rate control is selected Algorithm #1 uses the single torque component technique. It generates  $\vec{T}_{x-des}$  and arbitrary y and z components. If Algorithm #2 is used and scan rate control is needed a second selection of two component control modes is made, either one of which generates  $\vec{T}_{x-des}$ .

### 3. Baseline System Performance

Performance of the baseline scan mode control system was evaluated for a wide variety of conditions and orientation of the scan axis. Evaluations were made for solar pointing at various times of the year, galactic pole pointing, worst case declination pointing and capture for large initial errors. Results are presented here.

#### a. Solar Scan Winter-Solstice

Baseline performance for sun pointing at the winter solstice is shown in run #80 (Figure 16). For this condition the scan axis has a declination of  $-23^\circ 27'$  and is inclined to the orbit plane about  $52^\circ$ . Peak pointing errors are on the order of  $0.9^\circ$  and scan rate errors about 0.04 rpm.

#### b. Solar Scan-Vernal Equinox

A run using baseline conditions was made for the scan mode with the sun at vernal equinox (run #90, Figure 17) and the orbit node at  $180^\circ$  right ascension. These conditions place the scan axis in the orbit plane. At select times during each orbit, maximum gravity-gradient torques exist which tend to precess the spin axis from the solar vector. At other times during the orbit, these torques cause modulation of satellite spin rate. Results of run #90 indicate one brief period of several minutes duration in which the pointing error exceeded  $1.0^\circ$ . Otherwise peak pointing errors were on the order of  $0.9^\circ$ . Peak scan rate errors were 0.025 rpm.

(CASE #80)

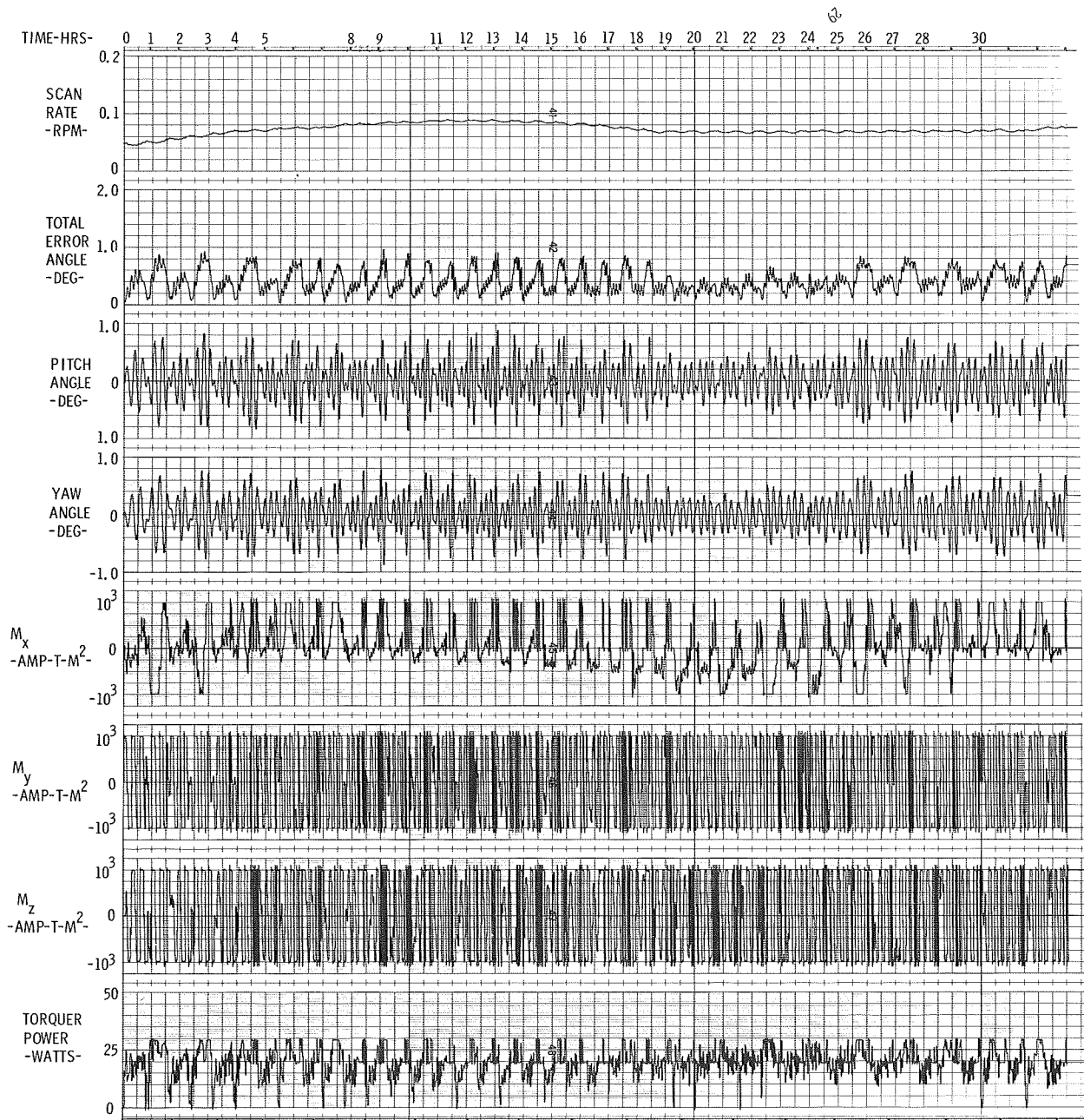


Fig. 16 SCAN MODE, SOLAR POINTING OF WINTER SOLSTICE

CONTROL LAW #14, ALGORITHM #1,  
1000 FT-LB-SEC WHEEL  
HEAO-A RUN #90

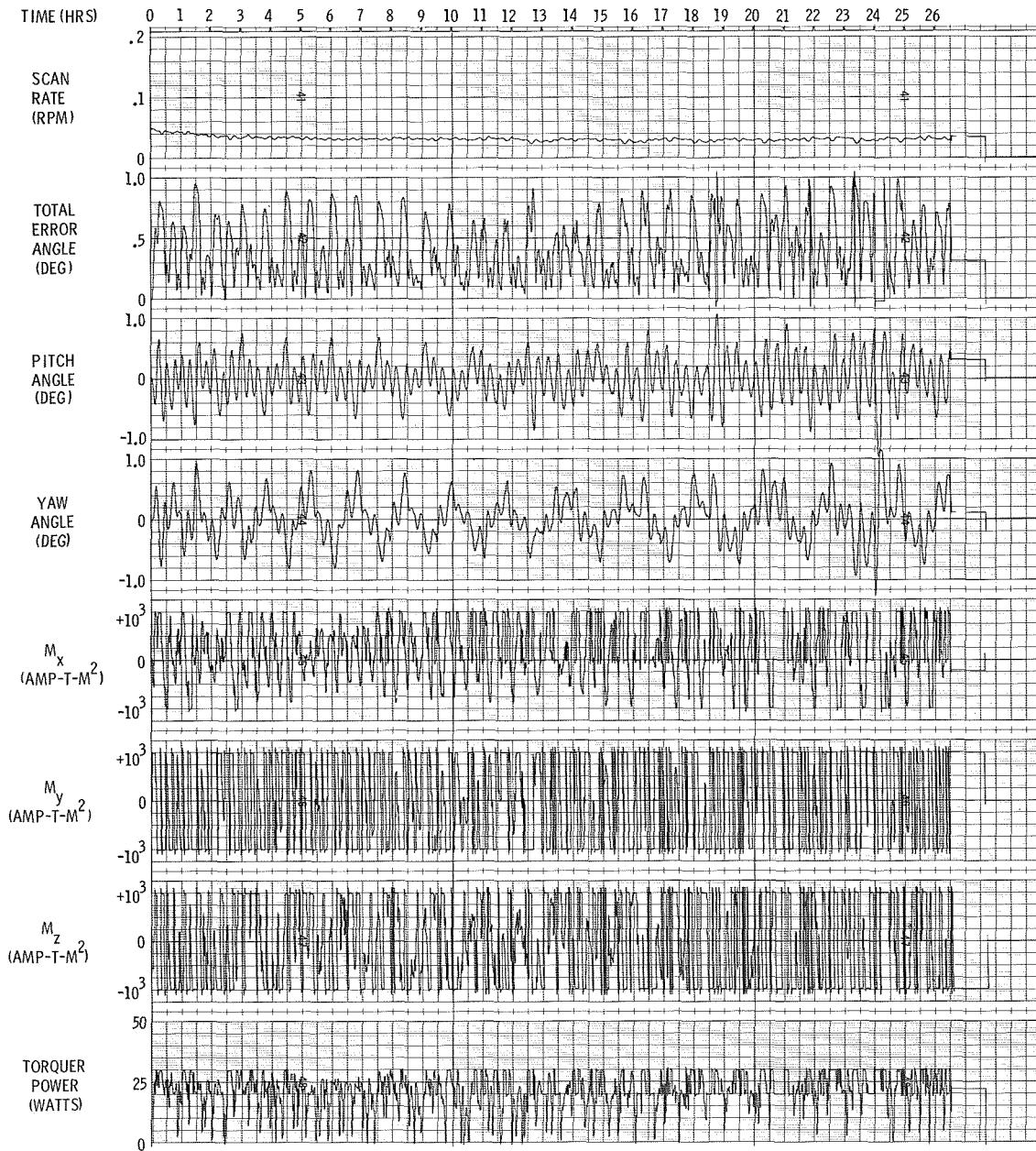


Fig. 17 SCAN MODE, SUN AT VERNAL EQUINOX

c. Galactic Pole Pointing

Coordinates for the north galactic pole are roughly  $192^\circ$  right ascension,  $+28^\circ$  declination. While pointing the scan axis at this pole in a 24 hour simulation (run #82), peak pointing errors experienced were close to  $0.9^\circ$  and peak scan rate errors, 0.02 rpm. Performance is shown in Figure 18.

A second run was made in which the orbit node was  $0^\circ$ . Results of that run (run #83, Figure 19) indicate pointing errors as great as  $1.4^\circ$ . The pointing error is below  $1.0^\circ$  roughly 90% of the time. The peak scan rate variation was 0.02 rpm.

d. Worst Case Declination

A worst case declination was considered to examine performance when the scan axis is more nearly aligned with the average magnetic field vector. This would occur for the scan axis at steepest declination. For this simulation the scan axis pointing coordinates were  $270^\circ$  right ascension  $-60^\circ$  declination.

In HEAO-A run #21 (Figure 20) the orbit node was  $180^\circ$  right ascension, thus the scan axis was almost normal to the orbit plane. For this condition gravity-gradient torques tend to modulate the spin rate. Over a 24 hour simulation peak pointing errors of about  $0.05^\circ$  were experienced along with scan rate errors less than 0.01 rpm.

e. Large Angle Maneuvers and Scan Rate Capture

In addition to maintaining scan axis pointing and scan rate control, HEAO-A must be capable of maneuvering from one source to another and be capable of achieving stabilization with large initial errors on attitude and rate.

Two large angle maneuver cases were run in which the desired scan axis pointing direction was the sun at winter solstice. In one run there was a  $45^\circ$  error in azimuth (in ecliptic coordinates), in the other a  $45^\circ$  error in declination. Both runs employed the baseline control system. The initial angular rate was 0.05 rpm.

CONTROL LAW #14, ALGORITHM #1, WITH DEADBAND  
1000 FT-LB-SEC WHEEL  
HEAO-A RUN #82

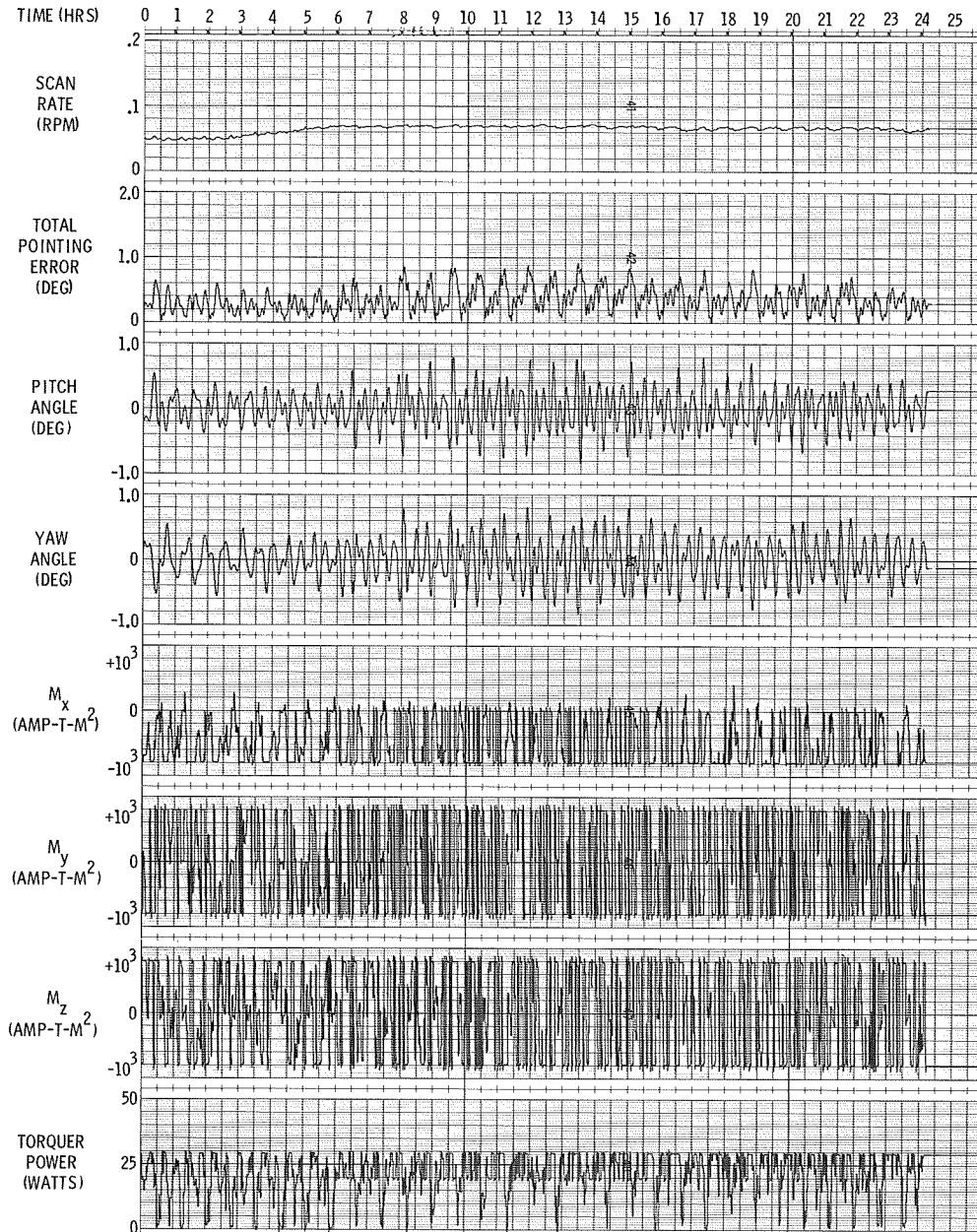


Fig. 18 GALACTIC SCAN (RAN - 180°)

CONTROL LAW #14, ALGORITHM #1, WITH DEADBAND  
1000 FT-LB-SEC WHEEL  
HEAO-A RUN #83

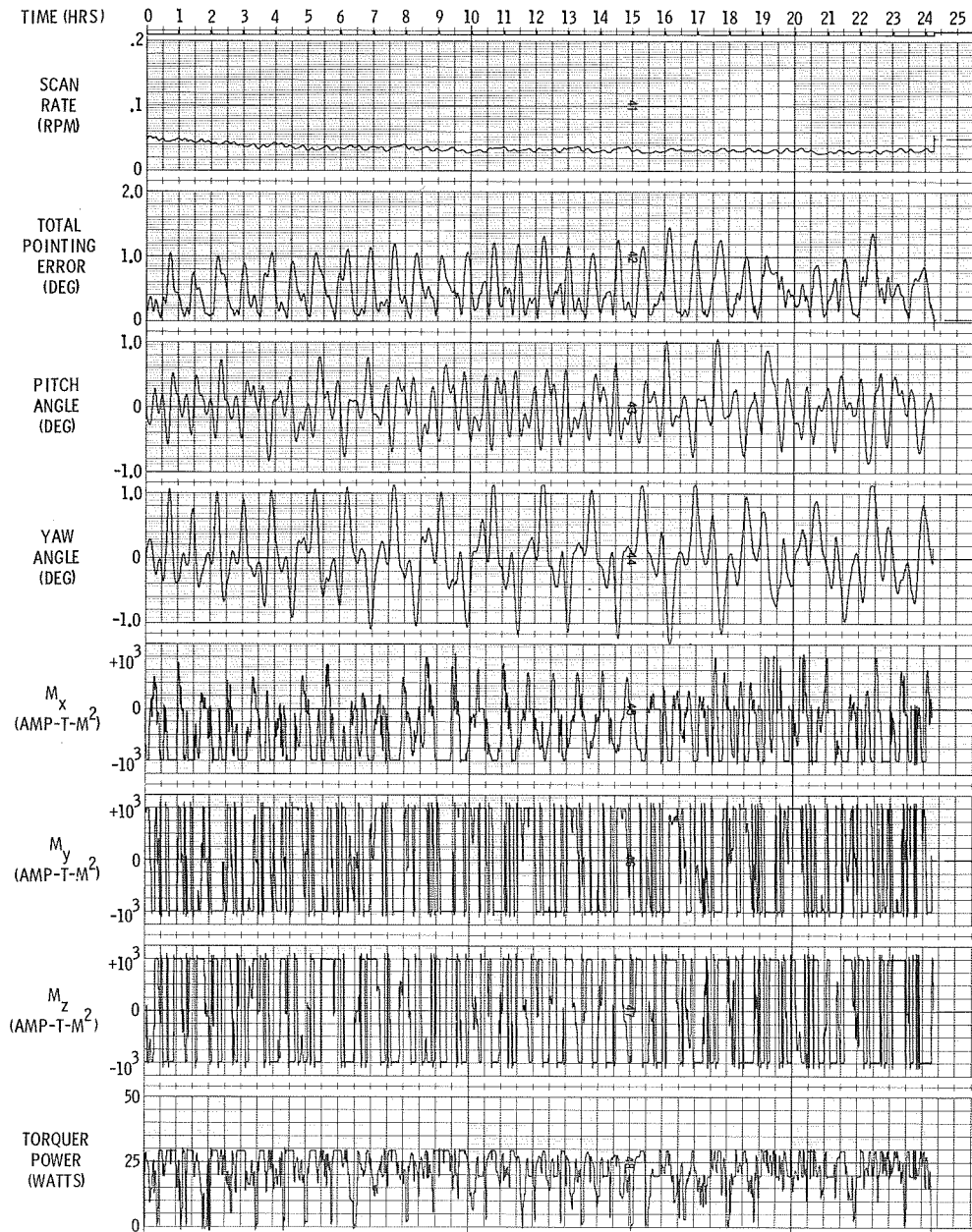


Fig. 19 GALACTIC SCAN, WORST CASE (RAN = 0)

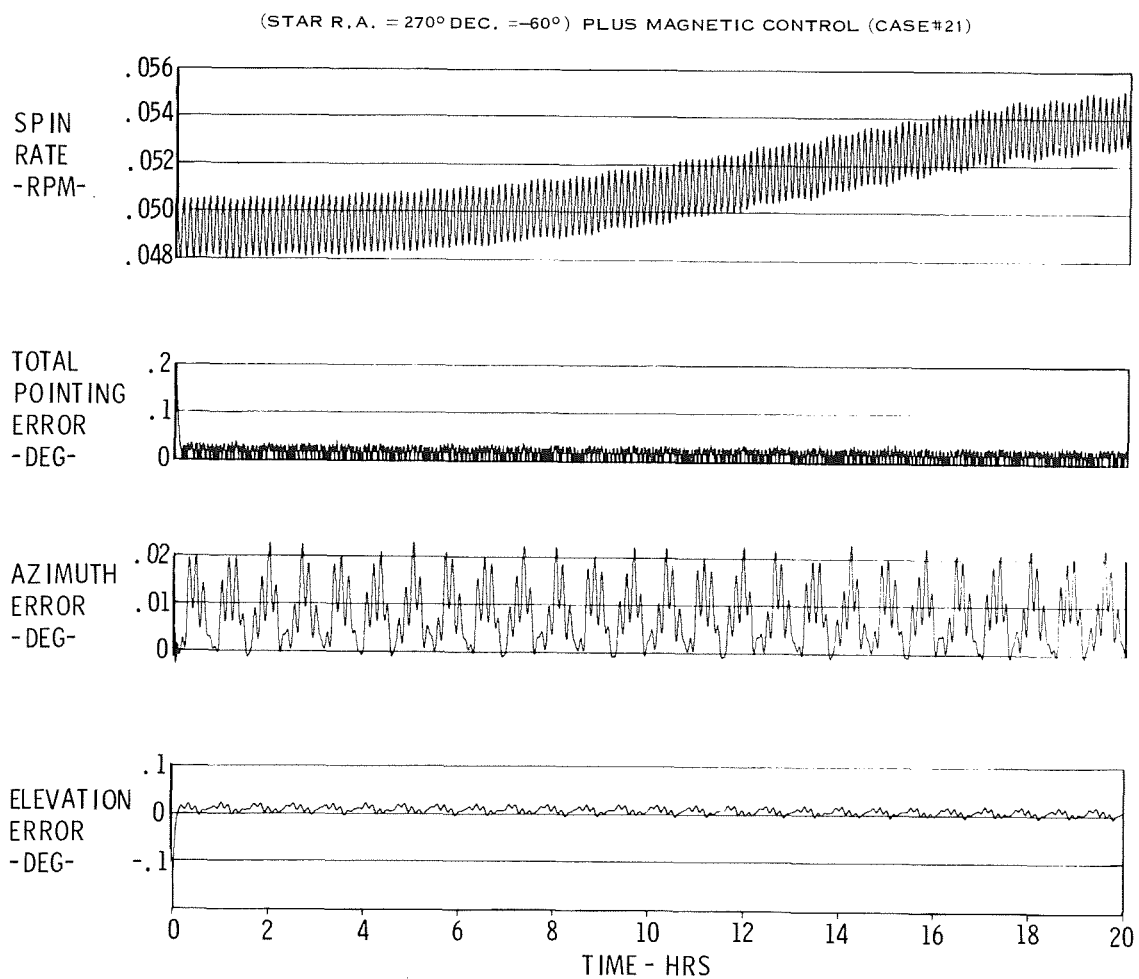


Fig. 20 WORST CASE DECLINATION OF SCAN AXIS



The 45° elevation maneuver is shown in Figure 21 (case #30). The maneuver was completed within 10 hours. During this time, variations in scan rate and azimuth error were small— 0.03 rpm and 3° in azimuth, respectively.

Performance of the baseline system for a 45° maneuver in azimuth was almost identical to that for the 45° elevation maneuver. The baseline system control law coefficients derived from linear optimal control analysis appear quite adequate for handling large angle conditions.

Capture from an initial scan rate of 0.15 rpm is shown in Figure 22. The baseline system maintains pointing control for small initial pointing errors while the scan rate is gradually decreased to 0.05 rpm. Approximately 24 hours are required for the scan rate to reduce from 0.15 rpm to 0.05 rpm. This operation could be expedited by changing the algorithm switching logic so that scan rate control action occurs more frequently.

Several attempts were made to achieve capture with both large errors in attitude and scan rate. Using the baseline algorithm switching logic the spacecraft could not capture. The problem appeared to be related to the fact that baseline pointing control coefficients are optimal for a scan rate of 0.05 rpm and are significantly different for much higher scan rates. By changing the switching logic slightly, however, capture from large angle and scan rate errors can be achieved. Such capture is demonstrated in HEAO-A run #95 (Figure 23). This is a simulation of scan mode acquisition from 30° azimuth error, 30° elevation error and an initial scan rate of 0.30 rpm. The technique used which effected capture was to alter the switching logic so that only spin rate control would be used until the spin rate was reduced below 0.10 rpm. When that rate was realized, switching logic was changed to baseline values and subsequent capture in attitude and rate proceeded normally.

(RUN #30)

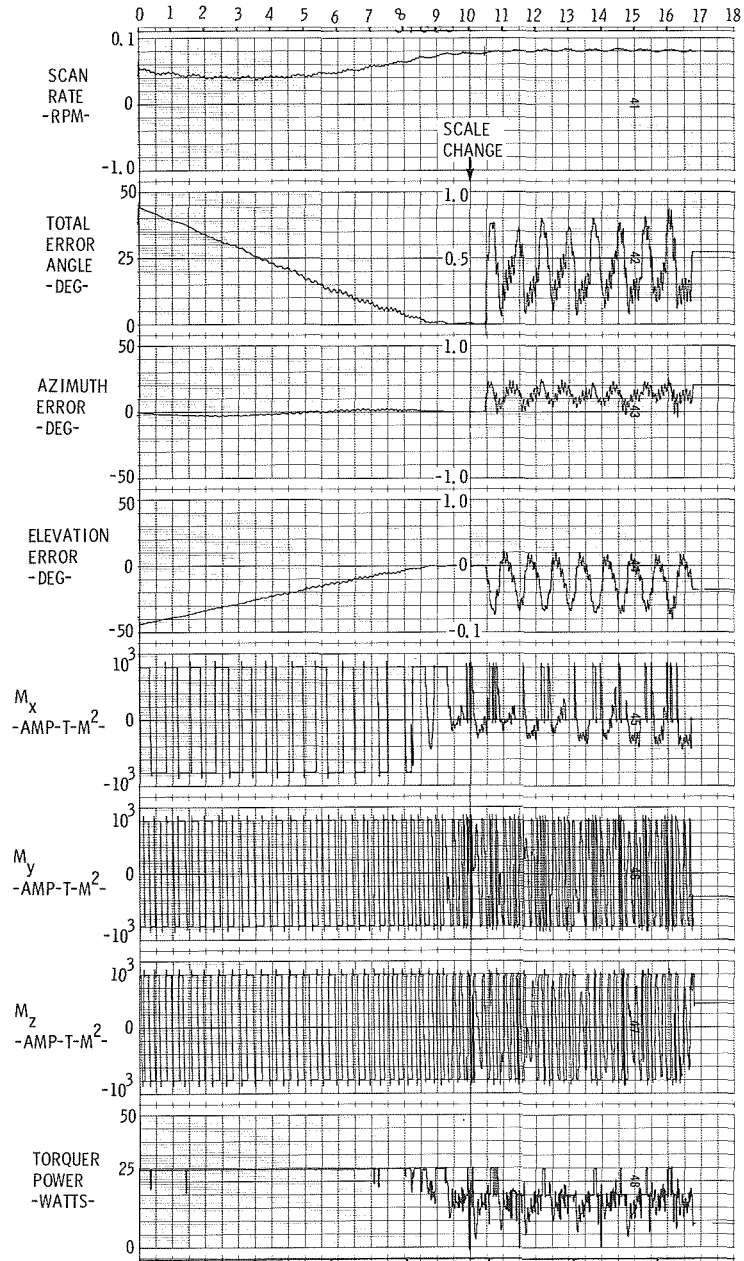


Fig. 21 CAPTURE FROM 45 DEG. ELEVATION ERROR

SCAN MODE, CONTROL LAW #14, ALGORITHM #2  
 DEADBANDS ON ANGLES AND RATES  
 1000 FT.-LB-SEC WHEEL  
 HEAO-A RUN #69

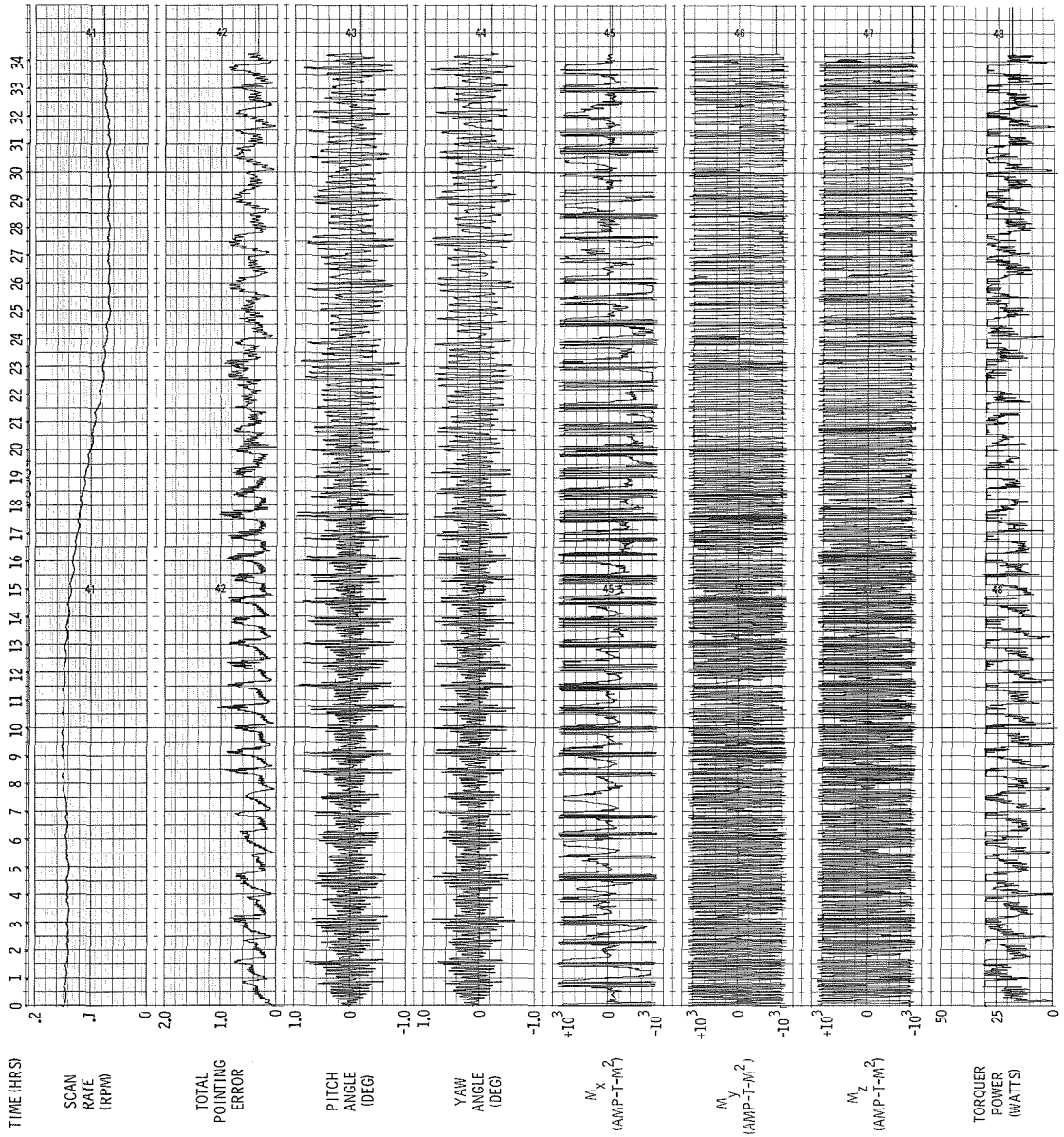


FIG. 22 CAPTURE FROM LARGE INITIAL SCAN RATE

SCAN MODE, CONTROL LAW #14, ALGORITHM #1,  
1000 FT-LB-SEC WHEEL  
HEAO-A RUN #95

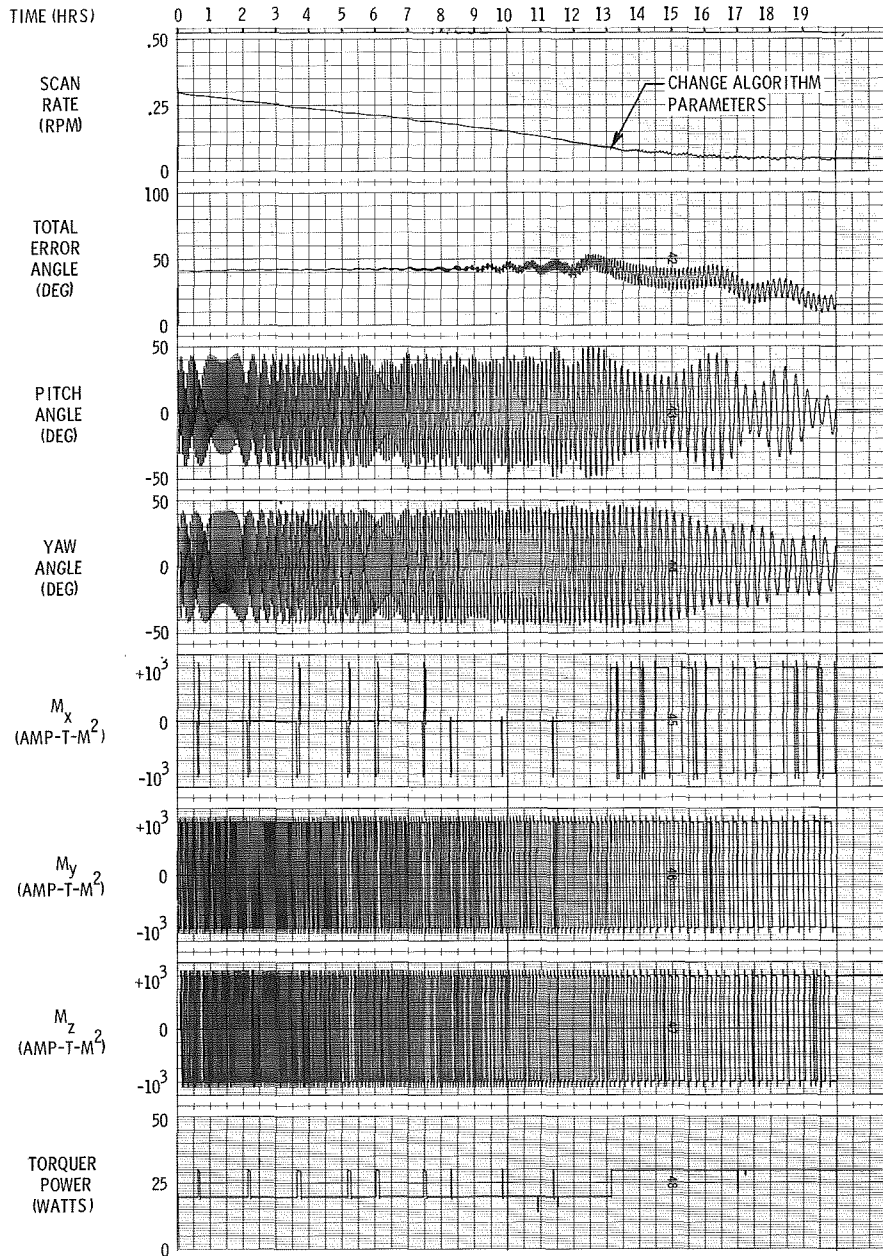


Fig. 23 CAPTURE FROM EXTREME INITIAL CONDITIONS

## F. Pointing Mode

### 1. Introduction to Problem of Pointing Mode Performance

The HEAO-A pointing mode is a problem involving 3-axis attitude stabilization with tight control of rotations (i.e. better than  $1^\circ$ ) maintained about two axes and somewhat looser control about the third ( $\pm 37^\circ$  to solar vector). Based on the performance obtained with the scan mode it would appear that pointing mode stabilization could be achieved if a momentum wheel were included which had its angular momentum aligned with the experiment axis to be controlled. For a general mission involving scan modes plus several experiment pointing modes this technique would call for three wheels and would require considerable space and weight.

The problem of pointing the Y or Z axis to within  $1^\circ$  of a specific celestial source is considerably more demanding when the control system is limited to the use of a single wheel whose momentum vector is aligned with the spacecraft X axis. Attempted here is the solution for pointing mode control in which the spacecraft uses a single wheel, aligned with the X axis, for both scan and pointing modes.

### 2. Fixed Speed Wheel

A set of runs was made using a wheel of constant angular momentum. Magnetic control algorithms and control law coefficients were varied in this set of runs to achieve pointing. HEAO-A runs #74, #75, and #76 in Figure 24 indicate performance for the Y pointing mode. Similar performance (not presented here) was obtained for the Z pointing mode. Generally it is observed that the spacecraft exhibits poor pointing control due to large angular motions about the momentum wheel axis. These large rotations appear whenever the magnetic control algorithm relaxes on generation of the desired X axis torque. Since there is no gyroscopic stiffness about the wheel axis gravity-gradient torques effect angular accelerations and the buildup of large angles of rotation.

HEAD-A RUNS #74, 75, AND 76

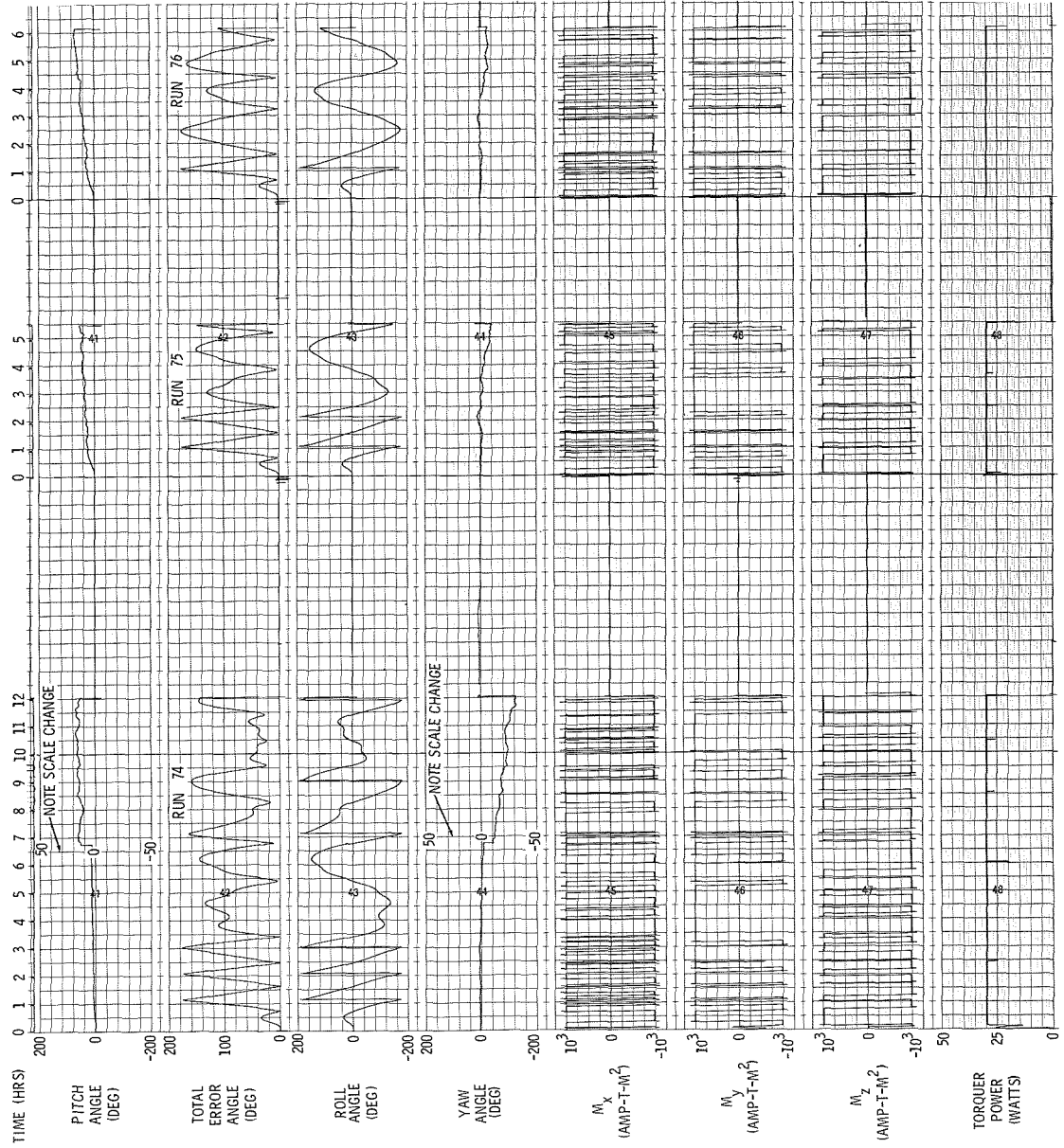


Fig. 24 Y POINTING MODE WITH NO WHEEL MODULATION

It must be noted that it is not possible to generate the desired X axis torque at all times due to (a) the position of the magnetic field (b) limits on dipole moments and (c) compromises in the algorithm necessary to control for rotations about the other two spacecraft axes.

### 3. Variable Speed Wheel - Y Pointing Mode

For the pointing mode then, it appears that we need to generate very close to the desired torque value along each spacecraft axis at all times. This can be done by using the magnetic control system to generate the correct torque about the Y and Z axes and generating the X axis torque by means of the wheel motor. This produces modulation of wheel speed. Run #79 (Figure 25) is an example of Y axis pointing control through wheel speed modulation. Over a 24 hour period the total y axis pointing error is less than  $0.5^\circ$  and rotation about the Y axis is controlled to better than  $3^\circ$ .

Simulation performance is based on the motor torquing characteristics of an induction motor. This means that the X axis torque value was established by that torque which could be delivered by the motor as a function of its speed, rather than the exact torque value desired. The motor torque characteristics assumed are given in Figure 26 and are based on motor data provided in Reference 6. The actual algorithm used for the wheel modulation solution consisted of:

(a) generating the dipole moments necessary to produce near desired values of torque for the Y and Z axes,

POINT AT RA=0°, DE=0°  
CONTROL LAW #24, ALGORITHM #2, WITH DEADBANDS  
HEAO-A RUN #79

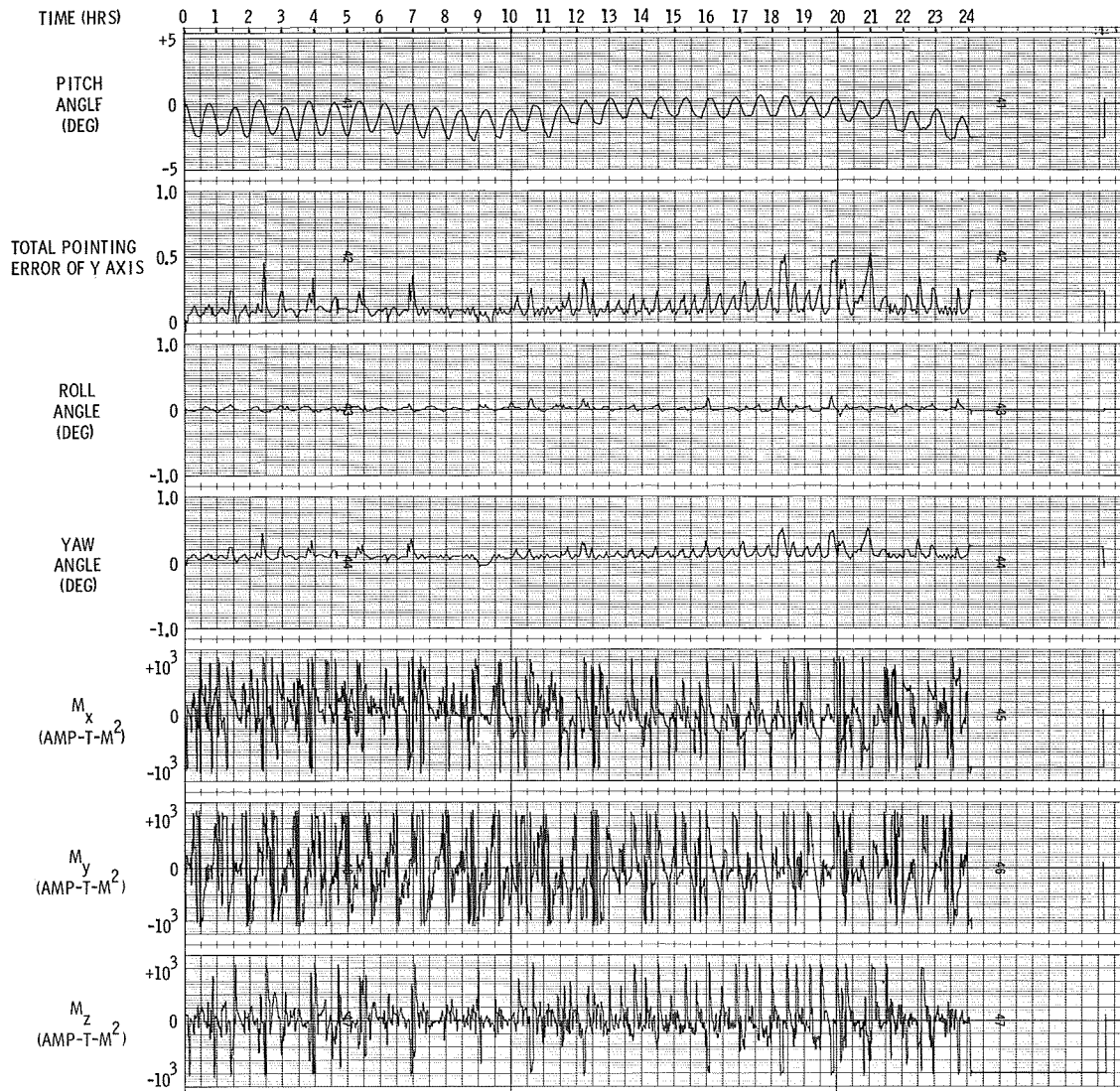


Fig. 25 Y POINTING MODE WITH WHEEL MODULATION



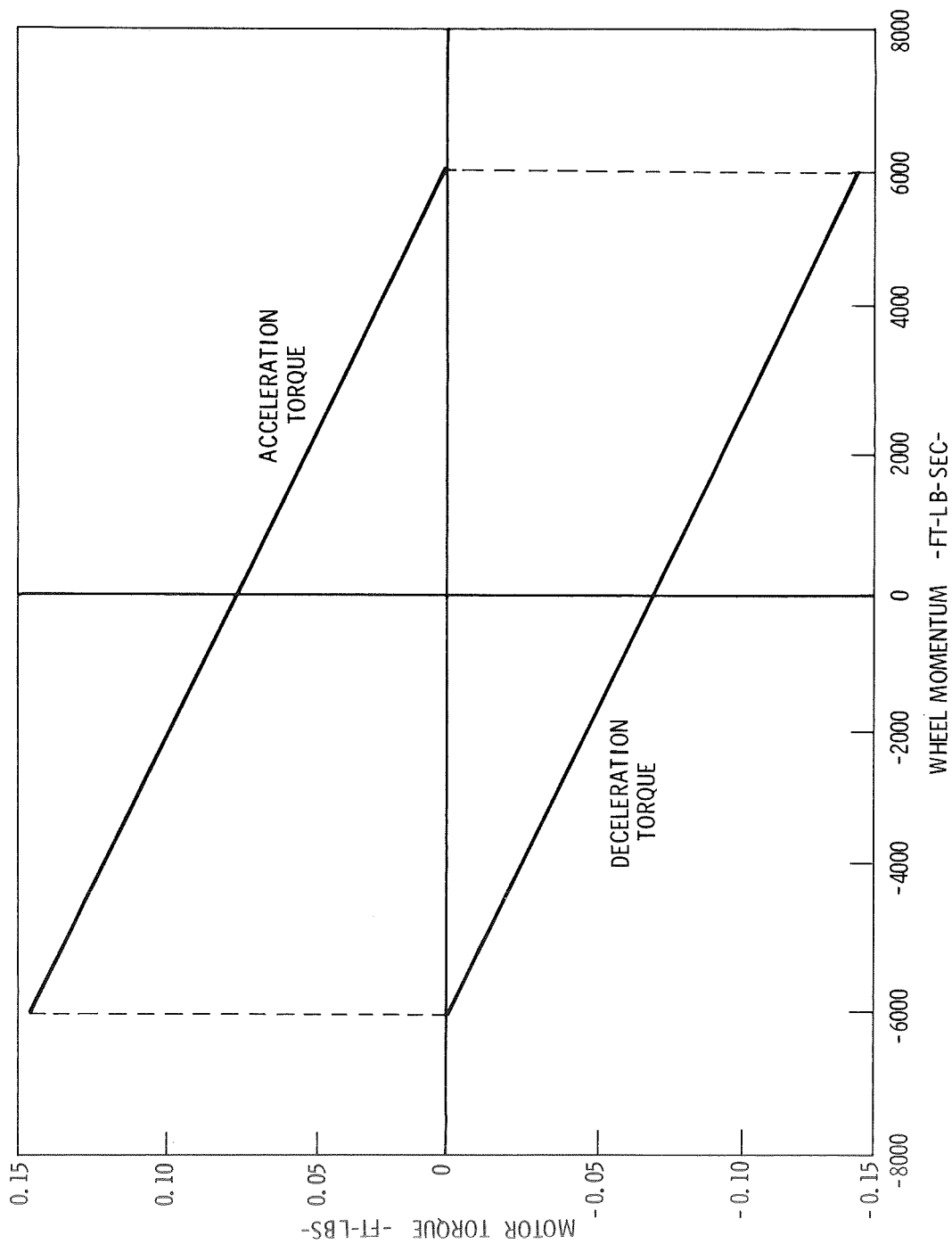


Fig. 26 ASSUMED MOTOR TORQUE CHARACTERISTICS

(b) Computing the magnetic torque which would be produced by these dipole moments, i.e.  $\vec{T} = \vec{M} \times \vec{H}$  ,

(c) computing X-axis torque difference of  $T_x(\text{desired}) - T_x(\text{produced})$  ,

(d) generating this torque difference by the momentum wheel motor (subject to inherent motor design characteristics) This algorithm produces excellent Y-axis pointing over a 24 hour period, as shown in Figure 25. For this run the Y-axis was in the orbit plane, pointed at  $0^\circ$  RA  $0^\circ$  DE with the sun at winter solstice.

The most demanding conditions for Y-axis pointing occur when the Y-axis is  $45^\circ$  to the orbit plane as the spacecraft experiences maximum gravity-gradient torques. If the Z-axis also happens to be in the orbit plane then an average gravity-gradient torque exists about the X-axis which tends to monotonically increase or decrease the wheel momentum. When the wheel momentum reaches its limit further modulation is impossible and pointing control is lost. This effect was simulated in a run where the Y-axis was  $28.5^\circ$  out of the orbit plane and the X-axis pointed at the sun at vernal equinox. An initial wheel momentum of 1000 ft-lb-sec was used with an assumed modulation limit of  $\pm 500$  ft-lb-sec. After 8 simulation hours saturation occurred and pointing control was lost. In a subsequent run the modulation limit was set at  $\pm 750$  ft-lb-sec with a starting value of 1000 ft-lb-sec. Here, pointing control was lost after 10 hours, not because of saturation but because the wheel momentum had reduced to a level ( $\sim 350$  ft-lb-sec) where it was no longer effective.

The problem of wheel saturation was reduced to a large extent by redesigning the magnetic control algorithm such that X axis torque was generated by the magnetic system more often than by wheel modulation. Employing this modification to the algorithm, Y axis pointing performance comparable to Run #79 (Figure 25) was obtained. In this test case the sun was at vernal equinox and the Y axis pointed  $90^\circ$ RA,  $16.5^\circ$ DE

(i.e.  $45^\circ$  to orbit plane). This represents a worst case gravity-gradient disturbance condition. Pointing control was maintained to better than  $0.3^\circ$  and rotation control to better than  $3^\circ$ . A considerable savings in power was also realized. For the wheel and magnetic torquer design assumed, about 100 watts average power is required with the modified algorithm as compared to about 190 watts average for continuous wheel modulation. The wheel speed still changed monotonically but at a much reduced rate. Pointing control could be maintained for two days before wheel desaturation would be required.

It is possible to further reduce the tendency to saturate the wheel by requiring the magnetic system to also partially compensate for the known average gravity-gradient torque. This was done by adding a gravity-gradient bias torque to the desired torque vector. Normally the desired torque is a function of the attitude errors and rates. The effect of both modifications (change in algorithm plus bias torque) is shown in run #112 (Figure 27). This run also simulated worst case gravity-gradient torques. Two important effects were noted:

(a) momentum change in the wheel was reduced to 290 ft-lb-sec over a 24 hour period as compared to 340 ft-lb-sec without the bias, and

(b) the roll angle was biased  $0.5^\circ$  by the bias torque. (The bias torque was 0.1 n-m as compared to 3.4 n-m for the average gravity-gradient torque.) It was found that doubling the bias torque doubled the error bias.

The conclusion of the Y-axis pointing study is that better than  $1^\circ$  pointing and control of rotation about the Y-axis to better than  $5^\circ$  can be maintained. This performance can only be achieved however if wheel speed modulation is used to augment the magnetic torquing system. The desired Y-axis pointing can be maintained under worst gravity-gradient disturbance conditions for two days before it is required to desaturate the wheel. The attitude control design conditions for Y-axis pointing included:

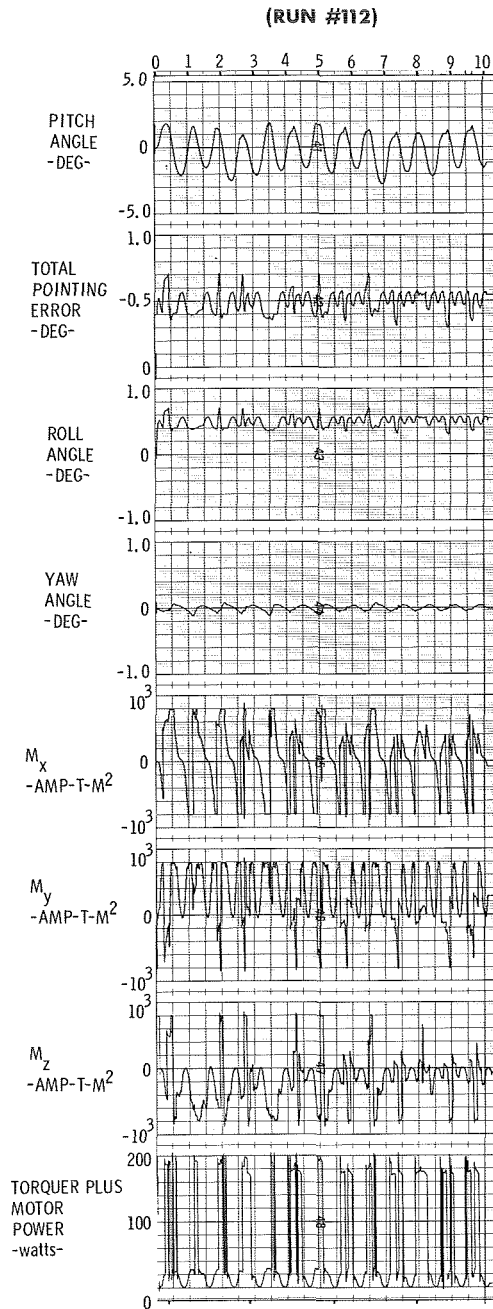


Fig. 27 Y POINTING WITH WHEEL MODULATION PLUS GRAVITY-GRADIENT COMPENSATION

- (a) minor change in the magnetic control algorithm,
- (b) a nominal wheel momentum of 1000 ft-lb-sec,
- (c) modulation of the wheel momentum to  $\pm 700$  ft-lb-sec limits, and
- (d)  $10^3$  amp-turn-m<sup>2</sup> dipole moment limits.

#### 4. Variable Speed Wheel - Z Pointing Mode

Using Y-axis pointing control system performance as a guide HEAO-A Z-axis pointing capability was investigated. For Z-axis pointing it is required to point the spacecraft Z-axis to a specific source to within  $1^\circ$  and to control the rotation about the Z-axis such that the X-axis points within  $37^\circ$  of the solar vector. For Z-axis pointing tight control must be maintained for rotations about the spacecraft X and Y-axes and somewhat looser control for rotations about the Z-axis. Based on experience with the scanning mode and Y-axis pointing mode, it can be said that tight control of motion about the Y-axis requires a momentum wheel and tight control of motion about the X-axis requires some degree of wheel speed modulation. (A run with no modulation for the Z-axis case indicated large rotations about the X-axis).

Several runs were made with wheel speed modulation for the Z-axis pointing mode. Variables in these runs were dipole moment limits, control law coefficients and parameters within the magnetic control algorithm. A summary of the effort is characterized by run #114 (Figure 28). The total pointing error was controlled to within  $2.5^\circ$  and rotations about the Z-axis controlled within  $2^\circ$ . In essence, the same attitude behavior evident for Y-axis pointing was observed for the Z-axis case, that is, relatively tight control was maintained for motions about the spacecraft X and Z-axes and looser control for motion about the Y-axis. Run #114 represents a minimum gravity-gradient disturbance condition wherein the Y-axis was in the orbit plane. The algorithm used, generated the desired torque vector about the Y and Z-axes magnetically (subject to dipole moment limits) and generated the X-axis torque component via wheel speed modulation. In all cases

POINT AT RA=90°, DE = 61.5°  
CONTROL LAW #27 ALGORITHM #2  
RUN #114

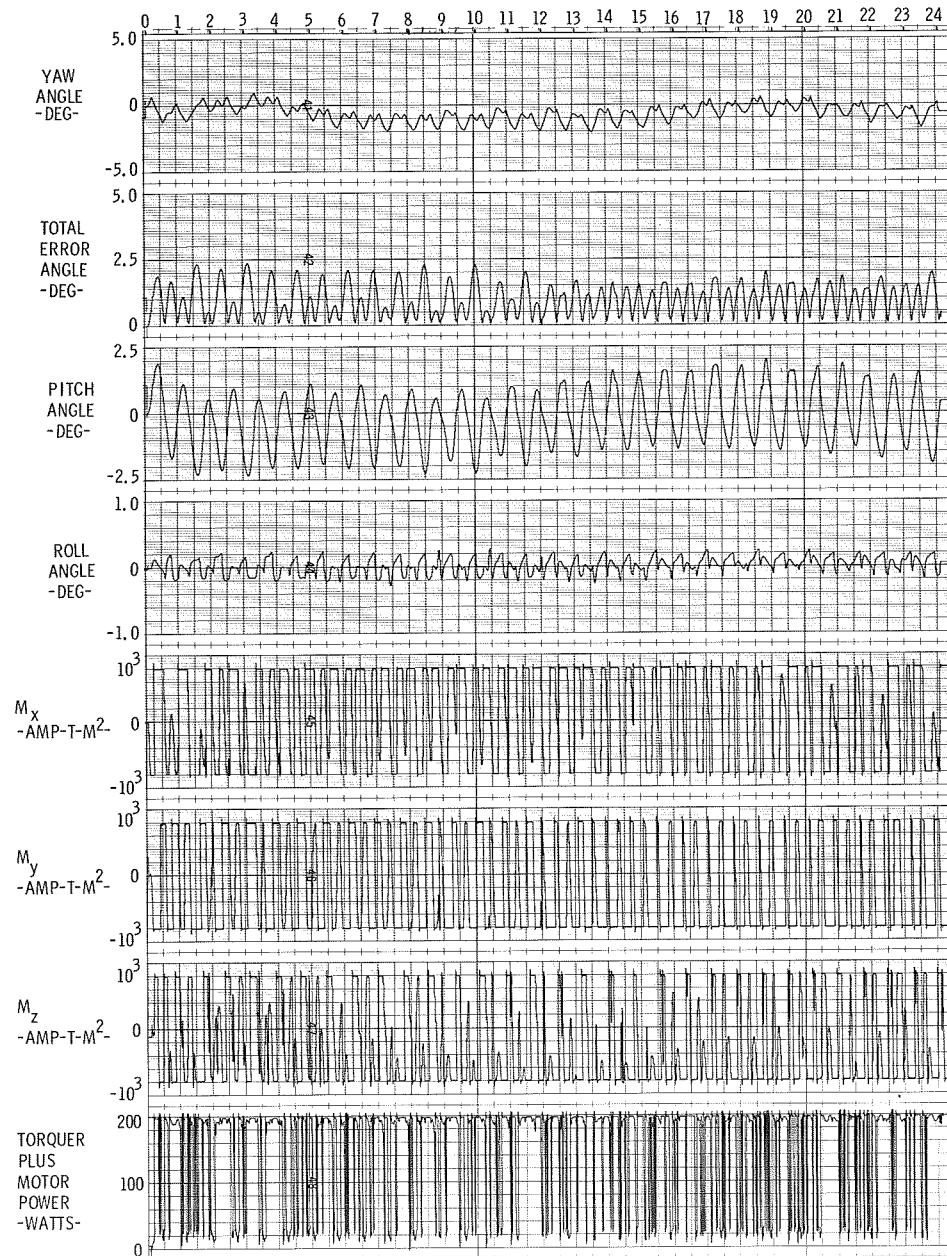


Fig. 28 Z POINTING MODE WITH WHEEL MODULATION

investigated, before termination of the study, Z-axis pointing was controlled to only within  $2.5^\circ$ . Approximately 50% of the time Z-axis pointing could be maintained to within  $1^\circ$ . Although the Z-axis pointing requirements were not fully demonstrated here the performance was close enough to estimate that reevaluation of the control algorithm could effect a solution for Z-axis pointing.

#### IV. CONCLUSIONS

The HEAO requirement of 1 degree accuracy is difficult for a magnetic control system because of the fundamental physical limitation of torquing against the earth's field, namely that no torque component parallel to the field can be produced at any given instant of time. However, as the satellite proceeds in orbit it passes over different portions of the earth's surface, and the local magnetic field changes in orientation. Therefore control action can be delayed until the magnetic field orientation is more favorable, or a more sophisticated control system conceived to make the best of existing conditions.

The APL study has focused on the problem of control law synthesis, magnetic torquer algorithm design, and has examined the trade-offs in pointing and scan rate performance associated with control system design, wheel momentum and magnetic torquer limits.

Control law synthesis uses techniques of optimal control theory which leads to linear control laws with specific values for the control law constants which minimize some measure of the squares of the error angles and squares of the control torques. This analysis ignores the inherent limitations of magnetic torquing; it provides desired control torques without consideration of the fact that these torques cannot in general be produced.

The magnetic torquer algorithm works out a compromise between the desired torques and those which can be produced, using the angle and rate information and the magnetic field components as measured by a three axis vector magnetometer.

Computer simulations of closed loop attitude control of HEAO with only magnetic control torques indicate that the desired pointing control cannot be obtained due to large gravity-gradient disturbance torques. However, addition to the system of a modest momentum wheel of 1000 ft-lb-sec momentum provides enough gyro-stabilization, to give HEAO



short-term attitude stabilization, and the magnetic torquing system can work effectively against long-term disturbances to meet the desired pointing requirements.

The APL study has also found that magnetic torquers can be limited to maximum dipole values of  $\pm 10^3$  ampere-turn-meter<sup>2</sup> without compromising the system performance. This has important implications on the weight and electrical power demands of the magnetic control system.

Based on computer simulation results, a baseline attitude control system for HEAO-A was defined which consisted of a specific optimal control law (control law #14), a specific logic for generating magnetic moments (algorithm #1), a 1000 ft-lb-sec momentum wheel and 1000 amp-turn-m<sup>2</sup> magnetic torquer limits. Typical baseline performance shows pointing errors less than 1.0 degree and scan rate bounded between zero and 0.1 rpm. This performance was observed for a galactic scan case and a  $-60^\circ$  scan axis declination case. This baseline system also demonstrated maneuver capability and acquisition from large initial attitude and scan rate errors.

In one galactic scan case where the orbit node was changed, from zero to  $180^\circ$  right ascension peak pointing errors in excess of 1.0 degrees were observed. The pointing error was less than 1.0 degree over 90% of the time, however. This run could indicate that although the baseline system meets attitude requirements for a variety of conditions, it may not satisfy the requirements for all combinations of scan axis orientations and orbit positions. A more exhaustive study is required to prove global performance of a selected HEAO-A scan mode attitude control system.

Another satellite operating mode requires a different axis to be pointed to 1 degree, and the wheel axis be maintained within  $\pm 37$  degrees of the sun-line to obtain the necessary solar array power. APL has found the constant speed momentum wheel with magnetic control inadequate for this case. However, by providing variable wheel speed capability, and operating the wheel to produce control torques by wheel speed variation the

desired control accuracy has been obtained. The baseline control system for the scan mode with slight modification to control constants and algorithm logic effects desired pointing of the Y-axis (long axis). Pointing of the Z-axis was only obtained to within 2.5 degrees.

The APL study has provided not only performance characteristics of a baseline system for magnetic control of HEAO-A but has provided background information to enable a designer to synthesize a control system. This background information is in the form of sections on optimal control theory and application, magnetic torquer design, earth's magnetic field description, magnetic control algorithms and performance trade-offs inherent to the selection of a particular control system.

REFERENCES

1. Hecht, E. and Manger, W. P. "Magnetic Attitude Control of the TIROS Satellites" Torques and Attitude Sensing, S. F. Singer, Editor, Academic Press, 1964.
2. Mobley, F. F., et al "Performance of the Spin Control System of the DME-A Satellite" Applied Physics Laboratory TG-929, June, 1967. Also AIAA/JACC Guidance and Control Conference Proceedings, p 463, August, 1966.
3. Mobley, F. F. "Gravity-Gradient Stabilization Results from the DODGE Satellite in 1967", Applied Physics Laboratory, TG-993, May, 1968.
4. Tossman, B. E. "Magnetic Attitude Control System for the Radio Astronomy Explorer-A Satellite" Journal of Spacecraft and Rockets, Vol. 6, No. 3, p 239, March, 1969.
5. Mobley, F. F. "Attitude Control System for the Atmosphere Explorer-B Satellite" AIAA Paper No. 65-432, AIAA 2nd Annual Meeting, July, 1965.
6. Duffie, J. M. (editor), "Conceptual Design of the High Energy Astronomy Observatory Spacecraft," Brown Engineering SMSD-PD-722, July, 1969.

## APPENDIX A

### Magnetic Torquer Design

#### Introduction

It is assumed that the control laws for HEAO attitude control will require the generation of magnetic dipoles parallel to each of three orthogonal satellite axes with continuous magnitudes varying over some limited range from full positive dipole to full negative dipole. These requirements can be met with electromagnets using ferromagnetic cores or air coil designs. The primary objectives of the design are minimum weight and electrical power. The examples worked here are addressed to the design for a maximum magnetic dipole of  $10^3$  amp-turn-meters<sup>2</sup>.

Symbols	Units
M    magnetic dipole moment	(amp-turn-m <sup>2</sup> )
N    number of turns of coil	
A    plane area enclosed by coil	(m <sup>2</sup> )
I    coil current	(amperes)
a    characteristic dimension of geometrical figure	(meter)
P <sub>e</sub> perimeter of figure	(meters)
W <sub>l</sub> total wire length	(meters)
W <sub>t</sub> total wire weight	(lbs)
R    total wire resistance	(ohms)
w    running wire weight	(lbs/meter)
r    running wire resistance	(Ω/meter)
P    power consumed by coil	(watts)
B <sub>av</sub> average magnetic flux density	(gauss)
V    core volume	(cm <sup>3</sup> )
μ    true permeability of core	(non-dimensional)
μ <sub>e</sub> effective permeability	(non-dimensional)
	(Δ B <sub>av</sub> /1.257(NI/ℓ))
H    nominal magnetizing force	(oersteds)
	(Δ 1.257/NI/ℓ)
ℓ    core and/or solenoid length	(cm)
d    core diameter	(cm)
n/4π    demagnetizing factor	(non-dimensional)
H <sub>c</sub> coercive force of core material	(oersteds)
ρ    core mass density	(gm/cm <sup>3</sup> )

## Air Coil Design

Assume a coil of  $N$  turns wound in a circle of diameter  $a$ , to produce a magnetic dipole  $M$ :

The required current  $I$  is

$$I = \frac{M}{NA} = \frac{M}{N\pi a^2} \quad (1)$$

Wire length,  $W_1$

$$W_1 = NP_e = N\pi a \quad (2)$$

Wire weight,  $Wt$

$$Wt = wNP_e = wN\pi a \quad (3)$$

Wire resistance,  $R$

$$R = rNP_e = rN\pi a \quad (4)$$

Power consumption

$$P = RI^2 = rN\pi a \left( \frac{M}{N\pi a^2} \right)^2 \quad (5)$$

Power-Weight Product,  $PxWt$

$$PxWt = rN\pi a \left( \frac{M}{N\pi a^2} \right)^2 wN\pi a \quad (6)$$

$$PxWt = \frac{16}{a^2} r w M^2 \quad (6)$$

The number of turns,  $N$ , cancels out of this last equation, indicating that the power-weight product is independent of  $N$ .  $N$  and  $I$  must be chosen to produce the required dipole moment  $M$ . This is a trade-off between current, voltage, and number of turns but does not affect the power-weight product.

The product  $rw$  is a characteristic of the material selected for the conductor. Aluminum provides the lowest value of this parameter among common conductor materials. For aluminum

$$(rw)_{\text{Aluminum}} = 1.70 \times 10^{-6} \frac{\text{ohm-lbs}}{\text{meter}^2}$$

Example: To produce a dipole of  $10^3$  amp-turn- $m^2$  with a coil of 9 ft diameter, what is the required power-wt product?

Using Equation 6,

$$P \times Wt = \frac{16}{(9 \times 3048)^2} (170 \times 10^{-6}) (10^3)^2$$

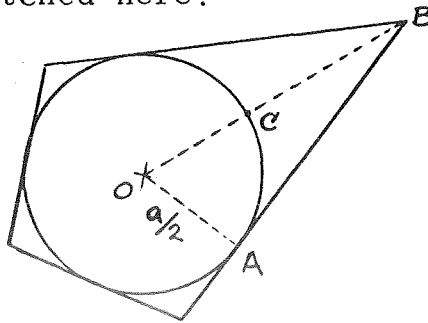
$$= 361.0 \text{ watt-lbs.}$$

Therefore, for instance, a 36 lbs coil would require 10 watts of electrical power. Wire size and number of turns would be selected to suit the available voltages. Lower coil weight could be achieved by allocating more electrical power.

If, for practical reasons, it is more convenient to configure the coil in a polygon rather than a circle the following results would be useful.

In the special case of a polygon superscribed on a circle the power-weight product will be shown to be the same as that of the inscribed circle

Consider an arbitrary polygon superscribed\* on a circle of diameter "a" as sketched here:




---

\*Note: By superscribed we mean a polygon all of whose sides are tangent to the circle.

Now the power-wt product for an air coil wound in any shape is

$$PxWt = rwN^2 \frac{P_e^2}{A^2} \frac{M^2}{N^2} = \frac{P_e^2}{A^2} rWM^2$$

which is proportional to the square of the perimeter to area ratio  $P_e/A$ . For any polygon superscribed on a circle of diameter "a" this ratio is  $4/a$ . The proof of this assertion follows:

Proof

The arc  $\widehat{AC}$  (above) has length  $\frac{a}{2} \theta$ . The area  $O\widehat{AC}$  is  $\frac{\theta}{2\pi} (\frac{\pi a^2}{4})$ . Therefore for  $O\widehat{AC}$  the perimeter-area ratio is

$$\frac{\frac{a}{2} \theta}{\frac{\theta}{2\pi} \frac{\pi a^2}{4}} = 4/a .$$

The line  $AB$  has length  $a/2 \tan \theta$ , and the area  $OAB$  is  $\frac{1}{2} (\frac{a}{2}) (\frac{a}{2} \tan \theta)$ . Therefore the ratio of line length  $AB$  to area  $OAB$  is.

$$\frac{a/2 \tan \theta}{\frac{1}{2} (\frac{a}{2}) (\frac{a}{2} \tan \theta)} = 4/a .$$

Since the perimeter to area ratio for any section of the circle is  $4/a$  it follows that it is  $4/a$  for the entire circle. Since the perimeter to area ratio for each line element of the superscribed polygon is  $4/a$  it follows that it is  $4/a$  for the entire polygon. Thus the assertion is proven.

The formula for this power-wt product is therefore the same as that for the inscribed circle, namely,

$$PxWt = \frac{16}{a} (rw) M^2 .$$



In the case of a rectangular coil configuration with short side "a" and long side "b" the power-wt product is:

$$PxWt = \frac{P_e^2}{A^2} rWM^2 = \frac{4(a+b)^2}{a^2 b^2} rWM^2 .$$

Example: For b = 30 ft and a = 100 inches, what is the power-weight product for a dipole of  $10^3$  amp-turn-meter<sup>2</sup>?

$$a = 100" = 2.54 \text{ meters}$$

$$b = 30' = 9.14 \text{ meters}$$

$$PxWt = \frac{4(2.54 + 9.14)^2}{(2.54 \times 9.14)^2} (170 \times 10^{-6}) (10^3)^2$$

$$= 172 \text{ watt-lbs}$$

This result is applicable to the HEAO configuration for use for the X axis and Z axis dipoles. If 10 watts are allocated for each coil then the coil weight would be about 17 lbs.

### Electromagnet Design

An electromagnet for efficient magnetic dipole moment production usually consists of a slender cylinder of ferromagnetic material, the core, wound with many turns of insulated wire, the solenoid. Energizing the solenoid with electric current magnetizes the core and produces a magnetic dipole moment.

Selection of Core Material - The dipole moment M of the core is related to the average flux density  $B_{Av}$  in the core by the formula

$$M = \frac{B_{Av} V}{4\pi} \frac{1}{1000} \quad (1)$$

The maximum dipole that can be developed in a given core is limited by the saturation value of  $B_{AV}$ , which is a property dependent on the core material. Obviously the higher  $B_{AV}$  the less volume (V) and correspondingly less weight of core is required.

The shape of the core is very important in electromagnet design due to the phenomenon of "demagnetization". When a cylindrical core is magnetized by an applied external field H it develops north and south poles near the ends of the core, which produce an additional field H which opposes the applied field. Thus the level of magnetization which is achieved is lower than that expected from the true permeability of the core material. The "effective" permeability  $\mu_e$  is lower than the true permeability  $\mu$ , and is given approximately by the formula

$$\frac{1}{\mu_e} = \frac{1}{\mu} + \frac{n}{4\pi} \quad (2)$$

where the parameter  $n/4\pi$  is called the demagnetization factor and depends on the  $l/d$  of the core. Table 1 gives typical values of  $n/4\pi$  for cylindrical cores of various  $l/d$  ratios, taken from Reference 1.

Table 1  
Demagnetizing Factor for Rods of Various  $l/d$  Ratio

<u><math>l/d</math></u>	<u><math>n/4\pi</math></u>
0	1.0
1	.27
2	.14
5	.040
10	.0172
20	.00617
50	.00129
100	.00036
200	.000090
500	.000014
1000	.0000036
2000	.0000009

The numbers given in this table are strictly valid for computing the flux density at the midpoint of the core, not the average over the entire core. The purpose in quoting them here is to make the point that the  $l/d$  ratio is a dominating factor in electromagnet design. As  $l/d$  becomes large the demagnetizing factor approaches zero and  $\mu_e$  approaches  $\mu$ .

It is desirable to have  $\mu_e$  large to minimize the required magnetizing force since

$$B_{Av} = \mu_e H_{\text{solenoid}} = 1.257 \mu_e \frac{NI}{l} \quad (3)$$

But with  $\mu_e$  in the range of  $10^5$  to  $10^6$  the core would be very responsive to the earth's field itself ( $\sim .3$  oersted at HEAO altitude), developing saturation dipole from the earth's field alone. This would interfere drastically with actual control dipole generation. It seems desirable to limit induced dipoles

to about 1% of the control dipoles. This is roughly achieved by limiting  $\mu_e$  to 1000 as a maximum. If we use an  $l/d$  of 80 for design purposes, then the demagnetizing factor can be found by interpolation from Table 1,  $n/4\pi = .0004$  and the desired true permeability can be calculated from Equation (2)

$$\frac{1}{\mu} = \frac{1}{\mu_e} - \frac{n}{4\pi} = \frac{1}{1000} - .0004 = .0006 \quad (4)$$

$$\mu = 1670 \quad (5)$$

If a material with  $\mu = 10,000$  is selected, then the effective permeability at  $l/d = 80$  would be

$$\frac{1}{\mu_e} = \frac{1}{\mu} + \frac{n}{4\pi} = \frac{1}{10,000} + .0004 = .0005 \quad (6)$$

$$\mu_e = 2000 \quad (7)$$

If  $\mu = \infty$ ,  $\mu_e = 2500$ . clearly the choice of  $l/d = 80$  has made  $\mu_e$  relatively insensitive to the true permeability above  $\mu = 2000$ . Any material with  $\mu = 1670$  or greater can be used for a core material.

Table 2 presents the physical characteristics of several popular ferromagnetic materials with sufficient permeability to meet the present requirements (from Reference 1).

Table 2

## Physical Properties of Some Ferromagnetic Materials

Name	Alloy (remainder Fe)	Density g/cm <sup>3</sup>	H <sub>c</sub> oersted	B <sub>MAX</sub> gauss
Iron		7.88	1.0	21,500
Silicon-iron		7.65	.5	19,700
45 permalloy	45Ni	8.17	.3	16,000
Hypernik	50Ni	8.25	.05	16,000
4-79 Permalloy	4Mo, 79Ni	8.72	.05	8,700
Mumetal	5Cu, 2Cr, 77Ni	8.58	.05	6,500
Permendur	50Co	8.3	2.0	24,500
AEM 4750	48Ni	8.2	.04	16,000

The weight of the final core is proportional to the density. The range of densities indicated above is fairly narrow, with silicon-iron the best. The high iron alloys show high B<sub>MAX</sub>, a desirable aspect to minimize weight. In this respect pure iron and permendur look most attractive. However, both have fairly large values of coercive force, H<sub>c</sub>. This implies significant residual magnetization at zero applied field and significant hysteresis. Hysteresis introduces some "indeterminacy" in the dipole moment since the resultant dipole is not exactly related to the instantaneous applied field. Too much indeterminacy would create control system problems.

Considering materials with low H<sub>c</sub> and high B<sub>max</sub>, iron and AEM 4750 look attractive.

Measurements of cylindrical cores of iron (actually Armco magnetic ingot iron) both before and after heat treatment, and AEM 4750 are given in Figure 1. The heat-treated iron shows a slight advantage in maximum flux density but the rather large hysteresis of 10% as compared to about 1 to 2%

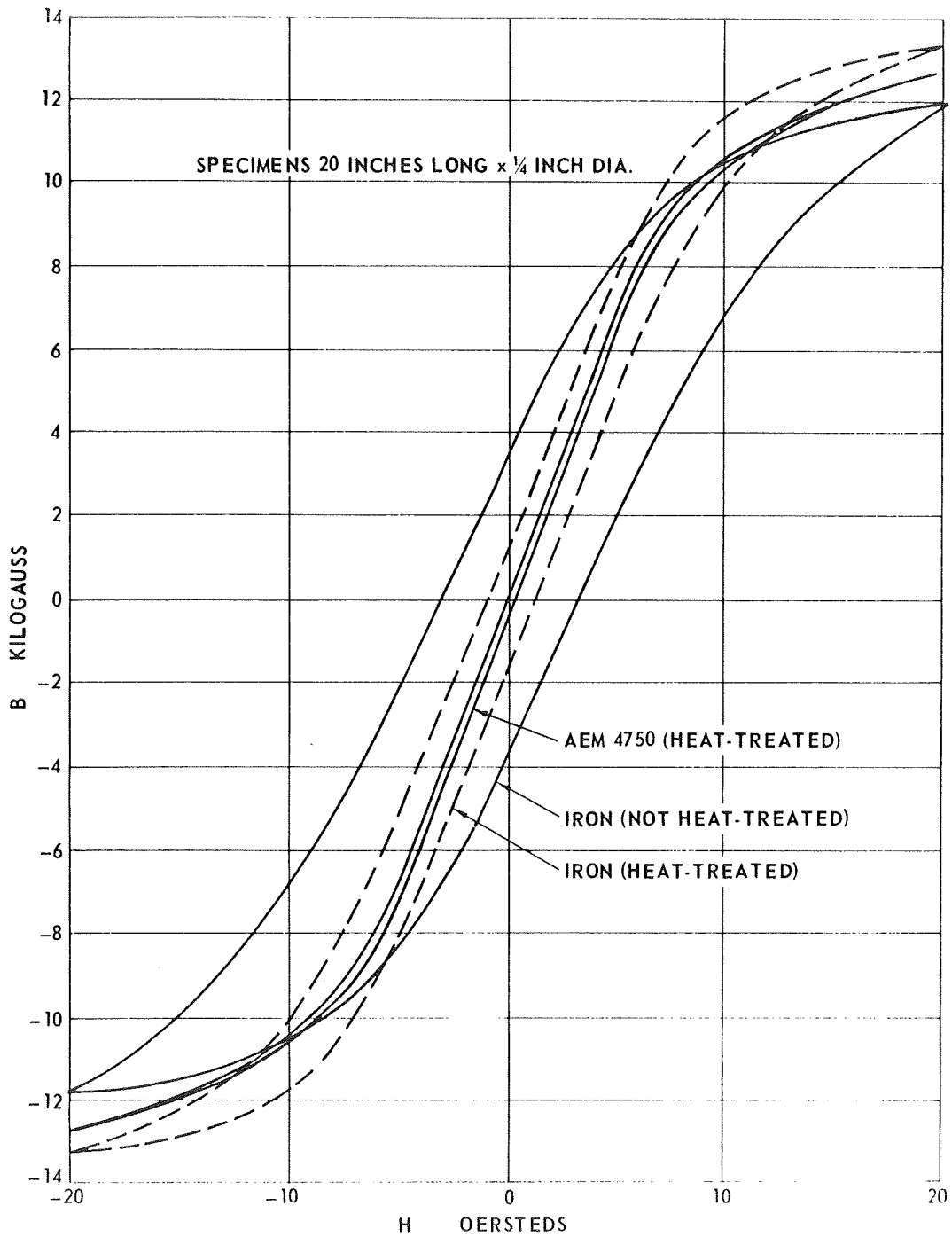


Fig. A-1 ELECTROMAGNET DESIGN COMPARISON OF CORE MATERIALS

for AEM 4750 makes the later more attractive for the present application.

Note that the maximum flux density achieved in these cores at  $H = 20$  oersteds is only 60-70% of the theoretical maxima listed in Table 2. In order to reach the peak flux density excessive values of magnetizing force would be required. This is indicated by the drop in the slope of  $B$  vs  $H$  around  $H = 10$  oersteds. We are in the region of diminishing returns — greater  $B$  can be obtained only with investment of more power and/or weight in the magnetizing solenoid.

#### Choice of Core Material

On the basis of low hysteresis and high  $B_{MAX}$  an alloy with 48 to 50% nickel, remainder iron, is recommended for HEAO control dipole electromagnets. A commercially available alloy of this type is AEM 4750 made by the Allegheny-Ludlum Steel Corp. This must be heat-treated in dry hydrogen to develop optimum properties. For long cores the availability of adequate size oven facilities may be a problem.

### Solenoid Design

The electrical power dissipated in the solenoid is

$$P = I^2 R \quad (8)$$

$$= I^2 r N \pi \left( \frac{d}{100} \right) \quad (9)$$

and the solenoid weight is

$$Wt = N \pi \left( \frac{d}{100} \right) w \quad (10)$$

The magnetizing force in the solenoid is given by

$$H = 1.257 \frac{NI}{\ell} \quad (11)$$

which can be rearranged to give

$$I = \frac{H\ell}{1.257N} \quad (12)$$

Using (8) and (10) the power-wt product is

$$PxWt = I^2 r w \left( \frac{N\pi d}{100} \right)^2 \quad (13)$$

and using (12) gives

$$PxWt = \left( \frac{H\ell}{1.257} \right)^2 r w \left( \frac{\pi d}{100} \right)^2 \quad (14)$$

Now the core diameter is related to the core volume by the expression

$$d = \sqrt[3]{\frac{4V}{\pi(\ell/d)}} \quad (15)$$



and

$$l = \left(\frac{l}{d}\right) d \quad (16)$$

Using (15) and (16) in eq. 14 yields the expression

$$P_x W_t = \left(\frac{\pi}{1.257}\right)^2 \left(\frac{4}{\pi}\right)^{4/3} r w H^2 \left(\frac{l}{d}\right)^{2/3} V^{4/3} \times 10^{-4} \quad (17)$$

The product  $r w$  is minimized by choosing aluminum wire, in which case  $r w = 170 \times 10^{-6}$  ohm-lbs/meter<sup>2</sup>

For the parameters selected here,  $H = 20$  oersted and  $l/d = 80$ , eq. (17) becomes

$$P_x W_t = 108.9 \times 10^{-5} V^{4/3} \quad \text{watt-lbs} \quad (18)$$

This expression gives the power-weight product for the sole-noid to drive the electromagnet core. The weight of the core must be added to get the total weight for the electromagnet.

#### Example

For  $M = 10^3$  amp-turn-m<sup>2</sup> and  $B_{MAX} = 12,000$  gauss

$$V = \frac{4\pi M \times 10^3}{B} = \frac{4\pi \times 10^6}{12,000} \cong 10^3 \text{ cm}^3$$

Therefore

$$V^{4/3} = 10^4$$

Therefore, from eq. (18)

$$P_x W_t = 108.9 \times 10^{-5} V^{4/3} = 10.89 \text{ watt-lbs.}$$

The core weight is

$$W_{t \text{ core}} = \rho V = 8.2 \times 10^3 \text{ grams} = 18.1 \text{ lbs.}$$

If we energize the electromagnet with 10 watts the solenoid weight would be 1.09 lbs. Therefore the total electromagnet weight is

Core	18.1 lbs.
Solenoid	<u>1.09 lbs</u>
Total	19.2 lbs.

This is about 1/2 the weight of the 9 ft. air coil design and comparable with the air coil design on a 30'x100' rectangle (assuming 10 watts of power). With greater power allotment the air coil designs are proportionally lighter - this is not the case for the electromagnet design since only about 1 lb out of a total of 19 lbs is involved in the constant power wt product. That is, even with infinite electric power the electromagnet weight would be 18.1 lbs, whereas the air coil weight would be reduced to nil.

For the HEAO application the electromagnet design for  $10^3$  amp-turn-meter<sup>2</sup> dipole is the better choice from a minimum power-weight standpoint for the Y axis dipole. It could be used for all three axes if desired.

Reference: 1 Bozorth, R. M.: "Ferromagnetism", D. Van Nostrand Company Inc., 1951.

APPENDIX B

Mathematical Model of the Earth's Magnetic Field

This appendix briefly describes the mathematical model for earth's magnetic field and MAGGY 4 which is a Fortran IV subroutine currently used by JHU/APL for computing the geomagnetic field vector at a particular location along a satellite trajectory.

The geomagnetic field is expressed as a series of solid spherical harmonics and their derivatives in geocentric spherical coordinates. The geomagnetic potential  $\underline{V}$  and field components are described by

$$\underline{V} = a \sum_{n=1}^{n=8} \sum_{m=0}^{m=n} \left( \frac{a}{r} \right)^{n+1} \cdot \left[ \frac{g_n^m}{r} \cos m\lambda + \frac{h_n^m}{r} \sin m\lambda \right] P_n^m(\cos\theta)$$

$$\underline{X} = \frac{1}{r} \frac{\partial \underline{V}}{\partial \theta} = \sum_{n=1}^{n=8} \sum_{m=0}^{m=n} \left( \frac{a}{r} \right)^{n+2} \cdot \left[ \frac{g_n^m}{r} \cos m\lambda + \frac{h_n^m}{r} \sin m\lambda \right] \frac{d}{d\theta} P_n^m(\cos\theta)$$

$$\underline{Y} = \frac{-1}{r \sin \theta} \frac{\partial \underline{V}}{\partial \lambda} = \sum_{n=1}^{n=8} \sum_{m=0}^{m=n} \left( \frac{a}{r} \right)^{n+2} \frac{-m}{\sin \theta} \cdot \left[ -\frac{g_n^m}{r} \sin m\lambda + \frac{h_n^m}{r} \cos m\lambda \right] P_n^m(\cos\theta)$$

$$\underline{Z} = \frac{\partial V}{\partial \underline{r}} = \sum_{\underline{n}=1}^{\underline{n}=8} \sum_{\underline{m}=0}^{\underline{m}=\underline{n}} - (\underline{n} + 1) \frac{a}{\underline{r}}^{n+2}$$

$$\cdot \left[ \underline{g}_{\underline{n}}^{\underline{m}} \cos \underline{m} \lambda + \underline{h}_{\underline{n}}^{\underline{m}} \sin \underline{m} \lambda \right] \underline{P}_{\underline{n}}^{\underline{m}} (\cos \theta)$$

where  $\underline{X}$ ,  $\underline{Y}$  and  $\underline{Z}$  represent, respectively, the northward, eastward, and downward components of the intensity in geocentric coordinates;  $a$ , the radius of the reference sphere;  $\underline{r}$ , the radial distance from the center of the reference sphere;  $\theta$ , the colatitude, or  $90^\circ - \beta$  where  $\beta$  is the latitude;  $\lambda$  the east longitude measured from greenwich;

$$\underline{P}_{\underline{n}}^{\underline{m}} (\cos \theta),$$

an associated Legendre function of degree  $\underline{n}$  and order  $\underline{m}$  and of the Schmidt quasi-normalized type; and

$$\underline{g}_{\underline{n}}^{\underline{m}} \quad \text{and} \quad \underline{h}_{\underline{n}}^{\underline{m}},$$

spherical harmonic coefficients.

The coefficients are defined for an epoch,  $\underline{t}_0$  and the value of a harmonic coefficient for another time  $\underline{t}$  is obtained from

$$\underline{C}_{\underline{n}}^{\underline{m}} (\underline{t}) = \underline{C}_{\underline{n}}^{\underline{m}} (\underline{t}_0) + \dot{\underline{C}}_{\underline{n}}^{\underline{m}} (\underline{t} - \underline{t}_0)$$

where  $\dot{\underline{C}}_{\underline{n}}^{\underline{m}}$  equals the secular change of the coefficient in gammas/year ( $1 \gamma = 10^{-5}$  gauss).

MAGGY 4 currently includes coefficients for a 7th order, 7th degree spherical harmonic expansion, defined by Cain 1964, with an epoch  $\underline{t}_0 = 1960$ . Inputs and outputs for using the subroutine are included in the listing. It is noted that the coefficients  $G(*,*)$ ,  $H(*,*)$ ,  $GT(*,*)$  and  $HT(*,*)$  in the listing are related to the spherical harmonic coefficients by

$$\underline{g}_n^m = G(\underline{n+1}, \underline{m+1})$$

$$\underline{h}_n^m = H(\underline{n+1}, \underline{m+1})$$

$$\underline{g}_n^m = GT(\underline{n+1}, \underline{m+1})$$

$$\underline{h}_n^m = HT(\underline{n+1}, \underline{m+1})$$

At an open meeting in Washington, D.C., on October 24, 1968, the IAGA Commission 2 Working Group No. 4 chose the International Geomagnetic Reference Field (IGRF) 1965.0. The reference field was endorsed by the International Association of Geomagnetism and Aeronomy (IAGA) World Magnetic Survey Board on October 28, 1968, and by the IAGA Executive Committee in February 1969. Table I shows the IGRF coefficients, which apply to the period 1955.0 - 1972.0. For dates after the epoch 1972.0, recommendations will be made at the XV General Assembly of the International Union of Geodesy and Geophysics (IUGG) in 1971; future modifications of the IGRF are likely to apply only to the secular change coefficients. A Fortran program to compute field values from the IGRF 1965.0 is obtainable from the U.S. National Space Science Data Center, NASA Goddard Space Flight Center, Greenbelt, Maryland, USA, 20771; the Institute of Geological Sciences, Royal Greenwich Observatory, Herstmonceux Castle, Hailsham, Sussex, England; or the World Data Center A for Geomagnetism, U.S. Coast and Geodetic Survey - ESSA, Rockville, Maryland, USA, 20852.

TABLE I  
IGRF 1965.0 COEFFICIENTS

$\underline{n}$	$\underline{m}$	Main field ( $\delta$ )		Secular change ( $\delta/\text{yr}$ )	
		$\underline{g}^{\underline{m}}_{\underline{n}}$	$\underline{h}^{\underline{m}}_{\underline{n}}$	$\underline{\dot{g}}^{\underline{m}}_{\underline{n}}$	$\underline{\dot{h}}^{\underline{m}}_{\underline{n}}$
1	0	-30339		15.3	
1	1	-2123	5758	8.7	-2.3
2	0	-1654		-24.4	
2	1	2994	-2006	0.3	-11.8
2	2	1567	130	-1.6	-16.7
3	0	1297		0.2	
3	1	-2036	-403	-10.8	4.2
3	2	1289	242	0.7	0.7
3	3	843	-176	-3.8	-7.7
4	0	958		-0.7	
4	1	805	149	0.2	-0.1
4	2	492	-280	-3.0	1.6
4	3	-392	8	-0.1	2.9
4	4	256	-265	-2.1	-4.2
5	0	-223		1.9	
5	1	357	16	1.1	2.3
5	2	246	125	2.9	1.7
5	3	-26	-123	0.6	-2.4
5	4	-161	-107	0.0	0.8
5	5	-51	77	1.3	-0.3
6	0	47		-0.1	
6	1	60	-14	-0.3	-0.9
6	2	4	106	1.1	-0.4
6	3	-229	68	1.9	2.0
6	4	3	-32	-0.4	-1.1
6	5	-4	-10	-0.4	0.1
6	6	-112	-13	-0.2	0.9
7	0	71		-0.5	
7	1	-54	-57	-0.3	-1.1
7	2	0	-27	-0.7	0.3
7	3	12	-8	-0.5	0.4
7	4	-25	9	0.3	0.2
7	5	-9	23	0.0	0.4
7	6	13	-19	-0.2	0.2
7	7	-2	-17	0.6	0.3
8	0	10		0.1	
8	1	9	3	0.4	0.1
8	2	-3	-13	0.6	-0.2
8	3	-12	5	0.0	-0.3
8	4	-4	-17	0.0	-0.2
8	5	7	4	-0.1	-0.3
8	6	-5	22	0.3	-0.4
8	7	12	-3	-0.3	-0.3
8	8	6	-16	-0.5	-0.3

	SUBROUTINE MAGGY4(DLAT,DLONG,ALT,TM,NMAX,L,	
	1BN,BE,BV,B)	20020
	DIMENSION SP(25),CP(25)	40010
	DIMENSION AID(11),FM(25)	40020
	DIMENSION FN(25),H(25,25)	40030
	DIMENSION G(25,25),P(25,25)	40040
	DIMENSION DP(25,25),CONST(25,25)	40050
	DIMENSION SHMIT(25,25),HT(25,25)	40060
	DIMENSION GT(25,25),HTT(25,25)	40070
	DIMENSION GTT(25,25),TH(25,25)	40080
	DIMENSION TG(25,25)	40090
	DOUBLE PRECISION A,G,H, P,R,T,AR,A2,A4,B2,CP,CT,DP,FM,FN,GT,	
	1HT,SP,ST,TG,TH,AOR,GTT,HTT,PNM,RAD,A2B2,A4B4,FLAT, RLAT,TEMP,	
	?CONST, RLONG,SHMIT,SINLA,TLAST,TZERO,AID,AA,BB,CC,DD,EE,FF	
C	MAGGY	70010
C	GEOMAGNETIC FIELD USING ANY NO. OF COEFFICIENTS	70020
C	INPUTS- DLAT= GEOCENTRIC LATITUDE (DEG)	70030
C	DLONG= GEOCENTRIC LONGITUDE (DEG)	70040
C	ALT= ALTITUDE(KM)	70050
C	TM= EPOCH REQUESTED( 1964.0 ETC.)	70060
C	NMAX= TERMS FACTOR ,COMPUTED EXTERNALLY BY-	70070
C	SQRTF(NO. OF DESIRED TERMS +ONE)	70080
C	L=COUNTER (SET TO 1 ON FIRST PASS)	70090
C	RESETS TO ZERO INTERNALLY	70100
C	OUTPUTS- BN= NORTH GEOC COMP OF FIELD (GAM)	70110
C	BE= EAST GEOC COMP OF FIELD (GAM)	70120
C	BV= VERTICAL GEOC COMP OF FIELD (GAM)	70130
C	B= TOTAL FIELD (GAM)	70140
	IF(L)9,9,1	
1	P(1,1)=1.	70160
	DP(1,1)=0.	70170
	SP(1)=0.	70180
	CP(1)=1.	70190
	RAD=57.295779513E0	70200
	A=6378.388	70210
	FLAT=1.-1./297.	70220
	A2=A**2	70230
	A4=A**4	70240
	B2=(A*FLAT)**2	70250
	A2B2=A2*(1.-FLAT**2)	70260
	A4B4=A4*(1.-FLAT**4)	70270
	CONST(2,1)=0.	70280
	CONST(2,2)=0.0	70290
	SHMIT(1,1)=-1.	70300
	DO 20 N=2,25	70310
	AA=2*N-3	
	BB=N-1	
	SHMIT(N,1)=SHMIT(N-1,1)*AA/BB	
	FN(N)=N	70330
	J=2	70340
	DO 20 M=2,N	70350
	CC=(N-M+1)*J	
	DD=N+M-2	
	SHMIT(N,M)=SHMIT(N,M-1)*DSQRT(CC/DD)	
20	J=1	70370
	DO 4 N=3,25	70380
	DO 4 M=1,N	70390
	FM(M)=M-1	70400
	FF=(N-2)**2-(M-1)**2	

EE=(2*N-3)*(2*N-5)	
4 CONST(N,M)=FF/EE	
9 IF (L)33,15,14	70420
15 IF (TM-TLAST)16,33,16	70430
14 TZERO=1960.0	70440
G(2,1)=-30431.1677E0	70450
G(2,2)=-2168.5602E0	70460
G(3,1)=-1535.8992E0	70470
G(3,2)=3000.3560E0	70480
G(3,3)=1571.9844E0	70490
G(4,1)=1313.1700E0	70500
G(4,2)=-2007.1055E0	70510
G(4,3)=1273.7626E0	70520
G(4,4)=879.6341	70530
G(5,1)=959.9695	70540
G(5,2)=797.8550	70550
G(5,3)=528.8060	70560
G(5,4)=-401.5577	70570
G(5,5)=271.8373	70580
G(6,1)=-242.0779	70590
G(6,2)=351.0913	70600
G(6,3)=226.4390	70610
G(6,4)=-29.6936	70620
G(6,5)=-143.7561	70630
G(6,6)=-79.8440	70640
G(7,1)=56.1731	70650
G(7,2)=73.4141	70660
G(7,3)=25.5949	70670
G(7,4)=-245.0623	70680
G(7,5)=-22.7866	70690
G(7,6)=-2.0980	70700
G(7,7)=-101.3779	70710
G(8,1)=90.7012	70720
G(8,2)=-49.7688	70730
G(8,3)=-5.5133	70740
G(8,4)=-24.2855	70750
G(8,5)=-9.9574	70760
G(8,6)=26.1497	70770
G(8,7)=6.1757	70780
G(8,8)=7.4069	70790
H(2,1)=0.	70800
H(2,2)=5764.0044E0	70810
H(3,1)=0.	70820
H(3,2)=-1950.0813E0	70830
H(3,3)=203.8712	70840
H(4,1)=0.	70850
H(4,2)=-439.5842	70860
H(4,3)=227.8224	70870
H(4,4)=-114.8944	70880
H(5,1)=0.	70890
H(5,2)=145.4854	70900
H(5,3)=-264.5039	70910
H(5,4)=-6.2607	70920
H(5,5)=-261.2573	70930
H(6,1)=0.	70940
H(6,2)=4.4806	70950
H(6,3)=126.4217	70960
H(6,4)=-103.5507	70970
H(6,5)=-97.3879	70980
H(6,6)=76.9685	70990



H(7,1)=0.	71000
H(7,2)=4.4359	71010
H(7,3)=80.6407	71020
H(7,4)=57.5413	71030
H(7,5)=-18.5516	71040
H(7,6)=-26.1826	71050
H(7,7)=5.3850	71060
H(8,1)=0.	71070
H(8,2)=-50.2589	71080
H(8,3)=-19.6576	71090
H(8,4)=6.2982	71100
H(8,5)=-35.5520	71110
H(8,6)=44.6752	71120
H(8,7)=-2.9338	71130
H(8,8)=-28.0237	71140
GT(2,1)=18.9341	71150
GT(2,2)=7.9063	71160
GT(3,1)=-24.0446	71170
GT(3,2)=-1.1733	71180
GT(3,3)=0.5387	71190
GT(4,1)=-1.2708	71200
GT(4,2)=-9.6570	71210
GT(4,3)=3.5994	71220
GT(4,4)=-1.8400	71230
GT(5,1)=0.8248	71240
GT(5,2)=5.6813	71250
GT(5,3)=-1.5957	71260
GT(5,4)=-0.3781	71270
GT(5,5)=0.4671	71280
GT(6,1)=3.6941	71290
GT(6,2)=-0.7427	71300
GT(6,3)=2.0015	71310
GT(6,4)=0.8213	71320
GT(6,5)=0.1702	71330
GT(6,6)=1.4983	71340
GT(7,1)=0.	71350
GT(7,2)=0.	71360
GT(7,3)=0.	71370
GT(7,4)=0.	71380
GT(7,5)=0.	71390
GT(7,6)=0.	71400
GT(7,7)=0.	71410
GT(8,1)=0.	71420
GT(8,2)=0.	71430
GT(8,3)=0.	71440
GT(8,4)=0.	71450
GT(8,5)=0.	71460
GT(8,6)=0.	71470
GT(8,7)=0.	71480
GT(8,8)=0.	71490
HT(2,1)=0.	71500
HT(2,2)=-1.3255	71510
HT(3,1)=0.	71520
HT(3,2)=-14.0029	71530
HT(3,3)=-17.4896	71540
HT(4,1)=0.	71550
HT(4,2)=2.2619	71560
HT(4,3)=3.3159	71570
HT(4,4)=-8.3190	71580
HT(5,1)=0.	71590

HT(5,2)=-1.1373	71600
HT(5,3)=-1.6846	71610
HT(5,4)=3.0572	71620
HT(5,5)=-5.2945	71630
HT(6,1)=0.	71640
HT(6,2)=1.9383	71650
HT(6,3)=3.1031	71660
HT(6,4)=-0.9935	71670
HT(6,5)=-0.5116	71680
HT(6,6)=0.0682	71690
HT(7,1)=0.	71700
HT(7,2)=0.	71710
HT(7,3)=0.	71720
HT(7,4)=0.	71730
HT(7,5)=0.	71740
HT(7,6)=0.	71750
HT(7,7)=0.	71760
HT(8,1)=0.	71770
HT(8,2)=0.	71780
HT(8,3)=0.	71790
HT(8,4)=0.	71800
HT(8,5)=0.	71810
HT(8,6)=0.	71820
HT(8,7)=0.	71830
HT(8,8)=0.	71840
MAXN=NMAX	71850
29 L=0	71860
31 DO 32 N=2, MAXN	71870
DO 32 M=1, N	71880
G(N, M)=G(N, M)*SHMIT(N, M)	71890
H(N, M)=H(N, M)*SHMIT(N, M)	71900
GT(N, M)=GT(N, M)*SHMIT(N, M)	71910
32 HT(N, M)=HT(N, M)*SHMIT(N, M)	71920
16 T=TM-TZERO	71930
DO 22 N=2, NMAX	71940
DO 22 M=1, N	71950
TG(N, M)=G(N, M)+(GT(N, M))*T	71960
22 TH(N, M)=H(N, M)+(HT(N, M))*T	71970
TLAST=TM	71980
33 RLAT=DLAT/RAD	71990
SINLA=DSIN(RLAT)	7200
RLONG=DLONG/RAD	72010
CP(2)=DCOS(RLONG)	7202
SP(2)=DSIN(RLONG)	7203
DO 10 M=3, NMAX	72040
SP(M)=SP(2)*CP(M-1)+CP(2)*SP(M-1)	72050
10 CP(M)=CP(2)*CP(M-1)-SP(2)*SP(M-1)	72060
18 R=ALT+6371.2	72070
CT=SINLA	72080
21 ST=DSQRT(1.0-CT**2)	7209
AOR=6371.2/R	72100
AR=AOR**2	72110
RN=0.	72120
BE=0.	72130
BV=0.	72140
DO 54 N=2, NMAX	72150
AR=AOR*AR	72160
DO 54 M=1, N	72170
IF (N-M)12, 11, 12	72180
11 P(N, N)=ST*P(N-1, N-1)	72190

	DP(N,N)=ST*DP(N-1,N-1)+CT*P(N-1,N-1)	72200
	GO TO 13	72210
12	P(N,M)=CT*P(N-1,M)-CONST(N,M)*P(N-2,M)	72220
	DP(N,M)=CT*DP(N-1,M)-ST*P(N-1,M)-CONST(N,M)*DP(N-2,M)	72230
13	PNM=P(N,M)*AR	72240
	TEMP=TG(N,M)*CP(M)+TH(N,M)*SP(M)	72250
	BN=BN-TEMP*DP(N,M)*AR	72260
	BE=BE-(TG(N,M)*SP(M)-TH(N,M)*CP(M))*FM(M)*PNM/ST	72270
	BV=BV+TEMP*FN(N)*PNM	72280
54	CONTINUE	72290
	B=SQRT(BN**2+BE**2+BV**2)	72300
23	RETURN	72310
	END	72320

## APPENDIX C

### Computer Program for HEAO-A Simulation

This appendix briefly describes the computer program used by JHU/APL for exact simulation of HEAO dynamics. The program itself is written in a specialized digital simulation language (DSL/91) which allows control of the program while it is in execution plus concurrent display (in analog and digital form) of system performance. Except for specialized interactive call statements the programming language is similar to FORTRAN IV.

The HEAO digital simulation simultaneously accounts for orbital motion of the spacecraft, evaluation of earth's magnetic field vector using a 48 term expansion of the geomagnetic potential, and exact rotational dynamics of the spacecraft. The program is the result of a long evolution of spacecraft dynamical simulations performed at APL. Therefore the spacecraft orbital and attitude equations of motion are exact and general in nature. Modifications to the general program for HEAO included only those transformations necessary to display spacecraft attitude in an ecliptic coordinate frame and the logic required for all interactive features. A new subroutine called ALGOR was added which generates the spacecraft magnetic dipole moments as determined by the control system algorithms.

Eulers dynamical equations are used for determination of the instantaneous angular accelerations about a set of principal axes. Spacecraft attitude is established by a 3x3 matrix  $\underline{A}$  whose elements are the direction cosines between spacecraft fixed axes and an inertial reference. Rates of change of the elements of this matrix are given by

$$\dot{\underline{A}} = - \underline{\omega} \underline{A}$$

where  $\underline{\omega}$  is the skew symmetric representation of the angular velocity vector  $\underline{\omega}$ . Integration of  $\dot{\underline{\omega}}$  and  $\dot{\underline{A}}$  provides for update

of angular rates and the attitude matrix. The orthogonality of A is established every time step.

The advantage of using the elements of the attitude matrix A as variables of integration rather than Euler angles is two-fold:

- 1) The zenith pointing problem is eliminated. This problem occurs when the spacecraft symmetry axis is aligned with the inertial reference system and rates of change of certain Euler angles approach infinity.
- 2) Outputs are rarely expressed by Euler angles directly but in terms of angles relative to an ecliptic or star reference frame. The attitude matrix A is involved in the transformation for generating these desired angles. Since A is an essential ingredient to the program and would be generated whether Euler angles were used or not, it is faster and more accurate.

For reference, a listing of the HEAO digital computer program follows:

INPUT FOR DSL/91 TRANSLATOR (VERSION 2)

```

TITLE ***      HEAD ATTITUDE SIMULATION IN DSL/91 BY B. TOSSMAN ***
*
STORAG DAVAR(8),KDAC(8),IDAC(8),DASF(8),INDX(8),TYC(12),TCNTRL(3),    ...    00000300
      XREF(3),YREF(3),ZREF(3),    ...
      HSPA(3),USPA(3),SSPA(3),TDES(3),ERRV(6),ECLNM(3)
* -----    00001300
*    00001400
INTGER I,J,K,ISAT,IDAY,IYR,ISTART,ISTOP,NYR,IHR,KDAY,L,NMAX,NTERMS,    ...
      JDAYP,IDAC,MIN,INDX,INITLP,INITSW,J4,J5,IGATE,NCALLS,IMODE,    ...
      ITSTOP,ITSTRT,IMRK,ICHNL,ISTRAN,ISWTCH,ISW1,ISW2,ISW3,ISW4,    ...
      ISEED,ISTRT,KDAC,ICDEF,JCOEF,MODE,IALGOR,IDELT,J8,ICL,IRSW,    ...
      MODWHL
* -----    00001900
*    00002000
CONTRL DFLT =4.0,DELMIN =3.,DELMAX =8.0,DELS =72.,DELNIX =300.,    ...
      DELSTP= 36.0
TABLE KDAC(1-8)= 8*+16384,ERRV(1-6) = 6*0.0
* -----    00002300
*    00002400
CONST PIE=3.1415927,PI2=6.2831853,RPD=0.01745329,OSE=7.2921157E-05,    ...
      RE=6378.166,CON=1.0E-05,DPR=57.29578,TAU=806.80947,    ...
      GM=3.986329E+20,CGSCON=1.3558E+7,ERFAC=1.0E+07,    ...
      NMAX=7,NTERMS=48,TAUKS=1.23945,RADTAU=16.297867E-5,    ...
      TAUKSF=1.23945,XCALLS=3.0
* -----    00003000
*    00003100
PARAM ISAT= 19730,IYR= 68,IM= 1968.0,STRDAY= 357.0,TSTOP= 0.0,    ...
      XDAY = 0.0,XNLOOP = 4.00,TSTART=0.0,    ...
      CXX= 36920.,CYY= 3992.,CZZ= 35187.,HWFHFL= 1000.,    ...
      CMXMAX= 1.0E+6,CMYMAX= 1.0E+6,CMZMAX= 1.0E+6,ALPHA0= 35.0,    ...
      WXD= 0.20,ERRT0= 0.75,HREMAX= 0.,AREMAX= 0.,WREMAX= 0.,    ...
      ERRK11= 0.0,ERRK12= 0.0,ERRK13= 0.0,ERRK14= 0.0,    ...
      ERRK15= 0.0,ERRK16= 31.4,ERRK21= 9.84,ERRK22= 6.84,    ...
      ERRK23=1.790,ERRK24=147.0,ERRK25= 0.0,ERRK26= 0.0,    ...
      ERRK31=1.790,ERRK32=391.3,ERRK33=-9.84,ERRK34=0.769,    ...
      ERRK35= 0.0,ERRK36= 0.0,    ...
      DAF1= 0.100,DAF2= 0.500,DAF3= 1.000,DAF4= 1.000,    ...
      DAF5=1.25E6,DAF6=1.25E6,DAF7=1.25E6,DAF8= 25.00,ISEED=0
* -----    00004400
*    00004500
INCON ROLLO= 0.0,PITCH0= 0.,YAW0=0.,OMEXC=0.0, OMEYC=0.,OMEZO=0.,    ...
      XNDX1 = 286.0,XNDX2 =289.0,XNDX3=287.0,XNDX4= 288.0,    ...
      XNDX5 = 268.0,XNDX6 =269.0,XNDX7=270.0,XNDX8= 278.0,    ...
      STRADE=100.000,SWTCHS=1112.01,HXBIAS= 0.,HYBIAS= 0.,HZBIAS= 0.,    ...
      WXDES= 0.00,PX= 0.,PY= 0.,PZ= 0.,AL=1.058069 ,CZIN= 28.5,    ...
      CAPO=0.,CRANO=180.0,EC=0.,CTP=0.0,DBSWX=0.0,DBSWY=0.0,    ...
      DBSWZ=0.0,CLALMD=11.0,TQLIM=0.0,XNTRCP=6181.8,YNTRCP=7.65E-2,    ...
      PCWM=0.50,TXBIAS=0.0,TYBIAS=0.0,TZBIAS=0.0
* -----    00005000
*    00005100
INTEG SIMP    00005200
* -----    00005300
ONLINE
*

```

```

ASSIGN A(ELPSTM,DELT,DBSWX,DBSWY,DBSWZ,STRDAY,CLALMD,ALPHAC,ERRTD,
      WXD),
      B(ROLLC,PITCHC,YAWC,CMEXC,CMEYC,CMEZC,STRAD,HWHEEL,WXDES,
      SWTCHS),
      C(ERRK15,ERRK16,ERRK21,ERRK22,ERRK23,ERRK24,ERRK31,ERRK32,
      ERRK33,ERRK34),
      D(CRAND,DAF1,DAF2,DAF3,DAF4,DAF5,DAF6,DAF7,DAF8),
      E(TOTERR,CMXMAX,CMYMAX,CMZMAX,HXBIAS,HYBIAS,HZBIAS,HREMAX,
      AREMAX,WREMAX)
* ----- 00005400
* 00006300
* 00006400
EXCLUDE I,J,K,IMRK,ISWTCH,ISW1,ISW2,ISW3,ISW4,ICDEF,JCDEF,ISTRAN,IMODE
* ----- 00006700
* 00006800
D DIMENSION UBOD(3),TTOR(3),AROD(3,3)
D DIMENSION HBOD(3),TMAG(3),TGRAV(3),C(9)
D DIMENSION ERRK(3,6),MTX(3,3),CURV(1)
D EQUIVALENCE (TIME , CURV(1))
* 00007100
* 00007700
INITIAL REGION 00007800
* 00008300
* 00009300
      IMODE = CLALMD+.01
* ICL IS THE NUMBER OF THE DESIRED CONTROL LAW
      ICL = IMODE/100
* IALGOR SWITCH - SELECTS CONTROL ALGORITHM
      IALGOR = (IMODE/10)-(ICL*10)
***** MODE SWITCH SELECTS POINTING MODE
* MODE=1 - X AXIS POINTED TO SUN
* MODE=2 - X AXIS POINTED TO STAR
* MODE=3 - Y AXIS POINTED TO STAR
* MODE=4 - Z AXIS POINTED TO STAR
      MODE = IMODE-(IMODE/10)*10
      ISWTCH = SWTCHS
      ISW1 = ISWTCH/10000
      ISW2 = (ISWTCH/1000)-(ISW1*10)
      ISW3 = (ISWTCH/100)-((ISWTCH/1000)*10)
      ISW4 = (ISWTCH/10)-((ISWTCH/100)*10)
      ISW5 = ISWTCH-((ISWTCH/10)*10)
      MODWHL = ISW1
      PMAGTQ = ISW2
      GRVTQ = ISW3
      CNTRLQ = ISW4
      INITLP = ISW5
      GO TO (5,10),INITLP

```





```

J4 = 24/IDELT
GO TO 12
11 IDELT = ((DELT*10.0)+.01)
J4 = 240/IDELT
12 XNLOOP = J4
L = 1
J8 = 1
RPMCDN = 30.0/PIE
ISTART = STRDAY+.01
ISTOP=ISTART+11
ITSTRT = TSTART
ITSTOP = TSTOP
KDAY=ISTART
YR=IYR+1900
NYR=IYR+1900
DAY=KDAY
DAYRUN=ISTOP-ISTART
TRUN=DAYRUN*86400.+TSTOP-TSTART
TIME=TSTART
TIMPST=TIME
TR=TIME
FINTIM=TRUN+TSTART
IHR=TIME/3600.
HR=IHR
MIN=TIME/60.-HR*60.
IDAY=XDAY
DDAY=0.1**IDAY
XHR=HR
IF(HR.LT.10.)XHR=HR+80.
XMIN=MIN
ELPSTM = DDAY*((XHR*1.0E-2)+(XMIN*1.0E-4))
NCALLS = XCALLS+.01
IGATE=J4*NCALLS
J5=IGATE
ZIN=CZIN*RPD
AP = CAPD*RPD
RAN=CRAND*RPD
TP=CTP*TAUKSF
JDAYP = STRDAY+.01
COEF=(+1.8027E-3*1.5)/(AL*(1.-EC**2))**2
TORB=84.489*AL*SQR(TAL)
ORTE=5.184E+5/TORB
CDAP=COEF*ORTE*(2.0-2.5*SIN(ZIN)**2)
CDRAN=-COEF*ORTE*COS(ZIN)
DAP=CDAP*RADTAU
DRAN=CDRAN*RADTAU
ORBCON=30.*TORB/PIE
* CONVERT MOMENTS OF INERTIA AND ROTOR MOMENTUM TO CGS UNITS
C24 = CXX*CGSCON
C25 = CYY*CGSCON
C26 = CZZ*CGSCON
HROTOR = HWHEEL*CGSCON
RTMOM = HWHEEL
IRSW = 0
RTORQ = 0.0

```

00016700

00017400

00017500

00017600

00017700

00017800

00017900

00018100

00018200

00018300

00018400

00018500

00018600

00018700

00018750

00018800

00018900

00019000

00019200

00020700

361

362

4

```

RMHGH = (1.0+PCWM)*HWHEEL
RMLDW = (1.0-PCWM)*HWHEEL
RMOM = HRDTR
SLOPE = -(YNTRCP/XNTRCP)
DESSPX = WXDES/RPMCON
COMPUTE DEAD BAND LIMITS
DO 27 I = 1,3
GO TO (20,21,22),I
20 ICDEF = DBSWX+.01
GO TO 23
21 ICDEF = DBSWY+.01
GO TO 23
22 ICDEF = DBSWZ+.01
23 JCOEF = ICDEF/100
ICDEF = ICDEF-(JCOEF*100)
ANGCOF = JCOEF
RTECOF = ICDEF
GO TO (24,25,26),I
24 DBXANG = ANGCOF*1.0E-2
DBXRTE = RTECOF*1.0E-5
GO TO 27
25 DBYANG = ANGCOF*1.0E-2
DBYRTE = RTECOF*1.0E-5
GO TO 27
26 DBZANG = ANGCOF*1.0E-2
DBZRTE = RTECOF*1.0E-5
27 CONTINUE

```

\* COMPUTE ALTITUDE OF A CIRCULAR ORBIT FOR GIVEN SEMI MAJOR AXIS

```

ALTKM = (AL-1.)*RE
ALTNMI = ALTKM*.53996
CALL GRNWH4(ISTART,IYR,GR)
SET L INDEX FOR USE IN MAGGY
NTERMS=NMAX**2-1

```

```

1206
00007900
00008000
00008100
00008200

```

```

NMAX=3 IMPLIES THAT NTERMS=8
NMAX=7 IMPLIES THAT NTERMS= 48

```

```

CALL MGFDC4(KDAY,IYR,TSTART,AL,EC,ZIN,AP,RAN,DAP,DRAN,JDAYP,TP,...
FLAT,FLDN,ALT,RK,ELDN,GR,TM,NMAX,L,HSPA,HTCT,CRAN,CAP,TA)
COMPUTE SUN RIGHT ASCENSION,DECLINATION IN INERTIAL SPACE
DAY = DAY + TSTART/86400.

```

```

CALL ALD4(DAY,IYR,RA,DE)

```

```

1233

```

```

COMPUTE NORMAL TO ECLIPTIC PLANE -- INCLINED 23(DEG)27(MIN)

```

```

ECLNM(1) = 0.
ECLNM(2) = -.39795
ECLNM(3) = .91741

```

```

1235
1236
1237

```

```

SSPA(1)=COS(DE)*COS(RA)
SSPA(2)=COS(DE)*SIN(RA)
SSPA(3)=SIN(DE)

```

```

COMPUTE STAR RIGHT ASC. AND DECL. FROM STRADE

```

```

ISTRAN = STRADE
ISTRAN = IABS(ISTRAN)
XSTRAN = ISTRAN
IF(STRADE.EQ.0.0)GO TO 13
DESGN = STRADE/ABS(STRADF)

```

```

      GO TO 14
13  DESGN = 1.0
**  SRA = STAR RIGHT ASCENSION
14  SRA = XSTRAN*RPD
**  SDE = STAR DECLINATION
      SDE= (STRADE-XSTRAN*DESGN)*100.0*RPD
      XRFF(1) = COS(SRA)*COS(SDE)
      XREF(2) = SIN(SRA)*COS(SDE)
      XREF(3) = SIN(SDE)
      DO 19 I=1,3
      YREF(I) = XREF(I)
19  ZREF(I) = XREF(I)
      CR = COS(ROLL0*RPD)
      SR = SIN(ROLL0*RPD)
      CP = COS(PITCH0*RPD)
      SP = SIN(PITCH0*RPD)
      CY = COS(YAW0*RPD)
      SY = SIN(YAW0*RPD)
***  SUB. AXGEN SETS UP LOCAL REF. AXES ACCORDING TO MODE SELECTION
      CALL AXGEN(MODE,SSPA,FCLNM,XREF,YREF,ZREF)
**  MTX = ATTITUDE MATRIX FOM LOCAL REF. AXES TO VEHICLE AXES
      GO TO (6,6,7,8),MODE
*   MATRIX TRANS. SEQUENCE IS ROLL,PITCH,YAW(FIRST TO LAST)
6   MTX(1,1) = CP*CY
      MTX(2,1) = -CP*SY
      MTX(3,1) = SP
      MTX(1,2) = CR*SY+SR*SP*CY
      MTX(2,2) = CR*CY-SR*SP*SY
      MTX(3,2) = -SR*CP
      MTX(1,3) = SR*SY-CR*SP*CY
      MTX(2,3) = SR*CY+CR*SP*SY
      MTX(3,3) = CR*CP
      GO TO 9
*   MATRIX TRANS. SEQUENCE IS PITCH,YAW,ROLL(FIRST TO LAST)
7   MTX(1,1) = CP*CY
      MTX(2,1) = SR*SP-CR*CP*SY
      MTX(3,1) = CR*SP+SR*CP*SY
      MTX(1,2) = SY
      MTX(2,2) = CR*CY
      MTX(3,2) = -SR*CY
      MTX(1,3) = -SP*CY
      MTX(2,3) = SR*CP+CR*SP*SY
      MTX(3,3) = CR*CP-SR*SP*SY
      GO TO 9
*   MATRIX TRANS. SEQUENCE IS YAW,PITCH,ROLL(FIRST TO LAST)
8   MTX(1,1) = CP*CY
      MTX(2,1) = -CR*SY + SR*SP*CY
      MTX(3,1) = SR*SY + CR*SP*CY
      MTX(1,2) = CP*SY
      MTX(2,2) = CR*CY + SR*SP*SY
      MTX(3,2) = -SR*CY + CR*SP*SY
      MTX(1,3) = -SP
      MTX(2,3) = SR*CP
      MTX(3,3) = CR*CP

```

```

9 CONTINUE
*** COMPUTE ABOD - ATTITUDE MATRIX FROM GEOCENTRIC FRAME TO VEH. AXES
ABOD(1,1)=MTX(1,1)*XREF(1)+MTX(1,2)*YREF(1)+MTX(1,3)*ZREF(1)
ABOD(1,2)=MTX(1,1)*XREF(2)+MTX(1,2)*YREF(2)+MTX(1,3)*ZREF(2)
ABOD(1,3)=MTX(1,1)*XREF(3)+MTX(1,2)*YREF(3)+MTX(1,3)*ZREF(3)
ABOD(2,1)=MTX(2,1)*XREF(1)+MTX(2,2)*YREF(1)+MTX(2,3)*ZREF(1)
ABOD(2,2)=MTX(2,1)*XREF(2)+MTX(2,2)*YREF(2)+MTX(2,3)*ZREF(2)
ABOD(2,3)=MTX(2,1)*XREF(3)+MTX(2,2)*YREF(3)+MTX(2,3)*ZREF(3)
ABOD(3,1)=MTX(3,1)*XREF(1)+MTX(3,2)*YREF(1)+MTX(3,3)*ZREF(1)
ABOD(3,2)=MTX(3,1)*XREF(2)+MTX(3,2)*YREF(2)+MTX(3,3)*ZREF(2)
ABOD(3,3)=MTX(3,1)*XREF(3)+MTX(3,2)*YREF(3)+MTX(3,3)*ZREF(3)
TYO(1)=OMEXO/RPMCON
TYO(2)=OMEYO/RPMCON
TYO(3)=OMEZO/RPMCON
K=4
DO 28 J=1,3
DO 28 I=1,3
TYO(K)=ABOD(I,J)
28 K=K+1
SRAD = RA*DPR
CALL HEADER
15 CONTINUE
DERIVATIVE REGION
NOSORT
IF(INITLP .NE. 2) RETURN
IF(INITSW .EQ. 0) GO TO 10000
INITSW=0
RETURN
10000 CONTINUE
TY1 = INTGRL(TYO( 1) , DTY1 )
TY2 = INTGRL(TYO( 2) , DTY2 )
TY3 = INTGRL(TYO( 3) , DTY3 )
TY4 = INTGRL(TYO( 4) , DTY4 )
TY5 = INTGRL(TYO( 5) , DTY5 )
TY6 = INTGRL(TYO( 6) , DTY6 )
TY7 = INTGRL(TYO( 7) , DTY7 )
TY8 = INTGRL(TYO( 8) , DTY8 )
TY9 = INTGRL(TYO( 9) , DTY9 )
TY10 = INTGRL(TYO(10) , DTY10)
TY11 = INTGRL(TYO(11) , DTY11)
TY12 = INTGRL(TYO(12) , DTY12)
GO TO (56,58),J8
58 CONTINUE
C(1) = TY4
C(2) = TY5
C(3) = TY6
C(4) = TY7
C(5) = TY8
C(6) = TY9
C(7) = TY10
C(8) = TY11
C(9) = TY12
CALL CONDTN(C)
TY4 = C(1)
TY5 = C(2)
TY6 = C(3)

```

```

00025100
00025400
00026800
00026900
00027000
00027200
00027300
00027400
00027500
00027600
00027800
00027900
00028000
00028100
00028200
00028500
00028600
00028700
00028800
00028900
00029000
00029100
00029200
00029300
00029400
00029500
00029600
00030100
00030200
00030800
00030900
00031000
00031100
00031200
00031300
00031400
00031500
00031600
00031700
00031800
00031900
00032000

```

	TY7 = C(4)	00032100
	TY8 = C(5)	00032200
	TY9 = C(6)	00032300
	TY10 = C(7)	00032400
	TY11 = C(8)	00032500
	TY12 = C(9)	00032600
	56 CONTINUE	00032700
	J8=2	00032800
*	ATTITUDE MATRIX RECOVERED FROM TY ARRAY	00032900
	ABOD(1,1) = TY4	00033000
	ABOD(2,1) = TY5	00033100
	ABOD(3,1) = TY6	00033200
	ABOD(1,2) = TY7	00033300
	ABOD(2,2) = TY8	00033400
	ABOD(3,2) = TY9	00033500
	ABOD(1,3) = TY10	00033600
	ABOD(2,3) = TY11	00033700
	ABOD(3,3) = TY12	00033800
	TR=TR+(TIME-TIMPST)	00033900
	J5=J5+1	00034000
	IF(IGATE.GT.J5)GO TO 35	
	J5=0	00052400
	IF(TR.LT.86400.)GO TO 32	
	TR=TR-86400.	00034300
	KDAY = KDAY + 1	00034400
	IDAY=IDAY+1	00034500
	DDAY=0.1**IDAY	00034700
	CALL GRNWH4(KDAY,IYR,GR)	00034800
32	CALL MGFDC4(KDAY,IYR,TR,AL,EC,ZIN,AP,RAN,DAP,DRAN,JDAYP,TP,...	
	FLAT,FLON,ALT,RK,ELON,GR,TM,NMAX,L,HSPA,HTCT,CRAN,CAP,TA)	
	IHR=TR/3600.	
	HR=IHR	00035500
	MIN=TR/60.-HR*60.	00035600
	XHR=HR	00035700
	IF(HR.LT.10.)XHR=HR+80.	00035800
	XMIN=MIN	00036000
	ELPSTM = DDAY*((XHR*1.0E-2)+(XMIN*1.0E-4))	
*	COMPUTE LOCAL VERTICAL	
	G=(.11958096E+07)/(RK**3)	
	USPA(1) = COS(FLAT*RPD)*COS(ELON*RPD)	
	USPA(2) = COS(FLAT*RPD)*SIN(ELON*RPD)	
	USPA(3) = SIN(FLAT*RPD)	
*	COMPUTE SUN DIRECTION USING FRACTIONAL DAY NOTATION	
	DAY = KDAY	
	DAY = DAY + TR/86400.	
	CALL ALD4(DAY,IYR,RA,DE)	
*		
	SSPA(1)=COS(DE)*COS(RA)	2174
	SSPA(2)=COS(DE)*SIN(RA)	2175
	SSPA(3)=SIN(DE)	2176
*		
	CALL AXGEN(MODE,SSPA,ECLNM,XREF,YREF,ZREF)	
*		
*		00043000
*	35 CONTINUE	
*		00051600

```

MTX(1,1)=ABOD(1,1)*XREF(1)+ABOD(1,2)*XREF(2)+ABOD(1,3)*XREF(3)
MTX(1,2)=ABOD(1,1)*YREF(1)+ABOD(1,2)*YREF(2)+ABOD(1,3)*YREF(3)
MTX(1,3)=ABOD(1,1)*ZREF(1)+ABOD(1,2)*ZREF(2)+ABOD(1,3)*ZREF(3)
MTX(2,1)=ABOD(2,1)*XREF(1)+ABOD(2,2)*XREF(2)+ABOD(2,3)*XREF(3)
MTX(2,2)=ABOD(2,1)*YREF(1)+ABOD(2,2)*YREF(2)+ABOD(2,3)*YREF(3)
MTX(2,3)=ABOD(2,1)*ZREF(1)+ABOD(2,2)*ZREF(2)+ABOD(2,3)*ZREF(3)
MTX(3,1)=ABOD(3,1)*XREF(1)+ABOD(3,2)*XREF(2)+ABOD(3,3)*XREF(3)
MTX(3,2)=ABOD(3,1)*YREF(1)+ABOD(3,2)*YREF(2)+ABOD(3,3)*YREF(3)
MTX(3,3)=ABOD(3,1)*ZREF(1)+ABOD(3,2)*ZREF(2)+ABOD(3,3)*ZREF(3)
GO TO (50,50,51,52),MODE

```

```

50 R = ATAN2(-MTX(3,2),MTX(3,3))
P = ARSIN(MTX(3,1))
Y = ATAN2(-MTX(2,1),MTX(1,1))
GO TO 53

```

```

51 R = ATAN2(-MTX(3,2),MTX(2,2))
P = ATAN2(-MTX(1,3),MTX(1,1))
Y = ARSIN(MTX(1,2))
GO TO 53

```

```

52 R = ATAN2( MTX(2,3),MTX(3,3))
P =-ARSIN(MTX(1,3))
Y = ATAN2( MTX(1,2),MTX(1,1))

```

```

53 CONTINUE

```

```

DO 36 I=1,3

```

```

HBOD(I)=0.

```

```

UBOD(I)=0.

```

```

DO 36 J=1,3

```

```

HBOD(I)=HBOD(I)+ABOD(I,J)*HSPA(J)

```

```

36 UBOD(I)=UBOD(I)+ABOD(I,J)*USPA(J)

```

```

CALCULATE MAGNETIC TORQUES

```

```

IF(PMAGTQ)38,38,37

```

```

37 TMAG(1) = PY*HBOD(3)-PZ*HBOD(2)

```

```

TMAG(2) = PZ*HBOD(1)-PX*HBOD(3)

```

```

TMAG(3) = PX*HBOD(2)-PY*HBOD(1)

```

```

GO TO 39

```

```

38 TMAG(1) = 0.

```

```

TMAG(2) = 0.

```

```

TMAG(3) = 0.

```

```

39 CONTINUE

```

```

CALCULATE GRAVITY TORQUES

```

```

CALL VERT(FLAT,ELON,RK,USPA,G)

```

```

$ THIS IS DONE IN MAIN EVER
J4 INTEGRATION TIME STEPS

```

```

G = 3GM/RK**3 WHERE RK IS RADIUS VECTOR GIVEN IN KM

```

```

IF(GPVTQ)41,41,40

```

```

40 TGRAV(1)=-G*UBOD(2)*UBOD(3)*(C25-C26)

```

```

TGRAV(2)=-G*UBOD(3)*UBOD(1)*(C26-C24)

```

```

TGRAV(3)=-G*UBOD(1)*UBOD(2)*(C24-C25)

```

```

GO TO 42

```

```

41 TGRAV(1) = 0.

```

```

TGRAV(2) = 0.

```

```

TGRAV(3) = 0.

```

```

42 CONTINUE

```

```

COMPUTE CONTROL TORQUES

```

```

IF(CNTRLQ)45,45,43

```

```

43 CONTINUE

```

```

00046700
00046800

```

```

3073
3074

```

```

HX = HBOD(1)+HREMAX*UNM1P1(ISEED)+HXBIAS
HY = HBOD(2)+HREMAX*UNM1P1(ISEED)+HYBIAS
HZ = HBOD(3)+HREMAX*UNM1P1(ISEED)+HZBIAS

```

```

*
* COMPUTE ERROR VARIABLES -- RATES AND ANGLES
* ERRV(I) ARE ERRORS IN STATE VARIABLE FORM WHERE

```

```

* ERRV(1) = Z-AXIS ROTATION ( YAW ANG. )
* ERRV(2) = OMEGA-Z ( YAW RATE )
* ERRV(3) = Y-AXIS ROTATION ( PITCH ANGLE )
* ERRV(4) = OMEGA-Y ( PITCH RATE )
* ERRV(5) = X-AXIS ROTATION ( ROLL ANGLE )
* ERRV(6) = OMEGA-X ( ROLL RATE )

```

```

* ERRV(1) = Y+UNM1P1(ISEED)*AREMAX*RPD
* ERRV(2) = TY3+(WREMAX/RPMCON)*UNM1P1(ISEED)
* ERRV(3) = P+UNM1P1(ISEED)*AREMAX*RPD
* ERRV(4) = TY2+(WREMAX/RPMCON)*UNM1P1(ISEED)
* ERRV(5) = R+UNM1P1(ISEED)*AREMAX*RPD
* ERRV(6) = TY1-DESSPX+(WREMAX/RPMCON)*UNM1P1(ISEED)

```

```

* IF(ABS(ERRV(1)).LE.(DBZANG*RPD))ERRV(1)=0.0
* IF(ABS(ERRV(2)).LE.(DBZRTE/RPMCON))ERRV(2)=0.0
* IF(ABS(ERRV(3)).LE.(DBYANG*RPD))ERRV(3)=0.0
* IF(ABS(ERRV(4)).LE.(DBYRTE/RPMCON))ERRV(4)=0.0
* IF(ABS(ERRV(5)).LE.(DBXANG*RPD))ERRV(5)=0.0
* IF(ABS(ERRV(6)).LE.(DBXRTE/RPMCON))ERRV(6)=0.0

```

```

* COMPUTE SUN POINTING ERROR IN BODY FRAME -- THETX,THETZ IN DEGREES

```

```

* COMPUTE DESIRED CONTROL TORQUES -- TDES(I)

```

```

DO 44 I=1,3
  TDES(I) = 0.

```

```

DO 44 J=1,6

```

```

44 TDES(I) = TDES(I) - ERRK(I,J)*ERRV(J)

```

```

TDX = TDES(1)+TXBIAS

```

```

TDY = TDES(2)+TYBIAS

```

```

TDZ = TDES(3)+TZBIAS

```

```

* CALL ALGOR(IALGOR,MODE,ERRV,HX,HY,HZ,TDX,TDY,TDZ,C24,C25,C26, ...
ALPHA0,WX0,ERRTD,WXDES,CMX,CMY,CMZ)

```

```

ACMX = ABS(CMX)

```

```

ACMY = ABS(CMY)

```

```

ACMZ = ABS(CMZ)

```

```

IF(ACMX.GT.CMXMAX)CMX = (CMXMAX*CMX)/ACMX

```

```

IF(ACMY.GT.CMYMAX)CMY = (CMYMAX*CMY)/ACMY

```

```

IF(ACMZ.GT.CMZMAX)CMZ = (CMZMAX*CMZ)/ACMZ

```

```

TCNTRL(1) = CMY*HBOD(3)-CMZ*HBOD(2)

```

```

TCNTRL(2) = CMZ*HBOD(1)-CMX*HBOD(3)

```

```

TCNTRL(3) = CMX*HBOD(2)-CMY*HBOD(1)

```

```

IF(MODWHL.LT.1)GO TO 62

```

```

DELTRQ = TDX-TCNTRL(1)

```

```

IF(DELTRQ.EQ.0.0)GO TO 64

```

```

TQSGN = DELTRQ/ABS(DELTRQ)

```

```

GO TO 65

```

```

64 TQSGN = 1.0
65 IF(ABS(DELTRQ).LE.(TQLIM*CGSCON))GO TO 60
   IF(IRSW.EQ.0)GO TO 61
   DELMOM = (TIME-WHSTM)*(-RTORQ)
   HROTOR = RMMOM+DELMOM
   GO TO 66
61 IRSW = 1
66 RTQFLB = SLOPE*((HROTOR/CGSCON)+(TQSGN*XNTRCP))
   RTORQ = -RTQFLB*CGSCON
   WHSTM = TIME
   RMMOM = HROTOR
   RTMOM = HROTOR/CGSCON
   IF(RTMOM.LT.RMHGH)GO TO 67
   IF((RTQFLB/RTMOM).LT.0.0)GO TO 62
   GO TO 60
67 IF(RTMOM.GT.RMLDW)GO TO 62
   IF((RTQFLB/RTMOM).GT.0.0)GO TO 62
60 IRSW = 0
   RTORQ = 0.0
62 CONTINUE
   GO TO 47
45 DO 46 I=1,3
   TDES(I) =0.
46 TCNTRL(I) =0.
   CMX = 0.
   CMY = 0.
   CMZ = 0.
47 CONTINUE

```

```

*
DO 48 I=1,3
48 TTOB(I) =TMAG(I)+TGRAV(I)+TCNTRL(I)

```

```

*
*
*
*
EQUATIONS OF ATTITUDE MOTION

```

```

DTY1 = (TTOB(1) +TY2*TY3*(C25-C26)+RTORQ)/C24
DTY2 = (TTOB(2) +TY3*TY1*(C26-C24)-TY3*HROTOR )/C25
DTY3 = (TTOB(3) +TY1*TY2*(C24-C25) +TY2*HROTOR )/C26
DTY4 = -(-TY3*TY5 + TY2*TY6)
DTY5 = -(+TY3*TY4 - TY1*TY6)
DTY6 = -(-TY2*TY4 + TY1*TY5)
DTY7 = -(-TY3*TY8 + TY2*TY9)
DTY8 = -(+TY3*TY7 - TY1*TY9)
DTY9 = -(-TY2*TY7 + TY1*TY8)
DTY10 = -(-TY3*TY11+ TY2*TY12)
DTY11 = -(+TY3*TY10- TY1*TY12)
DTY12 = -(-TY2*TY10+ TY1*TY11)

```

```

00050500
00050600
00050700
00050800
00050900
00051000
00051100
00051200
00051300
00051400
00052200
00052800
00052900
00053000
00053100

```

```

*
TIMPST=TIME

```

```

*
SAMPLE REGION

```

```

IF(INITLP .NE. 2) RETURN
IF(INITSW .NE. 0) RETURN
CALL DASCL(DAF1,DAF2,DAF3,DAF4,DAF5,DAF6,DAF7,DAF8,XNDX1,XNDX2,...
XNDX3,XNDX4,XNDX5,XNDX6,XNDX7,XNDX8,INDX,DASF)
OMEX = TY1*RPMCON
OMEY = TY2*RPMCON
OMEZ = TY3*RPMCON

```



```

TRQWHL=-RTORQ/CGSCON
* COMPUTE POWER AND CONVERT TO WATTS
RTRPWR=0.0
IF (RTORQ.NE.0.0)RTRPWR=170.0
ACMX = ABS(CMX)
ACMY = ABS(CMY)
ACMZ = ABS(CMZ)
POWER = (ACMX+ACMY+ACMZ)*1.0E-5
TOTPWR = POWER+RTRPWR
SUNDEC = (ARSIN(MTX(1,3)))*DPR
SIJNRA = (ATAN2(MTX(1,2),MTX(1,1)))*DPR
ROLL = R*DPR
PITCH= P*DPR
YAW = Y*DPR
GO TO (85,85,87,88),MODE
85 TOTERR=ARCOS(MTX(1,1))*DPR
CHNL1 = OMEX
CHNL3=PITCH
CHNL4=YAW
GO TO 90
87 TOTERR=ARCOS(MTX(2,2))*DPR
CHNL1=PITCH
CHNL3=ROLL
CHNL4=YAW
GO TO 90
88 TOTERR=ARCOS(MTX(3,3))*DPR
CHNL1=YAW
CHNL3=PITCH
CHNL4=ROLL
90 CHNL2 =TOTERR
RANFN1 = (ERRV(1)-Y)*DPR
RANFN2=(ERRV(2)-TY3)*RPMCON
RANFN3 = (ERRV(3)-P)*DPR
RANFN4=(ERRV(4)-TY2)*RPMCON
RANFN5 = (ERRV(5)-R)*DPR
RANFN6 = (ERRV(6)-TY1+DESSPX)*RPMCON
*
IMRK=0
IF (TIME.EQ.TSTART)IMRK=1
IF (AMOD(TIME,3600.).GE.3510.)IMRK=1
CALL WECSAW(3,11,IMRK)
DO 99 ICHNL=1,8
DAVAR(ICHNL)=CURV(INDX(ICHNL))
99 IDAC(ICHNL)=DAVAR(ICHNL)*DASF(ICHNL)
* TRANSFER D/A
CALL WDAQAW(0,IDAC,8)
RECORDER STEPPED BY USE OF SYSTEM VARIABLE DELSTP
*-----00059800
00059900
END 00060000
STOP 00060100

```

```

0045      DETXZ = -HY*HSQD
0046      CMX  = -(TDX*HX*HZ + TDZ*(HY**2 + HZ**2))/DETXZ
0047      CMY  = (HZ*TDX - HX*TDZ)/HSQD
0048      CMZ  = (TDZ*HX*HZ + TDX*(HX**2 + HY**2))/DETXZ
0049      GO TO 51
0050      72  CONTINUE
C          ALGORITHM FOR X-Y AXIS TORQUE CONTROL
C
0051      DETXY = HZ*HSQD
0052      CMX  = -(TDX*HX*HY + TDY*(HY**2 + HZ**2))/DETXY
0053      CMY  = (TDY*HX*HY + TDX*(HX**2 + HZ**2))/DETXY
0054      CMZ  = (HX*TDY - HY*TDX)/HSQD
0055      GO TO 51
0056      73  CONTINUE
C          ALGORITHM FOR Y-Z AXIS TORQUE CONTROL
C
0057      DET  = -HSQD*HX
0058      CMX  = ( HY*TDZ - HZ*TDY )/HSQD
0059      CMY  = ( HY*HZ*TDY + TDZ*( HX**2 + HZ**2 ) )/DET
0060      CMZ  = -( HY*HZ*TDZ + TDY*( HX**2 + HY**2 ) )/DET
0061      GO TO 51
0062      81  CONTINUE
C          ALGORITHM FOR X AXIS TORQUE CONTROL
0063      SPK = TDX/( HY**2 + HZ**2 )
0064      CMX = 0.
0065      CMY = HZ*SPK
0066      CMZ = -HY*SPK
0067      GO TO 51
0068      82  CONTINUE
C          ALGORITHM FOR Y AXIS TORQUE CONTROL
0069      SPK = TDY/( HX**2 + HZ**2 )
0070      CMX = -HZ*SPK
0071      CMY = 0.
0072      CMZ = HX*SPK
0073      GO TO 51
0074      83  CONTINUE
C          ALGORITHM FOR Z AXIS TORQUE CONTROL
0075      SPK = TDZ/( HX**2 + HY**2 )
0076      CMX = HY*SPK
0077      CMY = -HX*SPK
0078      CMZ = 0.
0079      GO TO 51
0080      50  CMX = 0.
0081      CMY = 0.
0082      CMZ = 0.
0083      51  CONTINUE
0084      RETURN
0085      END

```

```

0001      SUBROUTINE ALGOR(I ALGOR,MODE,ERRV,HX,HY,HZ,TDX,TDY,TDZ,C24,C25,
        IC26,ALPHA0,WX0,ERRTO,WXDES,CMX,CMY,CMZ)
        DIMENSION ERRV(6)
        DATA DPR/57.2978/
0004      DATA RPMCON/9.54930/
        DATA RPD/0.01745329/
0006      HSQD = HX**2 + HY**2 + HZ**2
0007      HTOT = SQRT( HSQD )
0008      GO TO (60,60,61,62),MODE
        60 I=1
0010      J=3
0011      L=6
0012      WXN = WX0/RPMCON
0013      HI = HX
0014      GO TO 63
        61 I=1
0016      J=5
0017      L=3
0018      WXN = WX0*RPD
0019      HI = HY
0020      GO TO 63
        62 I=3
0022      J=5
0023      L=1
0024      WXN = WX0*RPD
0025      HI = HZ
0026      63 ERRT = ( SQRT(ERRV(I)**2+ERRV(J)**2) ) * DPR
0027      IF(ERRT.GT.1.0) ERRT=(ARCOS(COS(ERRV(I))*COS(ERRV(J)))) * DPR
0028      ALPHA = ( ARSIN(HI/HTOT) ) * DPR
0029      ACCX = TDX/C24
0030      ACCY = TDY/C25
0031      ACCZ = TDZ/C26

C
C      GENERATE LOGIC FOR SELECTION OF ALGORITHM
C
C      ISN = 1 MEANS SPIN AXIS CONTROL
C      ISN = 2 MEANS SPIN RATE TYPE CONTROL
C
0032      IF(ABS(ALPHA)-ALPHA0)22,22,44
0033      22 IF(ABS(ERRV(L))-WXN)44,44,21
0034      21 IF(ERRT-ERRTO)23,23,44
0035      44 CONTINUE
C      ISN = 1
C      GO TO (73,73,71,72),MODE
0036      GO TO 73
0037      23 CONTINUE
C      ISN = 2
0038      25 IF(IALGOR-1)50,26,27
0039      26 GO TO (81,81,82,83),MODE
0040      27 GO TO (32,32,33,34),MODE
0041      32 IF(ACCY-ACCZ)71,71,72
0042      33 IF(ACCX-ACCZ)73,73,72
0043      34 IF(ACCX-ACCY)73,73,71
0044      71 CONTINUE
C      ALGORITHM FOR X-Z AXIS TORQUE CONTROL
C

```

```

0007      WRITE (6,98)INTERMS
0008      WRITE(6,104)AL,ALTNMI,ALTKM,EC,CZIN,CAPO,CRANO,CDAP,CDRAN,CTP,
1JDAYP,NYR,SRAD
0009      WRITE(6,203)DELS,J4,OMEXO,OMEYO,OMEZO,ROLLO,PITCHO,YAWO,DELT,
1TORB,PX,PY,PZ,CXX,CYY,CZZ,HWHEEL
0010      WRITE(6,205)ISTART,ITSTRT,ISTOP,ITSTOP
0011      98 FORMAT (1H1,10X,40HSOLUTION OF ATTITUDE EQUATIONS OF MOTION/20X,5H
1329      1OF AN/10X,27HEARTH SATELLITE FOR DESIRED/20X,5HORBIT/20X,18HMOMENT
1330      1S OF INERTIA/20X,26HORIENTATION AND SPIN RATES/20X,25HSATELLITE MA
1331      1GNETIC DIPOLE/10X,7HUSING ,I3,30H TERM EXPANSION OF EARTH FIELD/)
1332
C
0012      104 FORMAT (/34X,
1333      151H ORIENTATION ANALYSIS OF A MAG STABILIZED SATELLITE//8X,33HKEPL
1334      1ER ELEMENTS- SEMI MAJOR AXIS=F9.6/
1335      1' ALTITUDE BASED ON ASSUMING A CIRCULAR ORBIT OF GIVEN SEMI MAJO
1R AXIS = 'F6.1,' N MI. = 'F6.1,' KM'/
1
1CLINATION=F9.5,6H (DEG)/25X,16HARG. OF PERIGEE=F9.4,39H (DEG) RT.
1337      1 ASCENSION OF NODE AT EPOCH=F9.4,6H (DEG)/25X,16HPRECESSION PER.=
1338      1F9.5,10H (DEG/DAY),6X,19HPRECESSION OF NODE=F9.5,10H (DEG/DAY)/25X
1339      1,13HEPOCH- TIME =F7.3,8H (KS UT),13X,5HDAY =I4,18X,6HYEAR =I5//
1' RIGHT ASCENSION OF SUN AT START OF RUN = ' F8.2,'DEGREES' )
C
0013      203 FORMAT( /18H PRINT INTERVAL= F6.2,9H SECONDS ,10X,24H MAGNETIC F
1341      1IELD UPDATE =I3,11H TIME STEPS//17H ANG VEL COMPS= 3E15.8//
1' INITIAL ATTITUDE RELATIVE TO SUN LINE AND ECLIPTIC PLANE IS'/
1' ROLL = 'F6.2,'DEG. PITCH = 'F6.2,'DEG. YAW = 'F6.2,'DEG '//
1' TIME STEP = 'F6.2,'SECONDS ORBITAL PERIOD = 'F6.2,' MIN.'//
1' PERMANENT MAGNETIC DIPOLE COMPONENTS = '3E15.8,' POLE-CM '//
1' SPACECRAFT MOMENTS OF INERTIA = '3E15.8,' SLUG-FT-SQUARED '//
1' ROTOR ANGULAR MOMENTUM = 'F7.1,' LB-FT-SEC '// )
C
0014      205 FORMAT( 28H INITIAL CONDITIONS//,19H START ON DAY NO.
1350      1I3,' TIME ( HRS-MIN, UT ) = 'I4,/' STOP ON DAY NO. 'I3,' TIME (
1HRS-MIN, UT ) = 'I4/)
C
0015      RETURN
0016      END
1354      00068600
00068700

```

## APPENDIX D

### Derivation of Optimal Control Law Coefficients

#### INTRODUCTION

This appendix presents the derivation of the HEAO-A attitude control law. The analysis is based on the linearized equations of motion, and assumes that a control torque can be obtained in any direction.

Three modes of operation are studied: a scan mode, and two pointing modes. In the scan mode the satellite spins about the axis with the largest moment of inertia (X-axis), and this axis must be controlled to point within  $\pm 1^\circ$ . In the pointing mode the satellite does not spin, but one axis, either the Y axis or the Z axis, must be controlled to point within  $\pm 1^\circ$  of a celestial source. The satellite is allowed to move about this axis, but it must be controlled to within  $\pm 37^\circ$ . A momentum wheel aligned with the spacecraft X-axis, is assumed for additional gyrostabilization. The principal disturbance torques are due to gravity-gradients.

The control system must meet certain requirements:

- (1) Given any initial error (roll spin rate, roll angle, pitch angle, or yaw angle), the system must reduce this error to an acceptable level.
- (2) Given an external disturbance on the satellite the control system must reduce the effects of this disturbance to an acceptable error.

The object of the control law is to take the measured states of the attitude errors and rates and apply torques to the satellite to correct these errors and at the same time minimize the control energy required.

DESCRIPTION

In the analysis the satellite is treated as a rigid body with one momentum wheel along the roll (X) axis. The linearized equations of motion are derived in Appendix E and are repeated here in equation (1).

$$I_z \ddot{y} - \dot{r}_o \dot{p} (I_x - I_y - I_z) - \dot{p} H_x = T_z$$

$$I_x \ddot{r}_e = T_x \tag{1}$$

$$I_y \ddot{p} - \dot{y} \dot{r}_o (-I_x + I_y + I_z) + \dot{y} H_x = T_y$$

where:

- r = roll angle (positive rotation about x axis)
- y = yaw angle (positive rotation about z axis)
- p = pitch angle (positive rotation about y axis)
- I<sub>z</sub> = moment of inertia about the z axis
- I<sub>y</sub> = moment of inertia about the y axis
- I<sub>x</sub> = moment of inertia about the x axis
- H<sub>x</sub> = moment of the x axis momentum wheel
- T<sub>z</sub> = control torque about the z axis
- T<sub>y</sub> = control torque about the y axis
- T<sub>x</sub> = control torque about the x axis.

and

$$\dot{r} = \dot{r}_o + \dot{r}_e$$

where

- $\dot{r}_o$  = nominal roll rate = constant
- $\dot{r}_e$  = roll rate error

Equations (1) can be put into state variable form

$$\dot{X} = AX + BT \quad (2)$$

where in the Scan Mode

$$X = \begin{bmatrix} y \\ \dot{y} \\ p \\ \dot{p} \\ \dot{r} \end{bmatrix} \quad T = \begin{bmatrix} T_z \\ T_y \\ T_x \end{bmatrix}$$

$$A = \begin{bmatrix} 0 & 1 & 0 & 0 & 0 \\ 0 & 0 & 0 & \frac{(\dot{r}_0(I_x - I_y - I_z) + H_x)}{I_z} & 0 \\ 0 & 0 & 0 & 1 & 0 \\ 0 & \frac{(\dot{r}_0(I_z + I_y - I_x) - H_x)}{I_y} & 0 & 0 & 0 \\ 0 & 0 & 0 & 0 & 0 \end{bmatrix}$$

$$B = \begin{bmatrix} 0 & 0 & 0 \\ \frac{1}{I_z} & 0 & 0 \\ 0 & 0 & 0 \\ 0 & \frac{1}{I_y} & 0 \\ 0 & 0 & \frac{1}{I_x} \end{bmatrix}$$

In the Pointing Mode

$$X = \begin{bmatrix} y \\ \dot{y} \\ p \\ \dot{p} \\ r \\ \dot{r} \end{bmatrix} \quad T = \begin{bmatrix} T_z \\ T_y \\ T_x \end{bmatrix}$$

$$A = \begin{bmatrix} 0 & 1 & 0 & 0 & 0 & 0 \\ 0 & 0 & 0 & H_x/I_z & 0 & 0 \\ 0 & 0 & 0 & 1 & 0 & 0 \\ 0 & -H_x/I_y & 0 & 0 & 0 & 0 \\ 0 & 0 & 0 & 0 & 0 & 1 \\ 0 & 0 & 0 & 0 & 0 & 0 \end{bmatrix}$$

$$B = \begin{bmatrix} 0 & 0 & 0 \\ \frac{1}{I_z} & 0 & 0 \\ 0 & 0 & 0 \\ 0 & \frac{1}{I_z} & 0 \\ 0 & 0 & 0 \\ 0 & 0 & \frac{1}{I_x} \end{bmatrix}$$



The state vector X is of dimension 5 in the scan mode and is of dimension 6 in the pointing mode. The control torque vector T is of dimension 3. Mathematically this objective of optimal control technique is to choose T in such a way as to minimize the quadratic performance index.

$$J = 1/2 \int_0^{\infty} (X'QX + T'RT)dt$$

where Q and R are the weighting matrices which weight the angular errors and torques and the prime indicates matrix transpose.

In the scan mode

$$Q = \begin{bmatrix} q_1 & 0 & 0 & 0 & 0 \\ 0 & 0 & 0 & 0 & 0 \\ 0 & 0 & q_2 & 0 & 0 \\ 0 & 0 & 0 & 0 & 0 \\ 0 & 0 & 0 & 0 & q_3 \end{bmatrix}$$

$$R = \begin{bmatrix} 1 & 0 & 0 \\ 0 & 1 & 0 \\ 0 & 0 & 1 \end{bmatrix}$$

Thus the quadratic performance criteria becomes

$$J = 1/2 \int_0^{\infty} (q_1 y^2 + q_2 p^2 + q_3 \dot{r}^2 + T_y^2 + T_y^2 + T_x^2) dt$$

In the pointing mode

$$Q = \begin{bmatrix} q_1 & 0 & 0 & 0 & 0 & 0 \\ 0 & 0 & 0 & 0 & 0 & 0 \\ 0 & 0 & q_2 & 0 & 0 & 0 \\ 0 & 0 & 0 & 0 & 0 & 0 \\ 0 & 0 & 0 & 0 & q_3 & 0 \\ 0 & 0 & 0 & 0 & 0 & 0 \end{bmatrix}$$

$$R = \begin{bmatrix} 1 & 0 & 0 \\ 0 & 1 & 0 \\ 0 & 0 & 1 \end{bmatrix}$$

Thus the quadratic performance criteria becomes

$$J = 1/2 \int_0^{\infty} (q_1 y^2 + q_2 p^2 + q_3 r^2 + T_z^2 + T_y^2 + T_x^2) dt \quad (4)$$

The optimal solution for the control torques ( $T_o$ ) that minimizes the integral is well known and is given by equation (5):

$$T_o = -R^{-1} B' K(\infty) X(t) \quad (5)$$

where  $K(\infty)$  is the steady-state solution of the Matrix Riccati Equation (6):

$$-\frac{dK}{dt} = KA + A'K - KBR^{-1}B'K + Q \quad (6)$$

The general form for the optimal control torque is thus given by a linear combination of attitude errors and rates, specifically,

$$\begin{aligned} T_x &= -k_{11}y - k_{12}\dot{y} - k_{13}p - k_{14}\dot{p} - k_{15}r - k_{16}(\dot{r} - \dot{r}_{des}) \\ T_y &= -k_{21}y - k_{22}\dot{y} - k_{23}p - k_{24}\dot{p} - k_{25}r - k_{26}\dot{r} \\ T_z &= -k_{31}y - k_{32}\dot{y} - k_{33}p - k_{34}\dot{p} - k_{35}r - k_{36}\dot{r} \end{aligned} \quad (7)$$

Incorporating this torque expression with optimal coefficients into the linearized equations of motion results in a controlled dynamical system. The block diagram representation for the HEAO-A linearized attitude control system is shown in Figures D1, and D2.

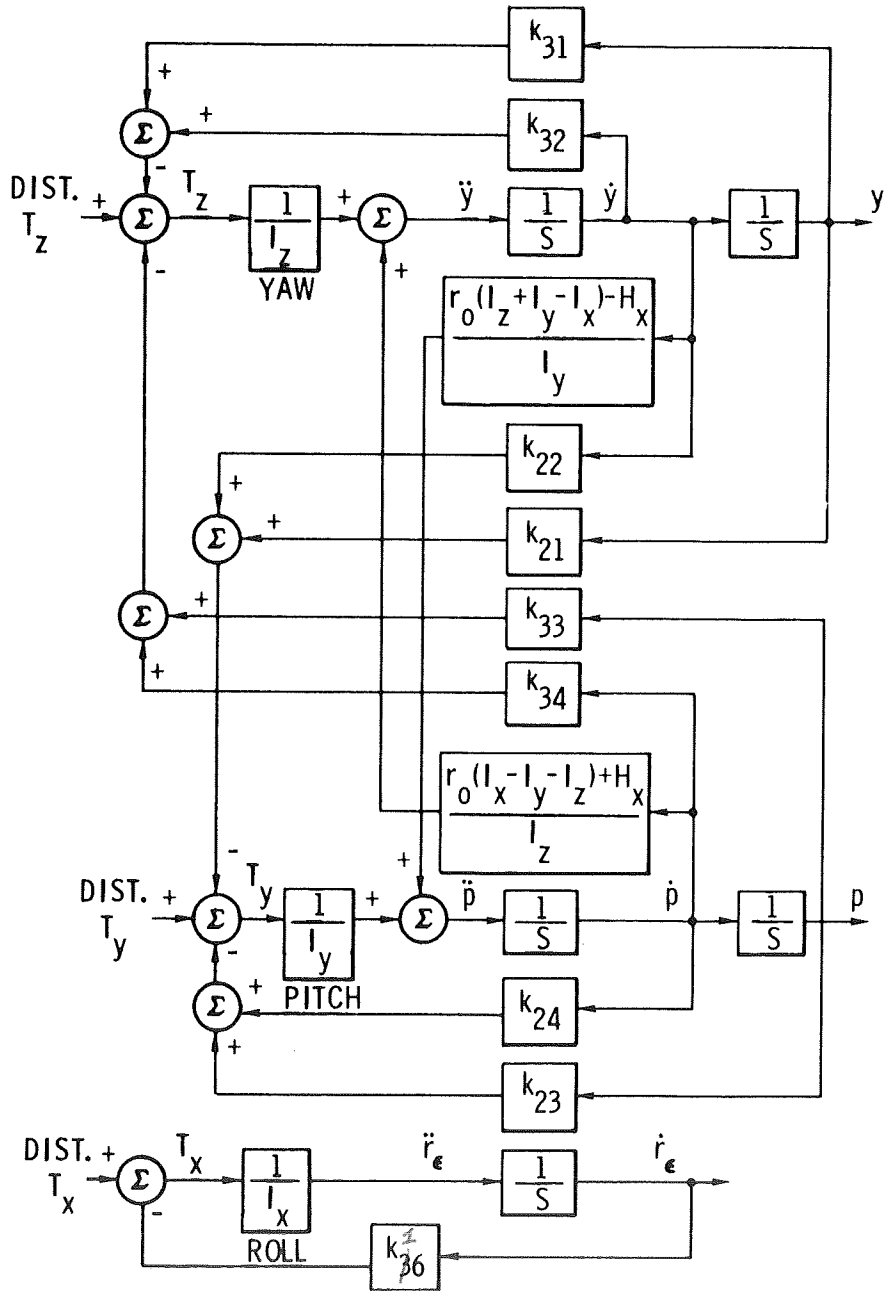


Fig. D-1 BLOCK DIAGRAM OF THE LINEARIZED SYSTEM (SCAN MODE)

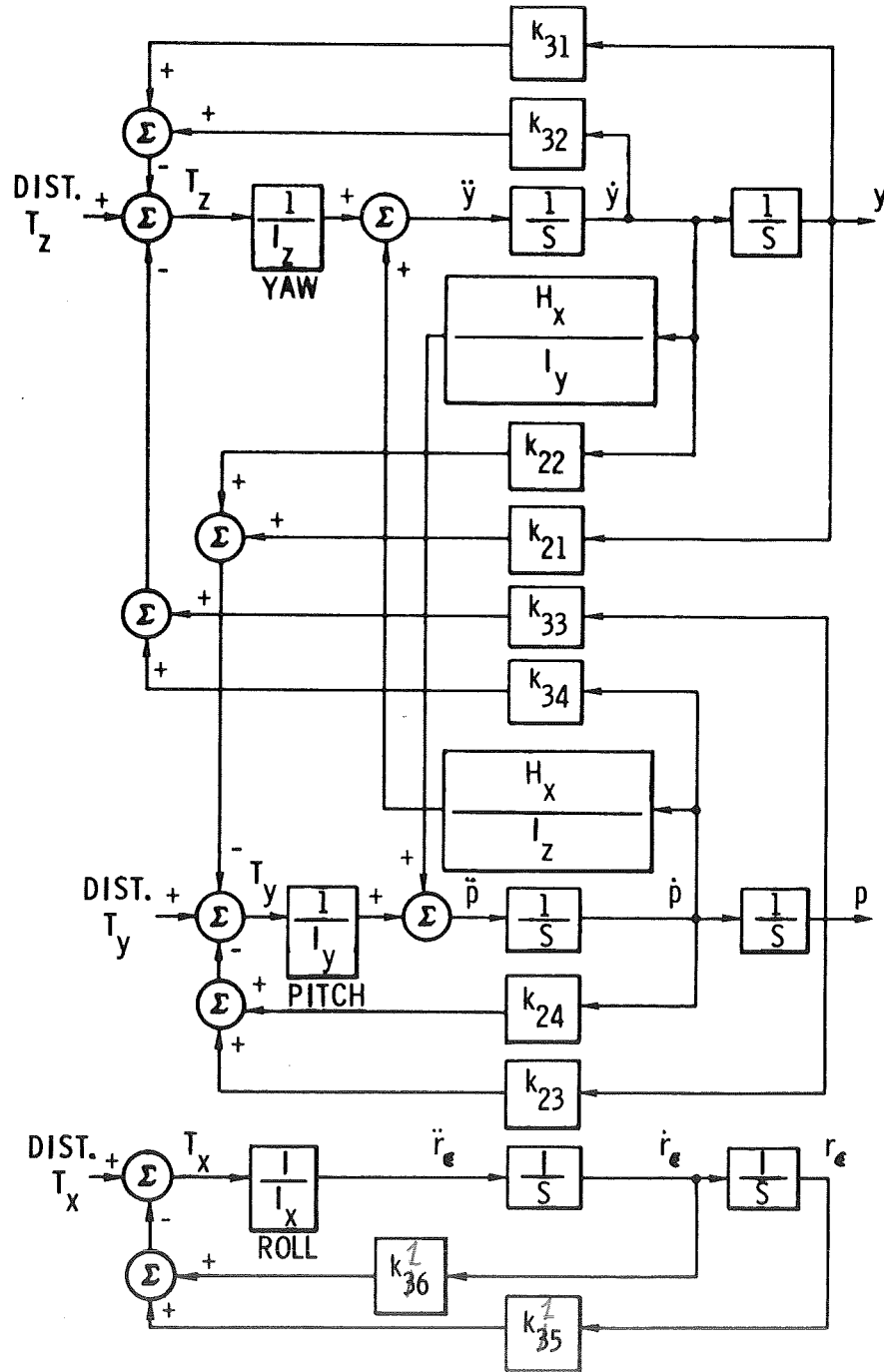


Fig. D-2 BLOCK DIAGRAM OF THE LINEARIZED SYSTEM (POINTING MODE)

Given spacecraft mass properties, and assumed values for wheel momentum nominal scan rate and weighting ratio, a computer program is used to generate specific values for all  $k_{ij}$ . These control coefficients are then used according to Equation (7) to generate the desired values of the torque components.

## APPENDIX E

### Derivation of Linearized Equations of Motion

#### Introduction

This section presents the derivation of a set of linearized dynamical equations for HEAO-A. This linearized set is used for determining the optimal control coefficients. The full up dynamical simulation for determining HEAO performance is based on exact generalized nonlinear equations of motion.

For HEAO-A, three separate derivations of linearized equations exist, one for each of the three following pointing modes:

- 1) X-axis toward sun or star,
- 2) Y-axis toward star, and
- 3) Z-axis toward star.

It shall be shown that for purposes of linearization separate derivations are necessary for the three modes but that all derivations result in an identical set of linearized equations.

#### X-Axis Pointing

The linearized equations are based on Eulers rigid body dynamical equations of motion and a preferred sequence of rotations which define the attitude of the spacecraft with respect to an inertial reference frame. Eulers equations of motion for a rigid body with a wheel spinning about the x-axis are

$$\begin{aligned} I_x \dot{\omega}_x - \omega_y \omega_z (I_y - I_z) &= T_x \\ I_y \dot{\omega}_y - \omega_x \omega_z (I_z - I_x) + \omega_z H_x &= T_y \\ I_z \dot{\omega}_z - \omega_x \omega_y (I_x - I_y) - \omega_y H_x &= T_z \end{aligned} \tag{E-1}$$

where  $H_x$  is the angular momentum of the wheel along the X-axis. The angular rates  $\omega_{x,y,z}$  and torques  $T_{x,y,z}$  are referenced to the X,Y,Z-axes fixed to the spacecraft.

### Rotation Sequence

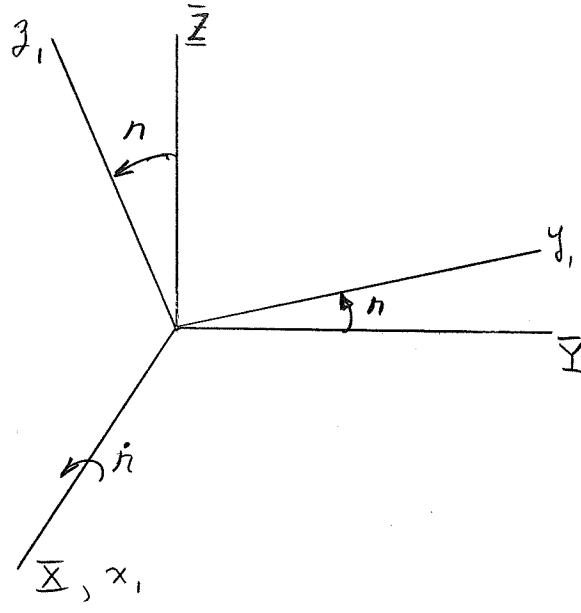
It is assumed that the spacecraft axes are initially aligned with an inertial reference set  $\bar{X}$ ,  $\bar{Y}$ ,  $\bar{Z}$  and that a sequence of rotations orients the spacecraft to some general attitude. It is noted that for each pointing mode, large angular rotations exist about one axis while small rotations (less than  $1^\circ$ ) occur about the other two. For subsequent linearization the large angle motion must be eliminated from the equations. This is done by beginning the rotation sequence with the axis about which large angular motion occurs.

For the X-axis pointing mode, then, the sequence of rotations is

- 1) rotation about X-axis through a roll angle,  $r$
- 2) rotation about Y-axis through a pitch angle,  $p$
- 3) rotation about Z-axis through a yaw angle,  $y$

Figures 1, 2, and 3 depict this sequence.

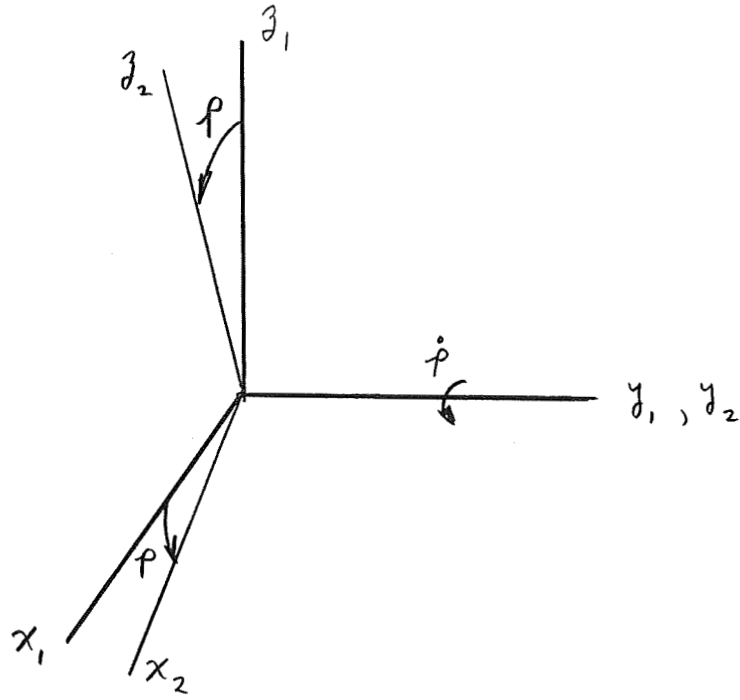
Each rotation is mathematically described by a matrix which transforms a vector from one frame to the next.



$$[R] = \begin{bmatrix} 1 & 0 & 0 \\ 0 & \cos r & \sin r \\ 0 & -\sin r & \cos r \end{bmatrix}$$

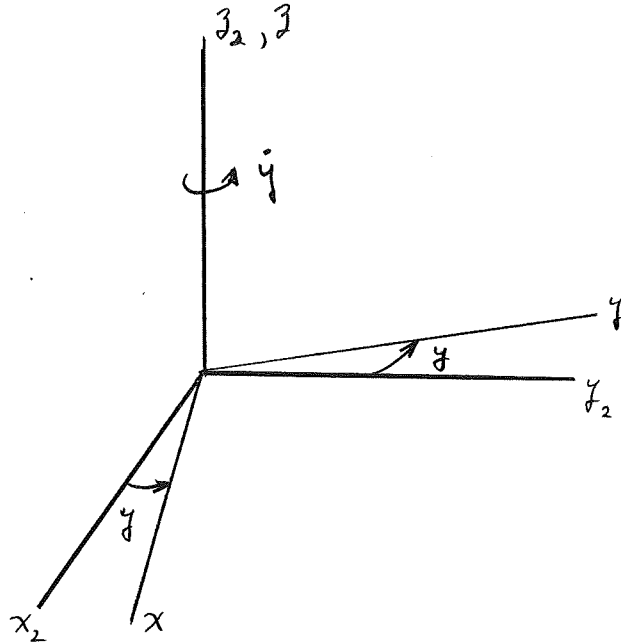
Figure 1 X-axis Rotation and Transformation Matrix





$$[P] = \begin{bmatrix} \text{cosp} & 0 & -\text{sinp} \\ 0 & 1 & 0 \\ \text{sinp} & 0 & \text{cosp} \end{bmatrix}$$

Figure 2 Y-axis Rotation and Transformation Matrix



$$[Y] = \begin{bmatrix} \cos\phi & \sin\phi & 0 \\ -\sin\phi & \cos\phi & 0 \\ 0 & 0 & 1 \end{bmatrix}$$

Figure 3 Z-axis Rotation and Transformation Matrix

The complete transformation then of a vector  $\vec{N}_I$  given in inertial coordinates to the same vector, but defined in body coordinates,  $\vec{N}_b$  is

$$\vec{N}_b = [Y] [P] [R] \vec{N}_I \quad (\text{E-2})$$

#### Transformation of Rates

The second step in the derivation of a linearized set of dynamical equations involves the transformation of the three rotation rates, roll rate, pitch rate and yaw rate, into the final body frame (x, y, z). This defines the three body rates  $\omega_x$ ,  $\omega_y$  and  $\omega_z$  in terms of rates of angles for substitution into Eulers equations.

The yaw rate  $\dot{y}$ , a rotation about the z-axis, is automatically in final body coordinates as seen in Figure 3. Thus the components of the angular rate vector  $\vec{\omega}$  in body coordinates due to yaw is

$$\vec{\omega}_{\text{yaw}} = \begin{bmatrix} 0 \\ 0 \\ \dot{y} \end{bmatrix} \quad (\text{E-3})$$

The pitch rate,  $\dot{p}$ , is a rotation about the  $y_2$  axis and is transformed to final body coordinates via  $[Y]$ . Thus  $\vec{\omega}$  due to pitch is

$$\vec{\omega}_{\text{pitch}} = [Y] \begin{bmatrix} 0 \\ \dot{p} \\ 0 \end{bmatrix} \quad (\text{E-4})$$

The roll rate,  $\dot{r}$ , is a rotation about the  $x_1$  axis (see Figure 1) and is transformed to final body coordinates via two matrix transformations  $[Y]$   $[P]$ . Thus  $\bar{\omega}$  due to roll is

$$\bar{\omega}_{\text{roll}} = [Y] [P] \begin{bmatrix} \dot{r} \\ 0 \\ 0 \end{bmatrix} \quad (\text{E-5})$$

The total angular rate vector, resulting from roll pitch and yaw rates is given by the sum of Eqs (3), (4), and (5), which is

$$\dot{\omega} = \begin{bmatrix} \omega_x \\ \omega_y \\ \omega_z \end{bmatrix} = \begin{bmatrix} \dot{p} \sin y & + & \dot{r} \cos p \cos y \\ \dot{p} \cos y & - & \dot{r} \cos p \sin y \\ \dot{y} & + & \dot{r} \sin p \end{bmatrix} \quad (\text{E-6})$$

Angular accelerations are

$$\begin{aligned} \dot{\omega}_x &= \ddot{p} \sin y + \dot{p} \dot{y} \cos y + \ddot{r} \cos p \cos y - \dot{r} \dot{p} \sin p \cos y - \dot{r} \dot{y} \cos p \sin y \\ \dot{\omega}_y &= \ddot{p} \cos y - \dot{p} \dot{y} \sin y - \ddot{r} \cos p \sin y + \dot{r} \dot{p} \sin p \sin y - \dot{r} \dot{y} \cos p \cos y \\ \dot{\omega}_z &= \ddot{y} + \ddot{r} \sin p + \dot{r} \dot{p} \cos p \end{aligned} \quad (\text{E-7})$$

where sine and cosine are abbreviated by s and c, respectively.

Linearization of Angles, Rates and Accelerations

The rates and accelerations given by Eqs (6) and (7) are substituted into Eulers Equations, Eq (1), and linearized. The final linearization process involves a breakdown of roll, pitch and yaw angles and rates into nominal plus perturbed motion. For example

$$y = y_0 + \underline{y}$$

and

$$p = p_0 + \underline{p}$$

where  $(-)_0$  is the nominal motion and  $(\underline{-})$  is the perturbed motion

The nominal motion for pitch and yaw is zero for both angles and rates which reflects the ideal stabilized condition. The nominal motion for roll rate,  $r_0$ , is finite and constant near 0.05 rpm. It is noted here that the roll angle which varies from 0 to 360° does not appear in the expressions for body rate or acceleration. This is due to the fact that the first rotation sequence was roll. Powers and products of the perturbed elements are neglected when linearizing. The resulting linearized equations of motion are:

$$I_x \ddot{\underline{r}} = T_x$$

$$I_y \ddot{\underline{p}} + \dot{\underline{y}} \left[ \dot{r}_0 (I_x - I_y - I_z) + H_x \right] = T_y$$

$$I_z \ddot{\underline{y}} - \dot{\underline{p}} \left[ \dot{r}_0 (I_x - I_y - I_z) + H_x \right] = T_z$$

(E-8)

### Y-Axis Pointing

The development of a linearized set of equations for the Y-axis pointing mode is similar to the development for X-axis pointing with the exception that the sequence of transformations must be different and that the nominal roll rate is now zero.

In the Y-axis pointing mode, the Y-axis must be pointed to a specific attitude with less than 1° half cone angle error. Large angular rotations can occur about the Y-axis (i.e. pitch motion) so long as the X-axis remains within 37° of the sun line. In the derivation it is essential that the pitch angle, which may be large, is not inherent to the equations. This is accomplished by selecting the Y-axis (pitch axis) as the first rotation in the sequence.

The rotation sequence for Y-axis pointing is thus:

- 1) rotation about Y-axis through a pitch angle
- 2) rotation about Z-axis through a yaw angle
- 3) rotation about X-axis through a roll angle

Following the procedure employed in the X-axis pointing mode, the body axis angular rates become

$$\vec{\omega} = \begin{bmatrix} \omega_x \\ \omega_y \\ \omega_z \end{bmatrix} = \begin{bmatrix} \dot{r} & + \dot{p} \sin\gamma \\ \dot{y} \sin r + \dot{p} \cos r \cos\gamma \\ \dot{y} \cos r - \dot{p} \sin r \cos\gamma \end{bmatrix}$$

Differentiating, substituting into Eulers equations of motion and linearizing, the following equations result:

$$\begin{aligned} I_x \ddot{\gamma} &= T_x \\ I_y \ddot{p} + \dot{\gamma} H_x &= T_y \\ I_z \ddot{y} - \dot{p} H_x &= T_z \end{aligned} \tag{E-10}$$

Equations (10) are identical to those for the X-axis pointing mode (Eqs(8)) if  $\dot{r}_0$  is set to zero in Eqs (8).

Z-Axis Pointing

Requirements for Z-axis pointing are similar to those for Y-axis pointing. In this case the Z-axis must be oriented to a specific source with less than 1° half cone angle error. Large angular motions can occur about the Z-axis (i.e. yaw motion) so long as the X-axis remains within 37° of the sun line.

Again, as in the Y-pointing mode, the large yaw motion must be kept out of the transformation equations for angular rates. This is done by selecting the following sequence of rotations:

- 1) rotation about Z-axis through a yaw angle.
- 2) rotation about Y-axis through a pitch angle.
- 3) rotation about ~~Z~~-axis through a roll angle.

Using this sequence, spacecraft angular rates in the body system are:

$$\vec{\omega} = \begin{bmatrix} \omega_x \\ \omega_y \\ \omega_z \end{bmatrix} = \begin{bmatrix} \dot{r} & -\dot{y} \sin p \\ \dot{p} \cos r + \dot{y} \sin r \cos p \\ -\dot{p} \sin r + \dot{y} \cos r \cos p \end{bmatrix} \quad (E-11)$$

Performing the required differentiation, substitution and linearization a set of equations identical to the Y-pointing mode results—Eqs (10).

### Conclusion-Appendix E

This appendix has presented the derivation of linearized equations for HEAO-A scan and Y-axis and Z-axis pointing modes. Although the transformation sequence for defining spacecraft attitude is different from each mode, the resulting linearized equations are the generalized set Eqs (8). For Y-and Z-axis pointing modes  $\dot{r}_0$ , the nominal roll rate, is set to zero.